Contents

Chapter 1

A Primer of Lattice Field Theory

1.1 Introduction — The Standard Model

In the last twenty years, the Standard Model (SM) has become the most successful model in explaining high–energy experimental data. Even at the highest attainable energies (approximately 10^5 MeV), there is no conclusive evidence indicating a significant deviation from the predictions of the SM. Low energy phenomena should also be explained fully by the SM. Some, for example electromagnetic interactions, have been found to be in very good agreement with theoretical predictions. The analysis of other low energy phenomena, in particular hadronic interactions, has been less thorough due to the complexity of the theory. If hadronic interactions could be studied accurately then a precise measurement of currently underdetermined parameters in the SM could be carried out. With these parameters calculated, the search for new physics would be significantly enhanced.

The SM links two areas of research in particle physics :

- The electromagnetic and weak interactions, using the Higgs mechanism to generate mass as investigated by Glashow [1], Weinberg [2], and others.
- The structure of hadrons and the strong interaction using Quantum Chromodynamics (QCD), investigated by Gell–Mann [3], Gross and Wilczek [4], and others.

As the latter topic is the focus of interest in this thesis, the former will not be discussed in detail[1].

1.1.1 Electro–weak and Higgs interactions

In the SM, fermions interact with each other via the exchange of gauge bosons which carry the electro–magnetic force and the weak and strong nuclear forces. These fermions are the six flavours of quark : up, down, strange, charm, bottom and top, which can interact via all three forces; the "electron–type" leptons: e, μ and τ which interact via the electromagnetic and weak forces and finally the "neutrino–type" leptons: ν, ν_μ and ν_τ which are only involved in weak interactions.

The masses of the first two classes of fermion are generated via a Yukawa–like coupling of each fermion with a doublet of complex scalar fields $\Phi(x)$, where

$$\Phi(x) = \begin{pmatrix} \phi^+(x) \\ \phi^0(x) \end{pmatrix} . \tag{1.1}$$

Because of the form of its self–interaction, this field undergoes spontaneous symmetry breaking, and $\Phi(x)$ can be rewritten as

$$\Phi(x) \to \frac{1}{\sqrt{2}} \begin{pmatrix} 0 \\ v + H(x) \end{pmatrix} , \tag{1.2}$$

where $v/\sqrt{2}$ is the vacuum expectation value $\langle 0 \, | \Phi(x) | \, 0 \rangle$. The residual scalar field $H(x)$ is referred to as the Higgs scalar field. As a result, the Yukawa coupling behaves like a mass term with the mass proportional to the vacuum expectation value of the field Φ and an interaction with the Higg's field.

The introduction of the scalar Higgs field is also extremely important in explaining the origins of the electromagnetic and weak (electro–weak) interaction. The violation of unitarity by a simple four–fermi Lagrangian suggests that weak interactions may occur via the exchange of a gauge boson with mass. However,

[1]Several excellent textbooks have been written on electro–weak and Higgs interactions including Renton [5], Cheng and Li [6] and Bailin and Love [7].

such a theory cannot be regulated, that is, it is non–renormalisable. In the SM, gauge fields are constructed which have the group symmetry $SU(2)_L \times U(1)_Y$ [2]. These fields couple to Φ, which after spontaneous symmetry breaking generate mass terms for three gauge fields, $W^{\pm}_{\mu}$ and Z^0_{μ}, which are a linear combination of the original four gauge fields. The remaining degree of freedom is associated with the $U(1)$ gauge symmetry of the electromagnetic interaction. Therefore, below the symmetry breaking scale the theory of Quantum Electrodynamics (QED) can be used. As a result, a renormalisable theory can be constructed which include massive vector bosons.

The weak interaction introduces a flavour–changing current between quarks. The size of this current between any two flavours is proportional to the magnitude of the elements of the Cabbibo–Kobayashi–Maskawa (CKM) matrix[3] [8]. The numerical values of some the CKM matrix elements are still underdetermined and their evaluation is an active topic of study [9].

1.1.2 The strong interaction

The theory of QCD is described by a gauge (gluon) field with the gauge symmetry $SU(3)$. The quark fields are in the fundamental representation of this group while the gluon field is in the adjoint representation. The QCD Lagrangian can be written in the form

$$\mathcal{L}_{QCD} = -\frac{1}{2} F_{\mu\nu} F^{\mu\nu} \ + \ \sum_{q=1}^{n_f} \bar{\psi}_q \left(i \not{D} - m_q \right) \psi_q \ , \tag{1.3}$$

where

$$\begin{aligned} F_{\mu\nu} &= \partial_\mu A_\nu \ - \ \partial_\nu A_\mu - ig \left[A_\mu, A_\nu \right] \ , & (1.4) \\ D_\mu &= \left(\partial_\mu - igA_\mu \right) \psi_q \ , & (1.5) \end{aligned}$$

[2]The subscripts L and Y stand for ‘weak isospin’ and ‘weak hypercharge’, used in comparison to the isospin and hypercharge of the quark model.

[3]The phase of these matrix elements provides information about CP violation in hadrons.

$$A_\mu = \sum_{a=1}^{8} A_\mu^a \frac{\lambda^a}{2}\,, \tag{1.6}$$

$$\psi_q = \begin{pmatrix} \psi_q^1 \\ \psi_q^2 \\ \psi_q^3 \end{pmatrix}, \tag{1.7}$$

the index n_f indicates the number of quark flavours, m_q is the mass of one the flavours and ψ_q^i are spinor fields. The matrices λ^a are the Gell–Mann matrices, which are the generators of $SU(3)$.

As free quarks or gluons in an asymptotic state have not been observed, it is believed that physical particles of QCD form singlets of the $SU(3)$ group. In classical terms, this implies that the quarks are confined in hadrons where the gluon potential increases as the distance between the quarks is increased. It is not clear that this is necessarily true for the Lagrangian of Eq.(1.3). Evidence that this does occur has been demonstrated by measuring the gluon potential between two infinitely heavy quarks in lattice field theory [10].

The calculation of expectation values from such a Lagrangian is far from trivial. The renormalisation group equation (RGE) demonstrates that for processes where the typical momentum scale μ is much greater than $\Lambda_{QCD} \sim 200-500$MeV, the effective coupling coefficient $\alpha_s(\mu)$ is much less than 1. The analysis proceeds in much the same way as low energy QED using perturbation theory. However, the RGE demonstrates that as μ approaches Λ_{QCD}, $\alpha_s(\mu) \to 1$, (as one would expect for a strongly interacting theory) and the perturbative approach breaks down.

QCD is therefore extremely frustrating. The agreement between theory and high energy experimental data is quite good [11, 12, 13] indicating that QCD is correct in that regime. At low energies, QCD and the electro–weak interaction in the SM provides a framework to explain an enormous range of phenomena, presenting an *ab initio* theory for nuclear physics in general. As will be demonstrated in chapter 4, new physics beyond the SM could be detected in the decays of B mesons. Even very subtle contributions could be detected with the high–luminosities of the B–meson factories that will be built at Stanford and Japan. However, soft (low energy) QCD contributions must be reliably calculated in order to achieve this goal. Such a tantalising opportunity lies beyond the grasp of standard analytic techniques of quantum field theory.

Lattice field theory presents a method for circumventing this difficulty. For a sufficiently small lattice spacing, low–energy QCD processes should give the same results as the continuum theory. High–energy processes can be included as radiative corrections, which can be determined perturbatively [14, 15, 16]. Furthermore, as QCD is (hopefully) a confining theory, then one expects that large volume calculations (for example, a spatial width of greater than 2 fm) would be unnecessary.

This thesis will derive the continuum matrix elements corresponding to a subset of two– or three–point functions for heavy hadrons (hadrons containing a quark whose mass is equal or greater than the mass of the charm quark). That is matrix elements of the form

$$\left\langle 0 \left| H(x)\bar{H}(0) \right| 0 \right\rangle , \left\langle H_1 \left| J_\mu \right| H_2 \right\rangle , \tag{1.8}$$

where $H(x)$ is an interpolating operator for some hadronic state and J_μ is a quark flavour–changing current. In general, this involves the calculation of

$$\left\langle 0 \left| T\left(\psi^{a_1}(x_1) \dots \psi^{a_n}(x_n) \bar{\psi}^{b_1}(y_1) \dots \bar{\psi}^{b_n}(y_n) \right) \right| 0 \right\rangle , \tag{1.9}$$

where T ensures the operators are time ordered, and a, b indicate the flavours of the quarks.

The time ordered product of Eq.(1.9) can be expressed in terms of a functional integral, which can then be expressed as a formal lattice calculation. A number of important approximations will be made and justified in order to proceed with a numerical evaluation by means of the Monte Carlo algorithm.

1.2 Formal solutions in Lattice Field Theory

The matrix element Eq.(1.9) can be expressed as

$$\begin{aligned}\langle 0 | T(\psi^{a_1}(x_1)\ldots\psi^{a_n}(x_n)\bar{\psi}^{b_1}(y_1)\ldots \quad \bar{\psi}^{b_n}(y_n) \quad)| 0 \rangle = \\ \frac{1}{Z}\int \mathcal{D}\Phi\psi^{a_1}(x_1)\ldots \quad \psi^{a_n}(x_n) \quad \bar{\psi}^{b_1}(y_1)\ldots\bar{\psi}^{b_n}(y_n)e^{iS[\Phi]},\end{aligned} \tag{1.10}$$

where Φ and $S[\Phi]$ is respectively the set of fields and the action of the theory and Z is the partition function. From Grassmann algebra, the integral over fermionic fields can be re-expressed in terms of propagators and the determinant of the Dirac operator. Assuming that there is only one quark flavour Eq.(1.10) can be expressed as

$$\begin{aligned}\left\langle 0 \left| T(\psi(x_1)\ldots\psi(x_n)\bar{\psi}(y_1)\ldots\bar{\psi}(y_n)) \right| 0 \right\rangle = \\ \sum_{i,j}\frac{1}{Z}\int \mathcal{D}AT_{i,j} \quad \det\left((-i)(i\not{D}-m)\right)e^{iS[A]} \ ,\end{aligned} \tag{1.11}$$

where $S[A]$ is the purely gluonic action, and

$$T_{i,j} = \prod_{k=1}^{n} G(P(x,i,k), P(y,j,k)). \tag{1.12}$$

$P(x(y), i(j), k)$ is the kth permutation of x_i (y_j) and $G(x,y)$ is the propagator, from y to x for a given configuration of the gauge field, satisfying the equation

$$(i\not{D} - m)\, P(x,y) = \delta^4(x-y) \ . \tag{1.13}$$

(Spin and colour indices have been dropped for clarity). In the case of N_f non-degenerate flavours occurring in Eq.(1.10), then the single determinant is replaced by

$$\det\left((-i)(i\not{D}-m)\right) \to \det\left((-i)(i\not{D}-m_1)\right)\ldots\det\left((-i)(i\not{D}-m_{Nf})\right) \ , \tag{1.14}$$

and $T_{i,j}$ replaced by $T^1_{i1,j1}\ldots T^{Nf}_{iNf,jNf}$.

The sum–over–histories approach has always been defined as the zero lattice spacing limit for a set of fields on a discrete lattice [17]. Hence, in this formalism, a numerical simulation is at least plausible. However, for even a very modest number of points, such a direct method of determining the integral is impossible for computational resources available [18]. Performing this integral by Monte Carlo methods is possible, if one accepts that all results will have a statistical, as well as a systematic error. This condition is not a particularly stringent one as the convergence of data with increasing statistics is well understood.

In order to use a Monte Carlo algorithm, the action in the exponential of Eq.(1.11) must be real. Hence one performs a Wick rotation where

$$t \rightarrow \tau = it. \tag{1.15}$$

As a result,

$$\begin{aligned} i\not{D} - m &\rightarrow \not{D}_E + m, & (1.16)\\ S[A] \rightarrow S_E[A] &= iS[A], & (1.17)\end{aligned}$$

and

$$\begin{aligned} \gamma^\mu &\rightarrow \gamma^\mu_E, \\ \gamma^0 &= \gamma^4_E, \\ \gamma^i &= i\gamma^i_E. \end{aligned} \tag{1.18}$$

Hence,

$$\left\langle 0 \left| T(\psi(x_1)\ldots\psi(x_n)\bar{\psi}(y_1)\ldots\bar{\psi}(y_n)) \right| 0 \right\rangle_E = \sum_{i,j} \frac{1}{Z_E} \int \mathcal{D}A\, T_{i,j} \quad \det\,(\not{D}_E + m) \quad e^{-S_E[A]}. \tag{1.19}$$

Assuming that such a rotation does not affect a non-perturbative calculation, one can in theory use a Monte Carlo algorithm to evaluate these matrix elements.

Once the required matrix element has been calculated, the rotations of Eq.(1.18) are utilised to rotate the result back into a Minkowski metric. As all future numerical calculations are carried out in a Euclidean metric, and rotated back into the Minkowski metric, the subscript E will be dropped.

Such calculations have been carried out, but it is extremely intensive numerically. It has been estimated that in order to obtain "reasonable" lattice spacings and volumes would require supercomputers which are of the order of 100 times current processing speeds (corresponding to 1–10 Tflop) [19]. The main reason for this is the determinant in Eq.(1.19) is a highly non-local object. In order to obtain results with current processing facilities, this determinant is assumed to be 1.

This is an uncontrolled approximation, as one cannot smoothly interpolate between a simulation with the determinant included and this approximation, commonly referred to as the "quenched" approximation. Furthermore, the size of the systematic error due to quenching cannot as yet be evaluated by analytic methods. Nonetheless, for the hadronic matrix elements that will be calculated here, it is reasonable to assume that errors due to such an approximation will not have a very large (i.e. greater than 20%) effect. This is for two reasons.

As the determinant corresponds to vacuum polarisation effects in the gluon field, it is clear that for a sufficiently large quark mass, the effect of the covariant derivative on the determinant will become more negligible. Physically, this corresponds to the fact that there is a very small probability that soft gluons will generate a quark anti–quark pair whose mass is very much greater than Λ_{QCD}. Hence for very large quark masses the quenched approximation is quite valid. One would expect, on the other hand, that vacuum polarisation effects would be very noticeable for systems involving light quarks, for example the light hadron mass spectrum. Indeed it can be shown that a quenched theory will exhibit logarithmic divergences as one approaches zero quark mass [20, 21]. However, the measurement of the light hadron mass spectrum has been remarkably successful, and is in agreement with experimental results to within 6%. Light hadron decay constants are in agreement with experiment to approximately 15% [19]. Indeed, unquenched calculations of the light hadron mass spectrum are in fact consistent with quenched calculations, although this is probably due to the very limited statistics available in such computations. As a result, it seems plausible to say that the mass spectrum for heavy–light hadrons would have similar properties. Furthermore, the simulation by several groups [22, 23, 24] of the transitions $D \to Ke\nu$, $D \to K^*e\nu$, and $D_s \to \phi e\nu$ is in relatively good agreement with experiment, even for quite coarse lattices and low statistical samples, indicating that other heavy–to–light decays should give similar results.

In practical terms, the evaluation of Eq.(1.19) in the quenched approximation for N_f non-degenerate flavours, is as follows : a distribution of gauge fields is generated which approximately satisfies the Boltzmann weight $\exp(-S[A])$.[4] Quark propagators are evaluated and combined as required in Eq.(1.19) to form

$$O(U_n) = T^1_{i1,j1;U_n} \dots T^{Nf}_{iNf,jNf;U_n}, \tag{1.20}$$

where U_n is the nth gauge configuration generated. Formally, the expectation value is

$$\langle 0 | O | 0 \rangle = \lim_{N\to\infty} \frac{1}{N} \sum_{n=1}^{N} O(U_n), \tag{1.21}$$

where N is the total number of gauge configurations calculated. By the central limit theorem, the statistical error associated with a finite number of samples falls off like $1/\sqrt{N}$.

The question of evaluating the quark propagator will now be considered. As will be seen, there are a wide range of possible methods to do this, even though only one will be utilised in this thesis. Each choice has its relative merits which will be compared.

[4] Lattice calculations do not generate the fields A_μ but the elements of the group $SU(3)$, U_μ. This method, which has proved to be highly successful, will not be discussed in any further detail here [25].

1.3 Fermionic Actions

As outlined in the previous section, the action including fermions is never actually required in the quenched approximation. However, it is necessary to determine the quark propagator for each gauge configuration at a number of bare quark masses. The choice of a discretised fermion action is by no means unique and is chosen for the typical mass scale of the quark simulated.

The equivalent of Eq.(1.13) in lattice field theory is

$$\sum_j F(i,j)P(j,k) = \delta_{i,k} , \tag{1.22}$$

where $F(i,j)$ is a discrete, Euclideanised form of the Dirac operator. The solution of Eq.(1.13) is transformed to an inversion of the Dirac matrix $F(i,j)$. The simulation of light quarks in this formalism is faced with two immediate difficulties. The inversion of the full Dirac matrix is numerically very intensive and its cost diverges as the quark mass approaches zero. Hence, the bare mass for "light" quarks (that is u and d) are typically simulated at masses in the strange quark mass regime. One then performs an extrapolation to the zero quark mass limit. The field of maximising the efficiency of an inversion algorithm has been explored intensively and will not be investigated any further here [26].

Furthermore, as demonstrated by Nielson and Ninomiya [27], any local action, defined on a regular lattice which satisfies hermiticity and translational invariance generates at least two states of opposite chirality. For calculations not concerned with generating states of a particular chirality, it is typically dealt with in two ways.

The doubling is accepted and is used to simulate 2 or 4 degenerate species using an action that extends the fermionic degrees of freedom over a number of lattice sites [28]. Referred to as staggered fermions, they are useful for light quark simulations, as one can treat the pair as satisfying isospin invariance. However, their utility is limited for heavier quark simulations where the concept of isospin breaks down. The second approach, which removes the doubling is outlined in the following section.

1.3.1 The Wilson Action

As suggested by Wilson [29], the constraint of hermiticity can be broken. The following action was suggested by him

$$S_F^W = a^4 \sum_x \frac{1}{a}\Big\{ \bar{q}(x)q(x) \quad + \quad \kappa \sum_\mu \big[\bar{q}(x)(\gamma_\mu - r)U_\mu(x)q(x+\hat{\mu}) \\ - \quad \bar{q}(x+\hat{\mu})(\gamma_\mu + r)U_\mu^\dagger(x)q(x)\big]\Big\}. \qquad (1.23)$$

This action has been used very successfully in light hadron calculations. In the limit of $\kappa \to 0$, corresponding to the bare quark mass going to infinity, the propagator behaves like a delta function. Therefore, as the bare quark mass is increased, one expects the propagator to be affected by discretization errors as its "width" falls below lattice spacing a.

The size of these discretisation errors have been explored in most detail through studies of the behaviour of the decay constant, f_P, of the pseudoscalar meson containing a heavy and light quark as a function of the heavy quark mass (approximately equal to the pseudoscalar mass). Heavy quark effective field theory (HQET) predicts that f_P will satisfy [30, 31, 32]

$$f_P\sqrt{m_P} = A + \frac{B}{m_P} + \mathcal{O}(\frac{1}{m_P^2}) \qquad (1.24)$$

where radiative corrections and terms of order $1/m_P^2$ are assumed to be negligible for $m_P \gtrsim m_D$. Initial analyses showed no agreement with this prediction at high mass scales. However, Lepage, Mackenzie and Kronfeld [33, 34, 35] have suggested that this is due to an incorrect normalisation of the fields $q, \bar{q}$. As demonstrated by Simone *et. al.* [36] and Bernard *et al.* [37], a new normalisation, using a mean field correction, does seem to eliminate the most pathological behaviour of the Wilson action for this parameter.

1.3.2 The Sheikholeslami–Wohlert Action

The question of discretisation errors is approached more directly by constructing an action which matches the continuum action at a higher order in a. This can be achieved by introducing next–to–nearest neighbour interactions

$$S_F^{II} = S_F^W + \Delta S^{II}, \tag{1.25}$$

where

$$\begin{aligned} \Delta S^{II} &= a^4 \sum_{x,\mu} \Big(\frac{\kappa r}{8a} \big[\bar{q}(x) U_\mu(x) U_\mu(x+\hat{\mu}) q(x+2\hat{\mu}) \\ &\qquad \bar{q}(x+2\hat{\mu}) U_\mu^\dagger(x+\hat{\mu}) U_\mu^\dagger(x) - 2\bar{q}(x) q(x) \big] \Big). \end{aligned} \tag{1.26}$$

By introducing the following substitution[5]

$$\begin{aligned} q(x) &\rightarrow \left(1 - \frac{1}{2} \overrightarrow{\not{\Delta}}\right) q(x) \\ \overline{q}(x) &\rightarrow \overline{q}(x) \left(1 + \frac{1}{2} \overleftarrow{\not{\Delta}}\right) , \end{aligned} \tag{1.27}$$

where Δ_μ is the discretised covariant derivative, operating on the quark fields as

$$\begin{aligned} a \overrightarrow{\Delta}_\mu \; q(x) &= \frac{1}{2} \Big(U_\mu(x) q(x+\mu) \; - \; U_\mu^\dagger(x-\mu) q(x-\mu) \Big) \; , \\ a \overline{q}(x) \; \overleftarrow{\Delta}_\mu &= \frac{1}{2} \Big(\overline{q}(x+\mu) U_\mu^\dagger(x) \; - \; \overline{q}(x-\mu) U_\mu(x-\mu) \Big) \; , \end{aligned} \tag{1.28}$$

the action S_F^{II} is transformed to S_F^I which Heatlie *et al.* [38] demonstrated to satisfy

$$S_F^I(q, \bar{q}, m_0) = S_F^C\left(q, \bar{q}, m_0 + \frac{ar}{2} m_0^2\right) + \mathcal{O}(a^2) \, , \tag{1.29}$$

where

$$S_F^C = S_F^W - ir\kappa \frac{a}{2} a^4 \sum_{x,\mu,\nu} \bar{q}(x) F_{\mu\nu}^C(x) \sigma_{\mu\nu} q(x) \, , \tag{1.30}$$

[5] The equations of motion of Dirac equation have been used to simplify this substitution.

and m_0 is the bare quark mass, satisfying

$$m_0 = \frac{1 - 8r\kappa/a}{2\kappa} \ . \tag{1.31}$$

The term $F^C_{\mu\nu}(x)$ is a lattice definition of the field strength tensor referred to as the "clover" term. This action (referred to as the Sheikholeslami–Wohlert (SW) [39] action, or more simply as the clover action), has the advantage that $F^C_{\mu\nu}$ acts like a purely local term, in that the quark fields are evaluated on the same site. In calculating the expectation value of any operator using the SW action, the improvement will be maintained if the substitution in Eq.(1.27) is applied for any occurence of the quark fields in the operator. Hence the SW action, though only involving nearest–neighbour interactions, matches the continuum action to a higher power of the lattice spacing than the Wilson action. Heatlie *et al.* demonstrated from lattice perturbation theory that the SW action eliminates terms of order $g_0^n a \log a^n$ where g_0 is the bare coupling coefficient, in n-th order perturbation theory.

Many simulations have been carried out in order to check if this holds in a non–perturbative regime. In particular, the expected scaling behaviour of f_P is satisfied [40]. Furthermore, as predicted by HQET, the vanishing of certain possible form factors in the decay $P \to P'l\nu$, where P and P' are sufficiently heavy pseudoscalar mesons has been demonstrated with this action [41].

The data presented in this thesis is based on the SW action.

1.3.3 The Static Approximation

Irregardless of the approach used, Wilson and SW actions cannot be used for $m_q a \gg 1$. The main difficulty is that at fixed lattice spacing the term in the Lagrangian corresponding to $m_Q \bar{\psi}\psi$ dominates. Hence, attempts have been made to construct a Lagrangian which does not contain this term. Eichten [42] determined a solution for the propagator in the limit of an infinite quark mass. In this case, the lower two components of the spinor vanish. The Lagrangian can be written as

$$\mathcal{L}_{static} = \phi^\dagger i D_t \phi. \tag{1.32}$$

This is a non–Lorentz–invariant theory, but as the heavy, or static, quark is at zero velocity, a non–relativistic formulation is perfectly acceptable.

Defining a simple discretised covariant derivative Δ_t as

$$a\Delta_t \phi(x) = \phi(x) - U_t^\dagger(x-\hat{t})\phi(x-\hat{t}), \tag{1.33}$$

implies that the propagator satisfies a remarkably simple evolution equation.

$$G^{static}(\vec{x}, t+a) = U_t^\dagger(x) G^{static}(\vec{x}, t) + \delta_{t,0}. \tag{1.34}$$

The numerical advantage of this method in comparison to a full inversion of the Dirac matrix is obvious. The simplicity of this equation comes at a cost as the propagator receives a very low statistical contribution from the gauge fields and hence the signal for two–point functions constructed from these propagators degrades much more rapidly than fully propagating quarks [43]. In order to counteract this, the δ function in Eq.(1.34) is multiplied by a function $\eta(\vec{x})$ which has some spatial extent. The use of this "smearing" function will be described in more detail later on in this chapter. Furthermore, static quarks cannot be used in simulating heavy to light quark decays, as it is unclear as to what the recoil of the light quark is. Finally, the static quark approximation cannot be used to explore any variation of parameters with respect to the heavy–quark mass, although it provides very useful information when used in conjunction with data at finite heavy–quark masses.

1.3.4 NRQCD

A systematic method of introducing a quark mass into the theory was suggested by Lepage and others [44, 45, 46]. In this approximation, the action is still non-relativistic and the lower spinor components are not present. Formally, one expands the action as a power series in v^2 and $1/M$, the velocity and inverse mass of the heavy quark. Including terms up to order Mv^4, one derives a continuum action of the form [47]

$$\mathcal{L}_{cont}^{NRQCD} = \phi^\dagger \left(D_t - \frac{\vec{D}^2}{2M} \right) \phi + \phi^\dagger \delta H_{cont} \phi, \tag{1.35}$$

where

$$\begin{aligned} \delta H_{cont} = & - \frac{c_1}{8M^3}(\vec{D}^2)^2 + \frac{ig_0 c_2}{8M^2}\left(\vec{D}\cdot\vec{E} - \vec{E}\cdot\vec{D}\right) \\ & - \frac{g_0 c_3}{8M^2}\vec{\sigma}\cdot\left(\vec{D}\times\vec{E} - \vec{E}\times\vec{D}\right) - \frac{g_0 c_4}{2M}\vec{\sigma}\cdot\vec{B}. \end{aligned} \tag{1.36}$$

The coefficients c_i are 1 at tree level, and their one–loop corrections are currently being calculated. The fields $\vec{B}, \vec{E}$ are the chromomagnetic and chromoelectric terms respectively. The discretised form of this action is obtained by replacing D_t, $\vec{D}$ by lattice operators. Hence,

$$\begin{aligned} \mathcal{L}^{NRQCD} & = \phi^\dagger(x)\phi(x) \\ - & \quad \phi^\dagger(x)\left(1 - \frac{aH_0}{2n}\right)_t^n U_t^\dagger \left(1 - \frac{aH_0}{2n}\right)_{t-a}^n (1 - a\delta H)_{t-a}\,\phi(\vec{x}, t-a), \end{aligned} \tag{1.37}$$

where n is an integer and H_0 and δH are respectively the lattice equivalents of the kinetic energy operator and the higher–order terms in the Hamiltonian.

From power counting, the term aH_0 is of order $1/Ma$, hence as $Ma \to 1$, the propagator will become more susceptible to instabilities due to this kinetic operator. Hence, the factor n needs to be increased accordingly.

Lattice simulations of heavy–heavy mesons have determined results in good agreement with experiment for hyperfine splitting in $c\bar{c}$ and $b\bar{b}$ states [48]. Recent research into calculations of f_P for heavy–light mesons by Davies *et al.* [49] and Hashimoto [50] are in good agreement with extrapolated results from Wilson and SW actions.

The differences between these actions are summarised in Table 1.1.

Action	$m_q a$	Numerically intensive ?	Main Use	Problems
Staggered	$\ll 1$	Yes	Light hadron spectrum, Dynamical simulations	Degeneracy
Wilson	< 1	Yes	Light and strange simulations	Behaviour unclear as $m_q a \to 1$
clover	< 1	Yes	Light, strange and charm simulations	Difficult to implement
Static	∞	No	Decay constants, Isgur–Wise function	Normalisation unclear, optimal smearing yet to be determined.
NRQCD	> 1	No	Bottom and charm simulations	Stability problems as $m_q a \to 1$

Table 1.1: Comparison of different discretised fermionic actions.

1.4 Two–Point Functions

The calculation of two–point functions is the simplest to do computationally and provides us with some of the most basic properties of the ground state hadron, that is, its mass and decay constant. By performing a Fourier transform on the spatial sites, one can fix the momentum of the state and test the behaviour of the dispersion relation. Theoretically, the same data could be derived for excited states of the hadron, but current lattice sizes and the number of configurations calculated generally exclude this.

From translational invariance in a Euclidean metric, it is clear that

$$\sum_{\vec{x}} e^{i\vec{p}\cdot\vec{x}} \left\langle 0 \left| H(\vec{x},t)\bar{H}(0) \right| 0 \right\rangle = \sum_{n} \frac{1}{2E_n} | \langle 0 \, | H | \, n(p) \rangle \, |^2 e^{-E_n t}, \tag{1.38}$$

where $|n(p)\rangle$ are all the possible states H can create and E_n satisfies the dispersion relation[6]

$$E_n = \sqrt{m_n^2 + p^2}. \tag{1.39}$$

As one would expect for a discrete lattice, the momenta are limited to increments of

$$\Delta p = \frac{2\pi}{La}, \tag{1.40}$$

where La is the physical size of the lattice. The damped exponential behaviour ensures that for large t

$$\sum_{\vec{x}} e^{i\vec{p}\cdot\vec{x}} \left\langle 0 \left| H(\vec{x},t)\bar{H}(0) \right| 0 \right\rangle \underset{t \gg (E_1 - E_0)^{-1}}{\longrightarrow} \frac{1}{2E_0} | \langle 0 \, | H | \, H_0(p) \rangle \, |^2 e^{-E_0 t}, \tag{1.41}$$

where E_1 and E_0 are respectively the first excited and ground state of the hadron. This needs to be modified if periodic or anti–periodic boundary conditions are used in evaluating the propagators for this function. One must then allow for

[6] It is tacitly assumed that all states generated are discrete, however as we are interested in the contribution of the ground state, it is a reasonable assumption.

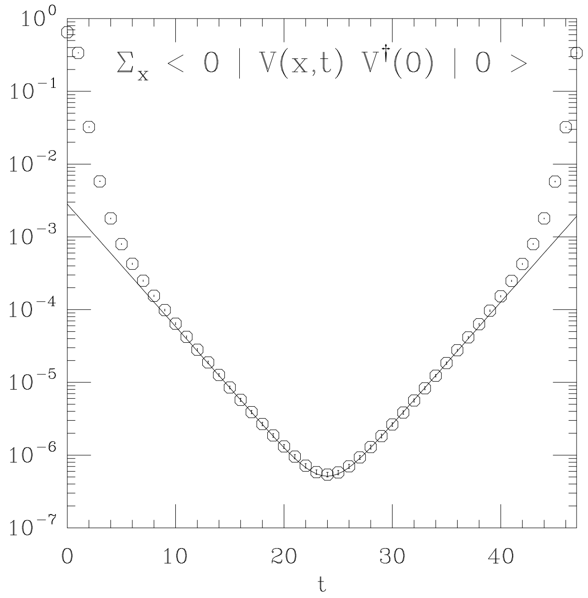

Figure 1.1: The two–point function of two vector ($\bar{\psi}\gamma^\mu\psi$) operators. The χ^2 per degree of freedom from the best fit of this data to the expected asymptotic form is 27/16.

backward propagating states from the final time slice T_f of the lattice. Hence

$$\sum_{\vec{x}} e^{i\vec{p}\cdot\vec{x}} \left\langle 0 \left| H(\vec{x},t)\bar{H}(0) \right| 0 \right\rangle \underset{t\gg(E_1-E_0)^{-1}}{\longrightarrow} \frac{1}{2E_0} |\left\langle 0 \left| H \right| H_0(p) \right\rangle|^2 (e^{-E_0 t} + e^{(-E_0(T_f - t))}). \tag{1.42}$$

An example of such a two–point function is shown in Fig.(1.1). Methods for obtaining the amplitude $\langle 0 | H | H_0(p)\rangle$ and the energy E_0 will be described in chapter 3.

1.4.1 Construction of Meson and Baryon fields

The construction of a meson interpolating field is quite straightforward. In general, the field M has the form

$$M = \bar{\psi}^a_{1\alpha} \Gamma_{\alpha\beta} \psi^a_{2\beta}, \tag{1.43}$$

where the Greek and Latin indices are respectively the spin and colour indices. By performing Wick contractions and assuming the quark fields are non–degenerate implies

$$\left\langle 0 \left| M(x) M^{\dagger}(0) \right| 0 \right\rangle = \lim_{N\to\infty} \frac{1}{N} \sum_{n=1}^{N} Tr(\gamma^5 G_1^{(n)\dagger}(x,0)\gamma^5 \Gamma G_2^{(n)}(x,0)\Gamma), \qquad (1.44)$$

where $G_i^{(n)}(x,0)$ is the propagator from 0 to x, calculated from the n^{th} gauge configuration and satisfies the relation

$$G^{(n)}(0,x) = \gamma^5 G^{(n)\dagger}(x,0)\gamma^5. \qquad (1.45)$$

The trace is taken over spin and colour. The matrix Γ is chosen to satisfy the quantum numbers of the meson, hence for a pseudoscalar meson, it is γ^5 and for a vector meson it is γ^{μ}.

The choice of baryonic operators is less clear as there exist a large number of combinations of the three quark fields which will have some overlap with the required quantum numbers [51]. In the simplified case of a baryon containing one heavy quark and two light quarks, the lowest spin 1/2 baryon operator can be written as

$$\begin{aligned} B_{\mu}(x) &= \varepsilon^{abc} h_{\mu}^{a}(x) l_{1\alpha}^{b}(x) \Gamma_{\alpha\beta} l_{2\beta}^{c}(x) \qquad (1.46) \\ \bar{B}_{\mu}(x) &= \varepsilon^{abc} \bar{h}_{\mu}^{a}(x) \bar{l}_{1\alpha}^{b}(x) \bar{\Gamma}_{\alpha\beta} \bar{l}_{2\beta}^{c}(x). \end{aligned}$$

If one assumes isospin symmetry between the light quarks and that $I = 0$, then Γ must be antisymmetric, for example $C\gamma^5$. Hence

$$\left\langle 0 \left| B_{\mu}(x) \bar{B}_{\nu}(0) \right| 0 \right\rangle = \lim_{N\to\infty} \frac{1}{N} \sum_{n=1}^{N} \varepsilon_{abc}\varepsilon_{def} \Gamma_{\alpha\beta} \bar{\Gamma}_{\gamma\delta} H_{\mu\nu}^{ad(n)}(x,0) L_{1\alpha\delta}^{be(n)}(x,0) L_{2\beta\gamma}^{cf(n)}(x,0)\ , \qquad (1.47)$$

where $H^{(n)}(x,0)$ and $L^{(n)}(x,0)$ are respectively, the heavy and light quark propagators.

1.5 Three–Point Functions

The purpose of calculating three–point functions is to determine the matrix element $\langle M_1 | J_\mu | M_2 \rangle$, where J_μ is some quark–flavour–changing current. For the purposes of this thesis, we will assume that $|M_1\rangle$ and $|M_2\rangle$ are mesonic states. Three–point functions can be used in calculating exclusive semi–leptonic and radiative decays, where the meson number is conserved[7]

Once again, from translational invariance and the fact that a Euclidean action is being used

$$\begin{aligned}\sum_{\vec{x},\vec{y}} \quad e^{i(\vec{p}\cdot\vec{x}+\vec{q}\cdot\vec{y})} \left\langle 0 \left| M_1^\dagger(x) O(y) M_2(0) \right| 0 \right\rangle = \\ \sum_{n_1,n_2} \frac{1}{4E_1^{n1}E_2^{n2}} \langle 0|M_1^\dagger|n_1\rangle \langle n_1|O|n_2\rangle \langle n_2 |M_2| 0\rangle \, e^{-E_1^{n1}t_y} e^{-E_2^{n2}(t_x-t_y)},\end{aligned} \tag{1.48}$$

where

$$E_1^{n1} = \sqrt{(m_{n1})^2 + |\vec{p}|^2} \quad E_2^{n2} = \sqrt{(m_{n2})^2 + |\vec{k}|^2} \tag{1.49}$$

and

$$\vec{k} = \vec{p} - \vec{q}. \tag{1.50}$$

(It is noted that if one of the states is a vector hadron, then there is an implicit sum over polarisations states.) Therefore, asymptotically

$$\begin{aligned}\sum_{\vec{x},\vec{y}} e^{i(\vec{p}\cdot\vec{x}+\vec{q}\cdot\vec{y})} \langle 0|M_1^\dagger(x) O(y) M_2(0)|0\rangle \xrightarrow[t_x \gg (E_1^1-E_1^0)^{-1}, t_x-t_y \gg (E_2^1-E_2^0)^{-1}]{} \\ \frac{1}{4E_1^0E_2^0} \left\langle 0 \left| M_1 \right| M_1^0 \right\rangle \left\langle M_2^0 \left| M_2^\dagger \right| 0 \right\rangle \left\langle M_1^0 \left| O \right| M_2^0 \right\rangle e^{-E_1^0 t_y} e^{-E_2^0(t_x-t_y)}.\end{aligned} \tag{1.51}$$

If the extension time slice t_x is held fixed at $T_f/2$, and periodic boundary conditions are used in the calculation of the propagators, then one creates two regions on the lattice ($0 \le t \le T_f/2$ and $T_f/2 \le t \le T_f$) where this asymptotic condition holds. This can be used to reduce the noise of the calculation.

---

[7] Decays of one hadron into two or more can be studied with four–point functions and higher. This has been tentatively studied by Bernard, Simone and Soni [52, 53] but will not be explored here.

As before, the meson fields are defined as

$$\begin{aligned} M_1 &= \bar{\psi}^a_\alpha \, \Gamma^1_{\alpha\beta} \, \phi^a_\beta, \\ M_2 &= \overline{\xi}^a_\alpha \, \Gamma^2_{\alpha\beta} \, \phi^a_\beta. \end{aligned} \tag{1.52}$$

The operator O takes the form

$$O = \bar{\psi}^a_\alpha \, \Gamma^O \, \xi^a_\beta. \tag{1.53}$$

If one assumes the quark fields are non–degenerate then

$$\langle 0 \,| M_1(x) \, O(y) \, M_2(0) | \, 0 \rangle = \lim_{N\to\infty} \frac{1}{N} \sum_{n=1}^{N} Tr(\Phi^{(n)}(x,0) \, \Gamma^2 \, \Xi^{(n)}(y,x) \, \Gamma^O \, \Psi^{(n)}(0,y) \,), \tag{1.54}$$

where $\Phi^{(n)}$, $\Xi^{(n)}$ and $\Psi^{(n)}$ are respectively the propagators for the fields ϕ, ξ and ψ calaulated for the n^{th} gauge configuration. The propagator $\Psi^{(n)}(0,y)$ is calculated at the origin, with the relevant δ–function at y, however this propagator is related to the calculable propagator $\Psi^{(n)}(y,0)$ by

$$\Psi^{(n)}(0,y) = \gamma^5 \Psi^{(n)\dagger}(y,0)\gamma^5 \; . \tag{1.55}$$

In the degenerate case where $\psi = \phi$,

$$\begin{aligned} \langle 0 \,| M_1(x) \, O(y) \, M_2(0) | \, 0 \rangle \;\; &= \\ \lim_{N\to\infty} \frac{1}{N} \sum_{n=1}^{N} \quad & \Big(Tr \left[\Phi^{(n)}(x,0) \, \Gamma^2 \, \Xi^{(n)}(y,x) \, \Gamma^O \, \gamma^5 \, \Psi^{(n)\dagger}(y,0) \, \gamma^5 \right] \\ + \quad & Tr \left[\Gamma^1 \, \Psi^{(n)}(0,0) \right] \; Tr \left[\Psi^{(n)}(x,y) \, \Gamma^2 \, \Xi^{(n)}(y,x) \, \Gamma^O \right] \Big) \; . \end{aligned} \tag{1.56}$$

The extra term on the r.h.s. of Eq.(1.56) corresponds to the annihilation of the $\bar{\psi}\psi$ pair and the creation of the $\overline{\xi}, \psi$ from purely gluonic processes, as schematically demonstrated in Fig.(1.2). Zweig's rule [54, 55, 56] states that such a process will be heavily suppressed for heavy or light quarks. Therefore, this extra term is ignored.

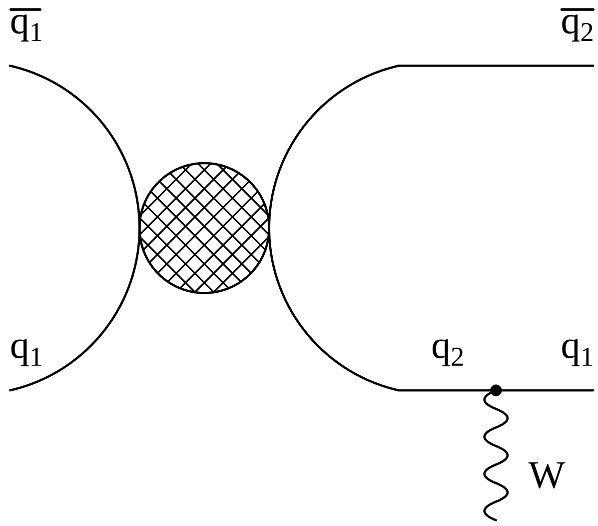

Figure 1.2: An example of a Zweig process. The quark pair $\bar{q}_1 q_1$ annihilate to some gluonic state (indicated by the blob), which forms the $\bar{q}_2 q_2$ quark pair. A flavour–changing current is introduced by the W boson.

In practical terms, the calculation of Eq.(1.54) is schematically demonstrated in figure Fig.(1.3). The propagators satisfy[8]

$$\begin{aligned} \sum_z F_\xi(y,z)\,\Xi(z,x) &= \delta_{y,x}\ , \\ \sum_z F_\psi(y,z)\,\Psi(z,0) &= \delta_{y,0}\ , \\ \sum_z F_\phi(x,z)\,\Phi(z,0) &= \delta_{x,0}\ , \end{aligned} \tag{1.57}$$

where F_ξ, F_ψ and F_ϕ are the lattice Dirac operators for the fields ξ, ψ and ϕ. Hence, one can define an extended propagator $E(y,t_x)$ as

$$E(y,t_x) = \sum_{\vec{x}} \Phi(x,0)\,\Gamma^2\,\Xi(y,x)\,e^{i\vec{p}\cdot\vec{x}}, \tag{1.58}$$

[8]The summation over gauge fields will be implicitely assumed for the rest of this chapter.

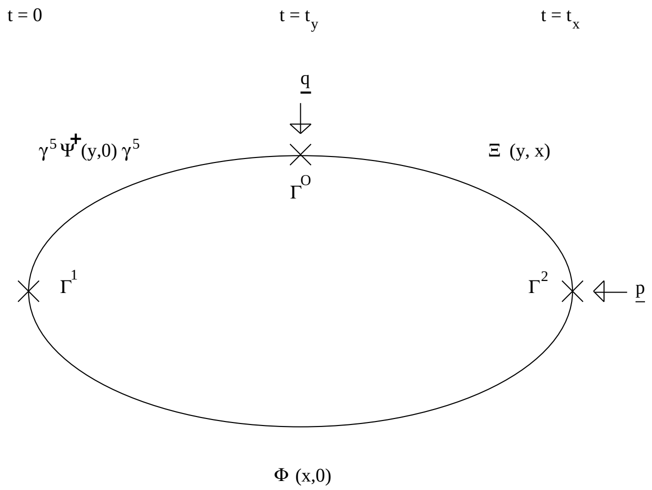

Figure 1.3: Calculation of a three–point function. The propagators $\Phi(x,0)$ and $\Psi(y,0)$ are calculated previously, hence the calculation of the three point function requires the evaluation of $E(y,0)$ and "tying" it with $\Psi(y,0)$.

which by Eq.(1.57) satisfies

$$\sum_z F_\xi(y,z)\, E(z,t_x) = \delta_{ty,tx}\, \Phi(\vec{y},t_x;0)\, \Gamma^2\, e^{i\vec{p}\cdot\vec{y}}. \tag{1.59}$$

Hence,

$$\begin{aligned} \sum_{\vec{x}\vec{y}} e^{i\vec{p}\cdot\vec{x}} e^{i\vec{q}\cdot\vec{y}} \left\langle 0 \left| M_1(x) O(y) M_2^\dagger(0) \right| 0 \right\rangle \quad &= \\ \lim_{N\to\infty} \frac{1}{N} \sum_{n=1}^{N} \sum_{\vec{y}} \quad e^{i\vec{q}\cdot\vec{y}} \quad & Tr(E^{(n)}(y,t_x)\, \Gamma^O\, \gamma^5\, \Psi^{(n)\dagger}(y,0)\, \gamma^5). \end{aligned} \tag{1.60}$$

The extended propagator can be calculated using Eq.(1.59). The propagator $\Phi(x,0)$ need only be calculated for one time slice t_x if that time slice is fixed and t_y varied. It is in fact calculated at all time slices. This is normally done as a separate phase and stored on disk, to be read in for the above calculation. The major advantage of fixing this time slice is that main memory requirements are significantly reduced.

The machinery for evaluating these functions has now been described. The ground–state signal for two– and three–point functions can be considerably improved for comparatively little numerical cost. This will now be discussed.

1.6 Smearing

It is assumed for Eq.(1.41) and Eq.(1.51) that the temporal extent of the lattice is large enough to eliminate the excited contributions to Eq.(1.38) and Eq.(1.48). However, as the ground–state contribution is also falling off exponentially, the amount of noise from the finite number of gauge configurations calculated may be too large to determine the parameters required. This lead Kenway [57] and Billoire *et al.* [58] to suggest that if operators can be picked which suppress the amplitudes of the excited states in Eq.(1.38) and Eq.(1.48), then a more accurate result can be determined. This is implemented by spatially extending the quark fields.

$$\bar{\psi}(0) \rightarrow \sum_{\vec{z}} f(\vec{z})\bar{\psi}(\vec{z},0), \tag{1.61}$$

$$\psi(x) \rightarrow \sum_{\vec{z}} g(\vec{x},\vec{z})\psi(\vec{z},t). \tag{1.62}$$

Substituting Eq.(1.61) into the propagator $G(x,0) = \psi(x)\bar{\psi}(0)$ implies a new propagator $G^{LS}(x,0)$ which satisfies

$$\sum_{z} F(x,z)\, G^{LS}(z,0) = f(\vec{x})\delta(t). \tag{1.63}$$

Hence, such a propagator can be easily evaluated numerically if one replaces the spatial δ function by the spatially extended function $f(\vec{x})$. The cost of evaluating Eq.(1.63) is comparable to evaluating the usual Dirac propagator equation (apart from the cost of evaluating f, which will be outlined below). This is referred to as smearing at the source. The second substitution Eq.(1.62) implies that the resulting propagator $G^{SL}(x,0)$ is formally defined as

$$G^{SL}(x,0) = \sum_{\vec{z}} g(\vec{x},\vec{z})\, G(\vec{z},t;0), \tag{1.64}$$

This is referred to as smearing at the sink. The propagator on the r.h.s. of Eq.(1.64) may have been determined using a local source, or with smeared source, defined in Eq.(1.63). The solution of that propagator is $G^{SS}(x,0)$.

Numerous smearing functions have been employed [59, 60, 61, 62, 63, 64, 65, 65]. As the parameters being measured are gauge covariant, the smearing functions should also be gauge covariant, thus avoiding the necessity to fix the gauge of each gauge configuration. One would also expect that the smearing function should be localised over a few spatial sites, roughly corresponding to the "shape" of the quark field. Finally, the generation of these functions should be as quick as possible, particularly in the case of Eq.(1.64) where the propagator must be evaluated for each spatial site, spin and colour index. A possible choice is to treat f and g as propagators of the discretised 3 dimensional Klein–Gordon equation

$$\sum_{\vec{x}'} \left[\delta_{\vec{x},\vec{x}'} - \kappa_{sc}\Delta\left(\vec{x},\, \vec{x}'\right)\right] f(\vec{x}') = \delta_{\vec{x},\vec{x}'}, \tag{1.65}$$

where

$$\Delta\left(\vec{x},\, \vec{x}'\right) = \sum_{\mu} \left(\delta_{\vec{x}',\vec{x}-\hat{\mu}} U^{\dagger}_{\mu}(\vec{x}-\hat{\mu}) \;+\; \delta_{\vec{x}',\vec{x}+\hat{\mu}} U_{\mu}(\vec{x}+\hat{\mu})\right) . \tag{1.66}$$

It can be shown that the propagator $G^{SL}(x,0)$ or $G^{SS}(x,0)$ is determined by this method as the solution to

$$\sum_{\vec{x}'} \left(\delta_{\vec{x},\vec{x}'} - \kappa_{sc}\Delta\left(\vec{x},\, \vec{x}'\right)\right) G^{SL}(\vec{x}',0;0) \;=\; G^{LL}(\vec{x},0;0) \,, \tag{1.67}$$

$$\sum_{\vec{x}'} \left(\delta_{\vec{x},\vec{x}'} - \kappa_{sc}\Delta\left(\vec{x},\, \vec{x}'\right)\right) G^{SS}(\vec{x}',t;0) \;=\; G^{SL}(\vec{x},t;0). \tag{1.68}$$

The r.m.s. "radius" of these propagators, defined as

$$r^2 = \frac{\sum_{\vec{x}} |\vec{x}|^2 |G^{SL}(\vec{x},0;0)|^2}{\sum_{\vec{x}} |G^{SL}(\vec{x},0;0)|^2} \,, \tag{1.69}$$

can be increased as κ_{sc} is increased. One can solve Eq.(1.67) and Eq.(1.68) completely, but for large κ_{sc} this can require as much time as a full Dirac inversion [66]. Another approach, referred to as the gauge–invariant Jacobi–smearing algorithm, is to treat the solution as a power series in κ_{sc}. For example, the solution to Eq.(1.65) is

$$f(\vec{x}) = \delta_{\vec{x},\vec{0}} + \sum_{n=1} \kappa_{sc}^n \Delta^n \left(\vec{x},\, \vec{0}\right) \ . \tag{1.70}$$

This series is divergent for large κ_{sc}. However if the series is truncated for some large n (typically of order 50 to 100), one still has gauge–covariant smearing function calculated at a comparatively low computational cost.

These techniques can now be employed in the evaluation of hadronic correlation functions.

Chapter 2

Heavy Quark Effective Field Theory

2.1 Introduction

In the last five years, the formulation of an effective theory in QCD involving the interaction of heavy quarks with light quarks and gluons – Heavy Quark Effective Theory (HQET) – has become very sophisticated. Not only is the infinite quark mass (m_Q) limit of the theory well understood, corrections of order $1/m_Q$ have been calculated for the important processes considered in HQET as well as the leading logarithmic radiative corrections to match the theory with full QCD.

Perhaps the most important use of HQET has been in the study of weak decays of bottom to charm hadrons. Heavy quark symmetry implies that in the first approximation, heavy decay modes can be related to each other by the mesonic [67, 68] and baryonic [69, 70] Isgur–Wise functions $\xi(v.v')$ and $\zeta(v.v')$. By determining the behaviour of these functions, one may obtain a better estimate of $|V_{cb}|$ than currently available [71, 72, 73].

HQET has also improved our understanding of the spectroscopy of charm and bottom hadrons [74]. It has been invaluable for lattice field theory as it provides a number of scaling laws which can be tested numerically.

Nonetheless, aspects of HQET require clarification. In particular, as m_Q is a scheme–dependent parameter, it is not immediately clear which definition is appropriate as the expansion parameter. This will be discussed in the following sections. Some attempts have been made to describe the light quark/soft gluon fields that surround the heavy quark (commonly referred to as the "brown muck") with chiral perturbation theory [75]. This approach, referred to as Heavy Hadron Chiral Perturbation Theory (HHCPT), presents a tantalising opportunity to describe entirely the dynamics of heavy–light hadrons. As of yet however, HHCPT has not made a significant contribution to our understanding of such systems.

The rest of this chapter is organised as follows. A heuristic picture of an extremely heavy quark within a hadron is described and the resulting symmetries that are satisfied by it. A more rigorous approach will be detailed, allowing for the introduction of higher–ordœ[Der corrections to the Lagrangian. Corrections to this Lagrangian will be outlined, in particular the radiative corrections required to match HQET with the continuum. The use of reparametrisation invariance and the potential difficulty of the residual mass term will be examined. Finally, an example of the use of HQET in heavy hadron spectroscopy will be addressed.

2.2 The Static Limit : A heuristic approach

It is somewhat misleading to refer to HQET as a result of heavy quark symmetry. How can charm, bottom and top, which have different masses, electric charge, CKM coupling coefficients etc. be related to each other by a symmetry transformation ? A more correct way of describing the symmetry is as a symmetry of the heavy degrees of freedom in the *effective* theory. To a first approximation, each of the heavy quarks has a mass much greater than the typical energy imparted by a soft gluon, that is an arbitrary quark Q is heavy if its mass, m_Q, satisfies

$$m_Q \gg \Lambda_{QCD}. \tag{2.1}$$

As the momentum imparted by such a soft gluon to the heavy quark is very small in comparison to the quark's total momentum, the quark's velocity will be changed very slightly. In the static limit, i.e. where $m_Q \to \infty$, the velocity of the quark is unchanged. This is referred to by Georgi [76] as the "velocity superselection rule". As with full QCD, the effect of hard gluons, whose momentum is of the of the order of m_Q, and $Q\overline{Q}$ pair production must be included in any calculation. However, as such processes occur, by definition, over short distances, one can treat them perturbatively and introduce them as radiative corrections to the theory. This will be discussed later on in this chapter.

The momentum of the quark p_Q^μ can be written as

$$p_Q^\mu = m_Q v^\mu + k^\mu, \tag{2.2}$$

where

$$k^\mu = \mathcal{O}(\Lambda_{QCD}) \;, \tag{2.3}$$

is then referred to as the residual momentum of the heavy quark. As the velocity of the quark is unchanged, one can parametrise its field, $Q(x)$ to be

$$Q(x) = e^{-im_Q v.x} h_v(x) \;. \tag{2.4}$$

The expectation value of the momentum of the field $h_v(x)$ is k^μ. If the quark was truly on–shell, then $h_v(x)$ would be a constant, and satisfy the constraint

$$\not{v} h_v(x) = h_v(x) \;. \tag{2.5}$$

As the quark is slightly off–shell, $h_v(x)$ has some extent. The residual field is still, however, independent of m_Q, and therefore the constraint Eq.(2.5) is still satisfied. Inserting Eq.(2.4) into the QCD Lagrangian implies

$$\begin{aligned} \overline{Q}(x)\,(i\not{D} - m_Q)\,Q(x) &= \overline{h}_v(x)\,(m_Q\,(\not{v} - 1) + i\not{D})\,h_v(x) \\ &= \overline{h}_v i\not{D} h_v(x) \;\;, \end{aligned} \tag{2.6}$$

by Eq.(2.5). By inserting $(1+\not{v})/2$ on either side of $\not{D}$ in Eq.(2.6) one finds

$$\mathcal{L}_{stat} = \overline{h}_v(x) iv.D h_v(x) \;\;. \tag{2.7}$$

There are three important points to note about the form of the Lagrangian in Eq.(2.7). Firstly, the Lagrangian is independent of the heavy quark mass, (hence the use of the term heavy quark symmetry). The Lagrangian has no spin structure, so the spin of the light degrees of freedom is independent of the heavy quark spin. Therefore, both spins are good quantum numbers. This point becomes very important in the spectroscopy of heavy hadrons. Finally, one could repeat this argument for antiquarks[1]. In this case, the field $Q(x)$ satisfies

$$Q(x) = e^{im_Q v.x} h_v(x), \tag{2.8}$$

where $h_v(x)$ now satisfies

$$\not{v} h_v(x) = -h_v(x). \tag{2.9}$$

However, the final static Lagrangian is the same as Eq.(2.7). As a result, the interaction of the light degrees of freedom with the heavy degrees of freedom is independent of whether the heavy fermion is in a quark or anti–quark state. One is therefore presented with the picture of a massive quark, moving at constant velocity, surrounded by the fields of light quarks and gluons. The only interaction that these fields have with the heavy quark is via the colour charge the heavy quark has. As the total spin of the hadron and the heavy quark is a good quantum number, so too is the spin of the light degrees of freedom.

The validity of this approach requires that the relationship Eq.(2.1), is satisfied. However, it is not clear that this is entirely true for heavy quarks, in particular charm. The mass of the charm quark in the $\overline{MS}$ scheme has recently been calculated to be approximately 1.5 GeV [77], which is not significantly larger than $\Lambda_{QCD}^{(4)\overline{MS}} \approx 0.3\,\mathrm{GeV}$. Corrections of order $1/m_Q$ to the theory must therefore be calculated. As will be demonstrated, the operators corresponding to the corrections of order $1/m_Q$ are equivalent to the kinetic energy of the heavy quark from the gluon field and a simple term coupling the spins of the brown muck to the heavy quark. This will be discussed in the following section.

[1]It is implicitly assumed that the heavy spinor is purely a quark or anti–quark. This is explicitly demonstrated from Eq.(2.5), if one uses the rest frame of the heavy quark.

2.3 The HQET Lagrangian

While several different derivations of these corrections have been calculated [78, 79, 80], the approach by Mannel, Roberts and Ryzak [81] is perhaps the most elegant, as it allows a systematic introduction of higher–order corrections to the Lagrangian, and is described here. In the static approximation, the heavy quark field $h_v(x)$ is only composed of the two upper spinor components in the rest frame of the quark. It is clear then that in a corrected Lagrangian, the lower components are included. One therefore decomposes the quark field $Q(x)$ into the fields $h_v(x)$ and $H_v(x)$, where

$$\begin{aligned} h_v(x) &= e^{im_Q v.x}\left(\frac{1+\not v}{2}\right)Q(x)\ \ ,\ \ \not v h_v(x) = h_v(x)\,, & (2.10)\\ H_v(x) &= e^{im_Q v.x}\left(\frac{1-\not v}{2}\right)Q(x)\ \ ,\ \ \not v H_v(x) = -H_v(x)\,. & (2.11)\end{aligned}$$

(Similar fields could be constructed assuming the fermion is in an anti–quark state). Inserting Eq.(2.10) and Eq.(2.11) into the full heavy quark Lagrangian one finds

$$\begin{aligned}\overline{Q}\,(i\not D - m_Q)\,Q \to \overline{h}_v i\,(v.D)\,h_v &+ \overline{H}_v i\,(v.D + 2m_Q)\,H_v\\ &+ \overline{h}_v i\not D^{\perp} H_v + \overline{H}_v i\not D^{\perp} h_v = \mathcal{L}_v, \quad (2.12)\end{aligned}$$

where

$$D^{\perp}_{\mu} = D_{\mu} - v_{\mu}\,(v.D)\,. \tag{2.13}$$

The Lagrangian of Eq.(2.12) can be used to derive a generating functional, $Z_v(r_v, \overline{r}_v, R_v, \overline{R}_v, l)$ for these fields,

$$Z_v(r_v,\overline{r}_v,R_v,\overline{R}_v,l) = \int \mathcal{D}h_v\mathcal{D}\overline{h}_v\mathcal{D}H_v\mathcal{D}\overline{H}_v\mathcal{D}l\,\exp\left(i\int d^4x\mathcal{L}_v + iS_l + iS_{source}\right), \tag{2.14}$$

where S_l is the action resulting from interactions only involving the light degrees of freedom and S_{source} is the source term rewritten in terms of h_v and H_v,

$$S_{source} = \int d^4x \left(\overline{\eta}Q + \overline{Q}\eta\right) = \int d^4x \left(\overline{r}h_v + \overline{h}_v r + \overline{R}H_v + \overline{H}_v R\right) \ . \tag{2.15}$$

The source variables r_v and R_v are derived from the original source variable η,

$$r_v = \left(\frac{1+\not{v}}{2}\right) e^{im_Q v.x}\eta \ , \tag{2.16}$$

$$R_v = \left(\frac{1-\not{v}}{2}\right) e^{im_Q v.x}\eta \ . \tag{2.17}$$

The "small" field H_v can be integrated out of $Z_v(r_v, \overline{r}_v, R_v, \overline{R}_v, l)$, and the sources $\overline{R}_v, R_v$ set to zero. The new generating functional $Z_v(\overline{r}_v, r, l)$ satisfies

$$Z_v(\overline{r}_v, r, l) = \int \mathcal{D}h_v \mathcal{D}\overline{h}_v \mathcal{D}l \Delta \exp\left(i\int d^4x \left(\mathcal{L}'_v + \overline{r}_v h_v + \overline{h}_v r\right) + iS_l\right) \ , \tag{2.18}$$

where

$$\mathcal{L}'_v = \overline{h}_v i\,(v.D)\,h_v - \overline{h}_v \not{D}^{\perp}\left(\frac{1}{i\,(v.D) + 2m_Q - i\epsilon}\right)\not{D}^{\perp} h_v, \tag{2.19}$$

$$\Delta = \exp\left(\frac{1}{2}Tr\ln\left(i\,(v.D) + 2m_Q - i\epsilon\right)\right). \tag{2.20}$$

Expanding Eq.(2.20), one finds

$$\Delta = \exp\left(\frac{1}{2}Tr\ln\left(i\,(v.\partial) - g\,(v.A) + 2m_Q - i\epsilon\right)\right). \tag{2.21}$$

By choosing the axial gauge, $v.A = 0$, it is clear that Δ is a merely a constant and does not alter any time–ordered products involving the heavy quark fields.

The non–local term in Eq.(2.19) can be expanded in powers of $1/2m_Q$. It can be shown

$$\overline{h}_v \not{D}^{\perp}\not{D}^{\perp} h_v = \overline{h}_v D^{\mu} D^{\perp}_{\mu} h_v \ + \ \overline{h}_v \sigma_{\mu\nu} F^{\mu\nu} h_v \ . \tag{2.22}$$

These operators correspond to the kinetic and magnetic energies of the heavy quark. This becomes clear when the rest frame of the quark is chosen, where $\vec{v} = \vec{0}$. One finds

$$\frac{1}{2m_Q}\overline{h}_v D^\mu D^\perp_\mu h_v \quad \rightarrow \quad -\frac{1}{2m_Q}\overline{h}_v \left(i\vec{D}\right)^2 h_v, \tag{2.23}$$

$$\frac{g}{4m_Q}\overline{h}_v \sigma_{\mu\nu} F^{\mu\nu} h_v \quad \rightarrow \quad -\frac{g}{m_Q}\overline{h}_v \vec{S}.\vec{B}_c h_v, \tag{2.24}$$

where $\vec{S}$ is the spin of the heavy quark and $\vec{B}_c$ is the chromo–magnetic gluon field.

As demonstrated by Georgi [82], the choice of operators in any effective field theory can be reduced by using the equation of motion for the Lagrangian. In this case, the equation of motion satisfies

$$i\,(v.D)\,h_v = \mathcal{O}(\frac{1}{m_Q}). \tag{2.25}$$

As a result, to order $1/m_Q$, the operator $D^\perp_\mu$ can be replaced by D_μ. Hence the Lagrangian can be expressed as

$$\mathcal{L} = \mathcal{L}_{stat} \ + \ \mathcal{L}_1 \ + \ \mathcal{O}(\frac{1}{4m_Q^2})\ , \tag{2.26}$$

where $\mathcal{L}_{stat}$ is defined in Eq.(2.7) and

$$\mathcal{L}_1 \ = \ O_{kin} \ + \ O_{mag}\ , \tag{2.27}$$

$$O_{kin} \ = \ -\frac{1}{2m_Q}\overline{h}_v D^2 h_v\ , \tag{2.28}$$

$$O_{mag} \ = \ -\frac{g}{4m_Q}\overline{h}_v \sigma_{\mu\nu} F^{\mu\nu} h_v\ . \tag{2.29}$$

As outlined previously, the effect of short–distance processes are included by radiative corrections. As will be demonstrated, some of the operators in the theory have non–trivial corrections of order α_s. Others are "protected" from radiative corrections by the ambiguity that exists in describing the quark mass and the residual momentum k^μ. Furthermore, the difficulties that arise when

when using the pole mass definition of the quark will be outlined.

2.4 Corrections to HQET

2.4.1 Radiative Corrections

In order to match the HQET to full QCD, the Lagrangian of Eq.(2.26) must be rewritten as

$$\mathcal{L}_{match} = \mathcal{L}_{stat} + C_{kin}(\mu) O_{kin} + C_{mag}(\mu) O_{mag} + \mathcal{O}(\frac{1}{4m_Q^2}). \tag{2.30}$$

The coefficients $C_{kin}(\mu)$, $C_{mag}(\mu)$ match both theories at $\mu = m_Q$ and are run down to an arbitrary scale via the renormalisation group equation. It should be noted that any operator evaluated using HQET (for example, the current $\overline{h}_v^1 \gamma^\mu h_v^2$) will also require a radiative correction and that the overall wave function renormalisation term in the Lagrangian has been implicitly assumed.

These coefficients can be evaluated from the heavy quark gluon vertex function, using a background gluon field [83, 84]. In the leading logarithmic approximation, they have been determined to be [78, 79, 80, 72],

$$C_{kin}(\mu) = 1 \ , \tag{2.31}$$

$$C_{mag}(\mu) = \left(\frac{\alpha_s(m_Q)}{\alpha_s(\mu)}\right)^{-9/(33-2N_f)} , \tag{2.32}$$

where N_f is the number of quark flavours appropriate for the interval m_Q to μ. Interestingly enough, the perturbative result for $C_{kin}(\mu)$ can be extended to all orders. This occurs because the operators $\overline{h}_v i(v.D) h_v$ and O_{kin} must be combined to form a single operator, in order that the Lagrangian satisfy a condition referred to as "reparameterisation invariance" [85].

2.4.2 Reparameterisation Invariance

As outlined previously, one expects the residual momentum k^μ to be of the order of Λ_{QCD}. However, the full momentum of the quark could be defined in a number of ways, satisfying Eq.(2.3), i.e.

$$\begin{aligned} p^\mu &= m_Q v^\mu + k^\mu \\ &= m_Q w^\mu + r^\mu , \end{aligned} \tag{2.33}$$

where

$$\begin{aligned} w^\mu &= v^\mu + \frac{q^\mu}{m_Q} , \\ r^\mu &= k^\mu - q^\mu , \\ w^2 &= (v + \frac{q}{m_Q})^2 = v^2 = 1 . \end{aligned} \tag{2.34}$$

Any matrix element obtained from HQET will be invariant under this transformation, referred to as reparameterisation invariance, and explored by Luke and Manohar [85].

For simplicity, a scalar field ϕ coupled to gluons is considered,

$$\mathcal{L}_{scalar} = D_\mu \phi^* D^\mu \phi - m^2 \phi^* \phi. \tag{2.35}$$

As before, for large m, one can express $\phi(x)$ in terms of an effective heavy field $\phi_v(x)$,

$$\phi(x) = \frac{1}{\sqrt{2m}} e^{-imv.x} \phi_v(x) . \tag{2.36}$$

The effective Lagrangian to order $1/m$ for such a field is

$$\mathcal{L}_{eff} = \phi_v^* iv.D\phi_v + \frac{A}{2m} \phi_v^* D^2 \phi_v , \tag{2.37}$$

where A introduces radiative corrections relative to the static operator $\phi_v^* iv.D\phi_v$. Under the residual momentum transformation of Eq.(2.33) and Eq.(2.36), the field $\phi_v(x)$ can be expressed in terms of the field $\phi_w(x)$ as

$$\phi_v(x) = e^{-iq.x} \phi_w(x). \tag{2.38}$$

Substituting Eq.(2.38) into Eq.(2.37), one finds

$$\begin{aligned}\mathcal{L}_{eff} &= \phi_w^* v.(iD+q)\phi_w + \frac{A}{2m}\phi_w^*(D-iq)^2\phi_w \\ &= \phi_w^*(w-\frac{q}{m}).(iD+q)\phi_w + \frac{A}{2m}\phi_w^*(D-iq)^2\phi_w. \end{aligned} \tag{2.39}$$

Expanding in powers of q, one finds

$$\delta\mathcal{L}_{eff} = (A-1)\phi_w^*\frac{iq.D}{m}\phi_w \;+\; \mathcal{O}(q^2;1/m^2) \;, \tag{2.40}$$

where

$$q.w = \mathcal{O}(q^2/m) \;, \tag{2.41}$$

by Eq.(2.34). If $\delta\mathcal{L}_{eff}=0$ for infinitesimal q, then A is forced to be unity, i.e. the renormalisation coefficient of the operator $\phi_v^* D^2\phi_v$ must be the same as $\phi_v^* iv.D\phi_v$.

In general any Lagrangian involving heavy fields can be written in the form

$$\mathcal{L}_h = \mathcal{L}_h\left(\mathcal{H}_v, iD^\mu, v^\mu\right) \;, \tag{2.42}$$

where $\mathcal{H}_v$ is the set of heavy fields. By Eq.(2.33), this transforms to

$$\mathcal{L}_h \to \mathcal{L}_h\left(\mathcal{H}_w, iD^\mu + q^\mu, w^\mu - q^\mu/m\right) \;. \tag{2.43}$$

In order to maintain reparameterisation invariance, v^μ and iD^μ must appear in the form

$$\mathcal{V}^\mu = v^\mu + \frac{iD^\mu}{m} \;. \tag{2.44}$$

The specific case for spinor fields is more complicated, but the argument is essentially the same. Under the transformation Eq.(2.33), the heavy quark field $h_v(x)$ is related to the field $h_w(x)$ by

$$h_w(x) = e^{iq.x}\tilde{\Lambda}(w,p/m_Q)\tilde{\Lambda}^{-1}(v,p/m_Q)h_v(x) \;, \tag{2.45}$$

where $\tilde{\Lambda}(w,p/m_Q)$ is a Lorentz boost matrix in the spinor representation. Defining

$$\tilde{h}_v(x) = \tilde{\Lambda}(p/m_Q, v) h_v(x) \ , \tag{2.46}$$

implies

$$\tilde{h}_w(x) = e^{iq.x} \tilde{h}_v(x) \ . \tag{2.47}$$

To order $1/m_Q$, the Lorentz boost satisfies

$$\tilde{h}_v(x) = \left(1 + \frac{i \not{D}}{2m_Q}\right) h_v(x) \ . \tag{2.48}$$

Bilinears formed from these fields will be reparameterisation invariant. In particular, one finds $\bar{\tilde{h}}_v \left(\mathcal{V}^2 - 1\right) \tilde{h}$ is invariant. It can be shown that

$$\frac{m_Q}{2} \int d^4x \bar{\tilde{h}}_v \left(\mathcal{V}^2 - 1\right) \tilde{h} = \int d^4x \overline{h}_v \left(iv.D + \frac{(iD)^2}{2m_Q}\right) h_v + \mathcal{O}(\frac{1}{m_Q^2}) \ , \tag{2.49}$$

demonstrating that the renormalisation coefficient of $(iD)^2/2m_Q$ is the same as that of $iv.D$.

2.4.3 The residual mass term

In all calculations involving HQET, there remains a somewhat worrying question: as the heavy quark mass is a scheme-dependent quantity, which scheme is the correct one ? Intuitively, one would expect that the choice is irrelevant. On an order–by-order basis this is true. However there are certain subtleties that must be considered, especially in the non–perturbative case.

As before, the momentum of the heavy quark can be defined in terms of different residual momenta. In this case however, the mass of the heavy quark can be redefined, as opposed to the velocity.

$$\begin{aligned} p^\mu &= m_Q v^\mu + k^\mu \\ &= m'_Q v^\mu + k'^\mu \ , \end{aligned} \tag{2.50}$$

where

$$\begin{aligned} m'_Q &= m_Q - \delta m_Q \ , & (2.51) \\ k'^{\mu} &= k^{\mu} + \delta m_Q v^{\mu} \ . & (2.52) \end{aligned}$$

Once again, a new heavy quark field $h'_v(x)$ can be defined in terms of the the original field $h_v(x)$. Here $h'_v(x)$ differs from $h_v(x)$ by a simple phase factor

$$h'_v(x) = e^{-i\delta m_Q v.x} h_v(x) \ , \tag{2.53}$$

and the covariant derivative acting on $h_v(x)$ can be reexpressed as

$$\begin{aligned} iD^{\mu} h_v(x) &= e^{i\delta m_Q v.x} \left(iD^{\mu} - \delta m_Q v^{\mu} \right) h'_v(x) \\ &= e^{i\delta m_Q v.x} i\mathcal{D} h'_v(x) \ . \end{aligned} \tag{2.54}$$

Inserting Eq.(2.53) and Eq.(2.54) into Eq.(2.26), one finds

$$\begin{aligned} \mathcal{L}_{HQET} \rightarrow \overline{h'}_v iv.\mathcal{D} h'_v &- \delta m_Q \overline{h'}_v h'_v - \frac{1}{2m'_Q} \overline{h'}_v (i\mathcal{D})^2 h'_v \\ &- \frac{g}{4m'_Q} \overline{h'}_v \sigma_{\mu\nu} F^{\mu\nu} h'_v + \mathcal{O}(\frac{1}{4m'^2_Q}) \ , \end{aligned} \tag{2.55}$$

introducing a small contact term in the Lagrangian.

Typically, the pole mass of the heavy quark, defined perturbatively, is used as the expansion parameter[2] and, by the intuitive arguments above, the residual mass term is set to zero. However, as demonstrated by Bigi *et al.* [87], such a definition has a systematic uncertainty of order Λ_{QCD}. This is due to long–distance effects in the perturbative calculation of the self–energy of the quark. By evaluating diagrams of the form shown in Fig.(2.1), it is claimed that

---

[2]HQET has also been formulated in terms of the running mass $m_Q^{\overline{MS}}$[86], however the constraint of Eq.(2.3) is altered to $k^{\mu} = \mathcal{O}(\alpha_s(m_Q) m_Q)$.

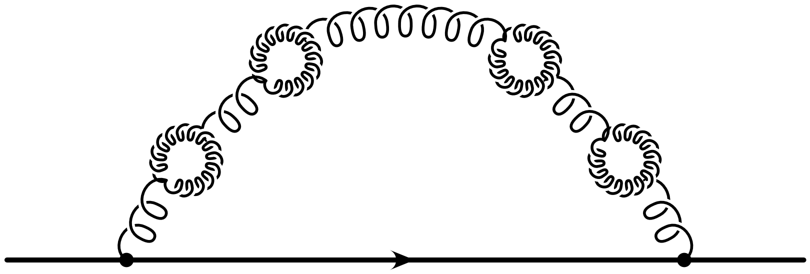

Figure 2.1: An example of a diagram contributing to the poor long distance behaviour of m_Q^{pole}.

$$m_Q^{pole} - m_Q(\mu) = \frac{4\alpha_s(\mu)}{3\pi}\mu \sum_n C_n \left(\frac{b\alpha_s(\mu)}{4\pi}\right)^n \ , \tag{2.56}$$

where $m_Q(\mu)$ is the running quark mass defined at some scale μ, b is the first coefficient in the Gell–Mann–Low function and

$$C_n = \int_0^1 dx \left(\ln\frac{1}{x^2}\right)^n \ , \tag{2.57}$$

which for large n grows factorially

$$C_n \underset{n\to\infty}{\longrightarrow} 2^n n! \ . \tag{2.58}$$

This series is divergent, and one is forced to truncate it, introducing the systematic uncertainty between $m_Q(\mu)$, which is well defined, and m_Q^{pole}, which is only defined in a perturbative sense.

As a result, the term δm_Q must be included in the Lagrangian. Fortunately, as demonstrated by Falk *et al.* [88], the addition of the residual mass term does not affect physical quantities calculated in the physical theory to order $1/m_Q$.

An example of how HQET can be implemented is now outlined.

2.5 Heavy Hadron Spectroscopy

In the static limit of HQET, the interpretation of hadron masses is quite clear. One can divide the mass of an arbitrary hadron into the mass of the heavy quark and the binding energy of the light degrees of freedom, that is

$$m_H^{static} = m_Q + \overline{\Lambda}_H \ . \tag{2.59}$$

By translational invariance, it can be shown that [89]

$$\langle 0 \left| O(x) \right| H(v) \rangle = e^{-i\overline{\Lambda}_H v.x} \langle 0 \left| O(0) \right| H(v) \rangle \ , \tag{2.60}$$

where $O(x)$ is the relevant operator to annihilate the heavy hadronic state $|H\rangle$. Hence, $\overline{\Lambda}_H$ can be defined as [90]

$$\overline{\Lambda}_H = \frac{\langle 0 \left| iv.\partial(O(x)) \right| H(v) \rangle}{\langle 0 \left| O(x) \right| H(v) \rangle} \ . \tag{2.61}$$

The corrections of order $1/m_Q$ can be seen as the extra energy the heavy quark acquires due to the kinetic energy from the light degrees of freedom and its spin coupling to the chromo–magnetic field. The mass is therefore written as

$$m_H = m_Q + \overline{\Lambda_H} + \frac{\Delta m_H^2}{2m_Q} + \mathcal{O}(\frac{1}{4m_Q^2}) \ , \tag{2.62}$$

where

$$\Delta m_H^2 = \frac{\langle H(v) \left| (-\mathcal{L}_1) \right| H(v) \rangle}{\left\langle H(v) \left| \overline{h}_v h_v \right| H(v) \right\rangle} \ . \tag{2.63}$$

Defining

$$\left\langle H(v) \left| \overline{h}_v D^2 h_v \right| H(v) \right\rangle = -2 m_H \lambda_1^H \ , \tag{2.64}$$

$$\left\langle H(v) \left| \overline{h}_v \frac{g}{2} \sigma_{\mu\nu} F^{\mu\nu} h_v \right| H(v) \right\rangle = -2 d_H m_H \lambda_2^H \ , \tag{2.65}$$

where, in the rest frame of the meson,

$$d_h = \langle \vec{s}_Q . \vec{s}_l \rangle \ , \tag{2.66}$$

and $\vec{s}_Q$ and $\vec{s}_l$ are the spins of the heavy quark and the light degrees of freedom respectively, and noting that in the rest frame of the meson

$$\left\langle H(v) \left| \overline{h}_v h_v \right| H(v) \right\rangle = 2m_H \ , \tag{2.67}$$

implies that

$$\Delta m_H^2 = -\lambda_1^H - C_{mag}(\mu) d_H \lambda_2^H \ . \tag{2.68}$$

In the case of the pseudoscalar and vector mesons, it can be shown that $d_H = 3$ and -1 respectively. For the simplest baryon Λ_Q, where the spin is carried entirely by the heavy quark, $d_H = 0$. Hence one can write these masses as

$$m_P = m_Q + \overline{\Lambda}_m + \frac{1}{2m_Q}(\lambda_1^m + 3C_{mag}(\mu)\lambda_2^m) + \mathcal{O}(\frac{1}{4m_Q^2}) \ , \tag{2.69}$$

$$m_V = m_Q + \overline{\Lambda}_m + \frac{1}{2m_Q}(\lambda_1^m - C_{mag}(\mu)\lambda_2^m) + \mathcal{O}(\frac{1}{4m_Q^2}) \ , \tag{2.70}$$

$$m_\Lambda = m_Q + \overline{\Lambda}_b + \frac{\lambda_1^b}{2m_Q} + \mathcal{O}(\frac{1}{4m_Q^2}) \ . \tag{2.71}$$

HQET introduces into the QCD Lagrangian the dynamics of the heavy quark on an order–by–order basis. However, it does not provide any indication of the size of the interaction of the light degrees of freedom at each order. For example, in this case HQET can not tell us anything about the size of the parameters λ_1^m, λ_2^m etc. These parameters must be determined non–perturbatively and will be discussed in the following chapter.

Chapter 3

Heavy Hadron Mass Splittings on the Lattice

3.1 Heavy Baryon Masses

The simulation of heavy–light mesons using lattice field theory techniques has been widely explored with the fermionic actions described in chapter 1. From the study of two–point mesonic functions, the decay constants f_B and f_D and a spectrum of masses and hyperfine splittings has been evaluated. Their study has also been crucial in simulations of semi–leptonic and radiative decays of B and D mesons. This shall be discussed in greater detail in chapter 4. The exploration of heavy–light baryons has been far less detailed [91, 92, 93]. This is primarily due to the fact that light baryons have far noisier signals than lighter mesons on the lattice and has been more susceptible to finite–size effects [94]. Nevertheless, as there is little experimental data for bottom baryon masses, the evaluation of these masses from lattice field theory would provide useful information. This would also lead on to the examination of heavy baryon decays such as $\Lambda_b \to \Lambda_c e\nu$ and $\Lambda_b \to \Xi_c e\nu$. HQET predicts that such decays would be determined by the baryonic Isgur–Wise function $\zeta(v.v')$, in the same way as heavy to heavy transitions in mesons are parametrised by the Isgur–Wise function $\xi(v.v')$ [72].

The simulation of heavy–light baryons may also be used to test algorithms for improving the signal for light baryons. The usual operators chosen for creating and annihilating heavy and light baryonic states have a large overlap with many states. If the operators for isolating heavy states can be optimised, then it is possible that those methods can be applied to light baryons.

An initial analysis is carried out by simulating the simplest heavy baryon, Λ_Q, where $I(J)^P = 0(1/2)^+$. As outlined previously in chapter 1, bare quark masses whose mass is approximately equal to the bottom quark mass, m_b, cannot be simulated using the SW action with the lattice spacing used in this thesis. One can however, simulate a number of quark masses in the region of the charm quark mass, m_c, and extrapolate the result to m_b, using a physical quantity, for example the mass of the B meson, m_B and the lattice spacing a.

As outlined in chapter 2, the mass of heavy–light hadrons can be expressed as a power series in the inverse heavy quark mass $1/m_Q$. The coefficients can be identified with the expectation values of physically meaningful observables, which can provide information about the behaviour of the heavy quark within the hadron. By calculating the mass splittings of hadrons, one obtains parameters whose behaviour is well defined in the static limit, and is the optimal method for extrapolating these masses to the bottom quark regime.

From chapter 2, it is clear that[1]

$$m_\Lambda - m_P = \overline{\Lambda}_b - \overline{\Lambda}_m - \frac{\lambda_1^b - \lambda_1^m - 3\lambda_2^m}{2m_Q} + \mathcal{O}(\frac{1}{m_Q^2}), \quad (3.1)$$

$$m_\Lambda - \frac{1}{4}(m_P + 3m_V) = \overline{\Lambda}_b - \overline{\Lambda}_m - \frac{\lambda_1^b - \lambda_1^m}{2m_Q} + \mathcal{O}(\frac{1}{m_Q^2}), \quad (3.2)$$

where m_P, m_V and m_Λ are the masses of the heavy–light pseudoscalar and vector mesons and Λ_Q. One therefore expects the following qualitative behaviour for a measurement of Eq.(3.1) and Eq.(3.2) on the lattice using a number of different quark masses. In the first instance, it is expected that both functions should behave linearly in $1/m_Q$ for sufficiently heavy quark masses. Furthermore, the slope of the "weighted" difference in Eq.(3.2) might be smaller than the "simple" difference of Eq.(3.1). Finally, one expects

$$\frac{m_\Lambda - m_P}{m_\Lambda - 1/4(m_P + 3m_V)} \underset{m_Q \to \infty}{\to} 1. \quad (3.3)$$

[1]Radiative corrections have been discarded as the statistical error is too large.

These relationships will now be tested.

3.2 Computational Details

Forty–four $SU(3)$ gauge configurations were generated in the quenched approximation for a $24^3 \times 48$ lattice at $\beta = 6.2$. These configurations were generated with periodic boundary conditions using the hybrid over-relaxed algorithm, and the standard discretised gluon action, defined in [95]. The configurations were separated by 2400 sweeps, starting at sweep number 16800. The inverse lattice spacing was determined to be 2.73(5) GeV, by evaluating the string tension [96]. In physical units, this corresponds to a spacing of approximately 0.07 fm and a spatial size of 1.68 fm. The quark propagators were evaluated from the SW action [39], using the over–relaxed minimal residual algorithm with red–black preconditioning for $\kappa = 0.14144$, 0.14226 and 0.14262; and 0.133, 0.129, 0.125 and 0.121 using periodic boundary conditions in the spatial directions and anti–periodic boundary conditions in the temporal direction. The first three κ values correspond to quark masses in the region of the strange quark mass, allowing for an extrapolation to the zero–light–quark mass (chiral) limit. The other four κ values correspond to heavy quark masses, ranging from approximately 1.48 GeV to 2.40 GeV.

As detailed in chapter 1, two–point functions for each of these hadrons can be defined as

$$\begin{aligned} C_P(t) &= \sum_{\vec{x}} \langle J_P^\dagger(t,\vec{x}) J_P(0) \rangle \\ &\underset{t,T\to\infty}{\longrightarrow} \frac{Z_P^2}{2E_P}\left(e^{-E_P t} + e^{-E_P(T-t)}\right), \qquad (3.4) \\ C_V(t) &= -\left(\frac{1}{3}\right) \sum_{\vec{x}} \langle J_{V\sigma}^\dagger(t,\vec{x}) J_V^\sigma(0) \rangle \\ &\underset{t,T\to\infty}{\longrightarrow} \frac{Z_V^2}{2E_V}\left(e^{-E_V t} + e^{-E_V(T-t)}\right), \qquad (3.5) \end{aligned}$$

$$\begin{aligned} C_\Lambda^{\alpha\beta}(t) &= \sum_{\vec{x}} \langle \overline{J_\Lambda^\alpha}(t,\vec{x}) J_\Lambda^\beta(0) \rangle \\ &\xrightarrow[t,T\to\infty]{} \frac{Z_\Lambda^{\alpha\beta^2}}{2E_\Lambda} \left(e^{-E_\Lambda t} + e^{-E_\Lambda (T-t)} \right). \end{aligned} \tag{3.6}$$

These operators are defined as

$$J_P(t,\vec{x}) = \sum_{\vec{y}} Tr \left(f(t,\vec{x};\vec{y})\, \bar{l}(x) \gamma_5 h(t,\vec{y}) \right), \tag{3.7}$$

$$J_\rho^V(t,\vec{x}) = \sum_{\vec{y}} Tr \left(f(t,\vec{x};\vec{y})\, \bar{l}(x) \gamma_\rho h(t,\vec{y}) \right), \tag{3.8}$$

$$J_\Lambda^\alpha(t,\vec{x}) = \sum_{\vec{y}} \varepsilon^{abc} f(t,\vec{x};\vec{y})\, h_a^\alpha(t,\vec{y}) l_b^\mu(x) \left(C\gamma_5 \right)_{\mu\nu} l_c^\nu(x), \tag{3.9}$$

where the trace is carried out over spin and colour indices. The smearing function $f(t,\vec{x};\vec{y})$ is either

$$f(t,\vec{x};\vec{y}) = \delta^3_{\vec{x},\vec{y}}, \tag{3.10}$$

or is spatially extended by the gauge–invariant Jacobi algorithm [66], with an r.m.s. smearing radius of 5.2. The operators J_P, J_V and J_Λ^α were calculated using the latter smearing function at $t = 0$. The operators $J_P^\dagger$, $J_V^\dagger$ and $\overline{J_\Lambda^\alpha}$ were calculated using both smearing functions for $t > 0$. The resulting correlators are referred to as smeared–local (SL) and smeared–smeared (SS) respectively.

The signal of the two–point functions was improved by considering the behaviour of the correlators under the discrete symmetries C and P. As outlined by Bernard [97], a quark propagator $Q(x,y;U)$, evaluated on the lattice for some gauge configuration U, satisfies the following equations under the operation of C and P

$$P : Q(x,y;U) = \gamma^0 Q(x^P, y^P; U^P) \gamma^0, \tag{3.11}$$

$$C : Q(x,y;U) = \mathcal{C} Q(x^P, y^P; U^P) \mathcal{C}^{-1}, \tag{3.12}$$

where $\mathcal{C} = \gamma^0\gamma^2$. As the masses obtained will be invariant under these operations, one can consider the average of an arbitrary correlator C_{2pt}

$$C_{2pt} = \frac{1}{4}\left(C^I_{2pt} + C^P_{2pt} + C^C_{2pt} + C^{PC}_{2pt}\right), \tag{3.13}$$

where I is the identity transformation. Each of the transformed correlators can be related to C^I_{2pt} by inserting Eq.(3.11) and Eq.(3.12) into Eq.(3.4), Eq.(3.5) and Eq.(3.6). In the case of $C_P(t)$, $C_V(t)$ and $C_\Lambda(t)$, this average is equal to the real component of $C^I_P(t)$, $C^I_V(t)$ and $C^I_\Lambda(t)$, respectively[2].

The symmetric behaviour of the correlators around $t = T/2$ was also used to improve the signal for the analysis. In the case of the mesons, $C_P(t)$ and $C_V(t)$, for $t < T/2$ were averaged with $C_P(T-t)$ and $C_V(T-t)$[3]. In order to isolate the forward and backward propagating states in $0 < t < T/2$ and $T/2 \leq t < T$ for $C^{\alpha\beta}_\Lambda(t)$, the average

$$C_\Lambda(t) = \frac{1}{2}\left(I + \gamma^0\right)_{\alpha\beta} C^{\beta\alpha}_\Lambda(t) + \frac{1}{2}\left(I - \gamma^0\right)_{\alpha\beta} C^{\beta\alpha}_\Lambda(T-t). \tag{3.14}$$

was evaluated.

3.3 Analysis

3.3.1 Optimisation of fit range

Having calculated a statistical ensemble for the two–point functions of the heavy–light mesons and the baryon Λ_Q, one can obtain the masses by fitting the data to the functions Eq.(3.4), Eq.(3.5) and Eq.(3.6). However, it is not *a priori* clear what range of time–slices this data should be fitted to. Clearly, as these equations are satisfied asymptotically, a lower bound is $\inf(t_{min}) = 1/m$. As $ma > 0.5$, one can assume $\inf(t_{min}/a) = 4$. However, excited states can still make a significant contribution. For example, a single excited state with an energy 1 GeV greater

[2] This relation is more generalised for non–zero momenta, where for each of the three correlators, the average implies $\sum_{\vec{x}} \cos(\vec{p}\cdot\vec{x})\langle J^\dagger(x)J(0)\rangle$ is required.

[3] The contribution of the current $J^0_V(x)$ to $C_V(t)$ was discarded as this component is zero due to polarisation vector decomposition.

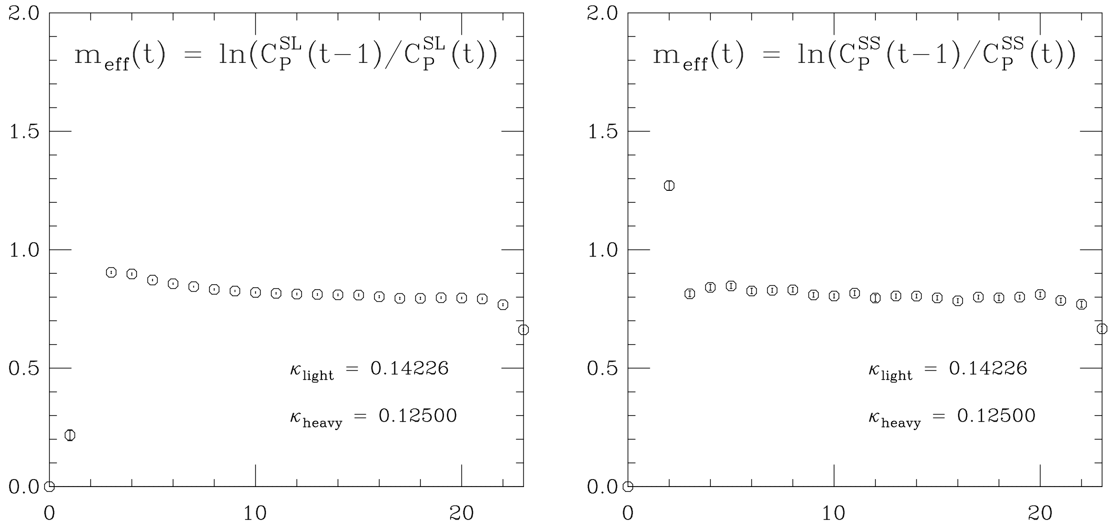

Figure 3.1: An example of effective mass plots for the pseudoscalar two–point function using local and smeared operators at the sink.

than the ground state energy will still make the correlator vary by greater than 2% at time–slice 10 for a lattice with this spacing – assuming the amplitudes of both states are equal to each other.

A direct method for estimating the range of time–slices is to calculate the effective mass $m_{eff}(t)$, defined as

$$m_{eff}(t) = \ln \frac{C(t-1)}{C(t)}, \tag{3.15}$$

where $C(t)$ is an arbitrary correlator. Given the general asymptotic form of the two–point functions, it is clear that for $1/(m_1 - m_0) \ll t \ll T/2$, where m_1 and m_0 are respectively the first excited and ground states of the hadron, Eq.(3.15) will isolate the ground–state mass. Any systematic variation from a constant will indicate excited state contamination for small t and a reduction of the SNR for large t.

The effective mass was determined for each two–point function with each

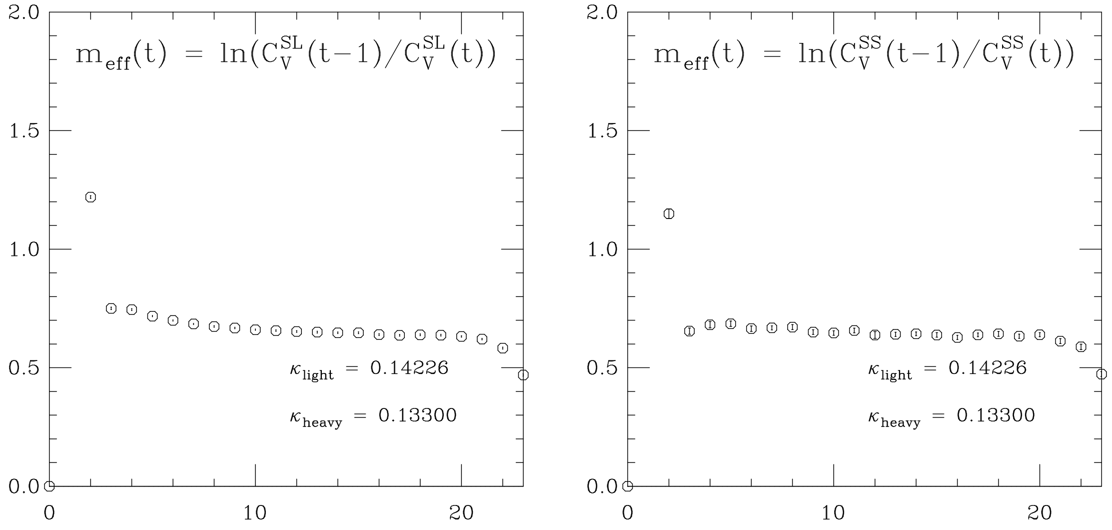

Figure 3.2: An example of effective mass plots for the vector two–point function using local and smeared operators at the sink.

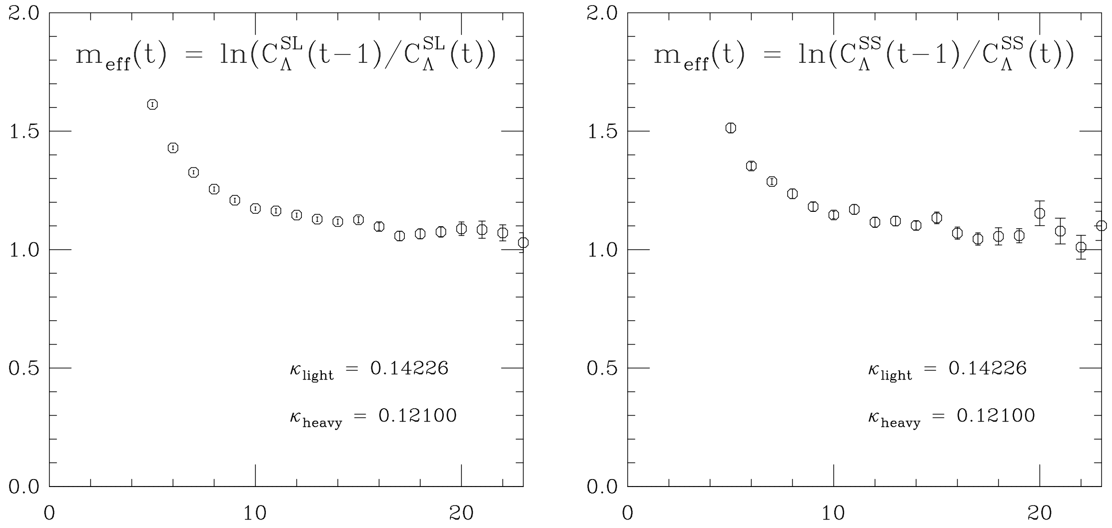

Figure 3.3: An example of effective mass plots for the two–point function $C_\Lambda(t)$ using local and smeared operators at the sink.

combination of κ and for spatially and non-spatially extended operators at the sink. Examples of these plots are shown in Fig.(3.1) to Fig.(3.3), where the errors have been calculated by the jack knife method [99].

The use of smeared operators at the sink ensured that a plateau occurs significantly earlier for both mesons. However, the error associated with each time–slice is increased substantially.

On the other hand, the use of smeared operators did not eliminate excited state contributions for the baryon. This indicates that the choice of smearing function for J_Λ was not optimal. From HQET, a heuristic picture of such a system is a point–like heavy quark, moving at constant velocity, with light quarks distributed around it. However, in this analysis, the heavy quark field was spatially extended and the light diquark pair was point–like. Improved signals for baryon correlators using smeared light propagators has been verified by Borelli *et al.* [93] and preliminary results by Maclean *et al.* [92].

While the effective mass plot gives an indication of the appropriate fit range, the backward propagating state gives increasingly large contributions as $t \to T/2$, which will vary considerably the effective mass. Hence more subtle criteria were chosen to determine the optimal fit range. It was assumed that the best fit is obtained by maximising the interval $t_{max} - t_{min}$, where $t_{min(max)}$ is the minimum (maximum) time–slice of the fit. This range was also chosen so that the χ^2 per degree of freedom (d.o.f.) was as small as possible. Finally, as it assumed that t_{min} lies in the region where higher states are sufficiently suppressed, the resulting mass must not change by more than one standard deviation as t_{min} is increased.

As a result, for each possible correlator, t_{max} was varied from time–slice 20, where the backward propagating state made a contribution of less than 2% to time–slice 23. The minimum time–slice, t_{min} was varied from 10 to $t_{max} - 2$. A fit to the appropriate function for each hadron was carried out from t_{min} to t_{max}. Correlations between different time–slices were included in the fit. Errors were determined using the bootstrap algorithm [99], with 250 bootstrap subsamples of the configurations. Examples of the resulting masses and χ^2/d.o.f. as t_{min} is varied are shown in Fig.(3.4) to Fig.(3.6).

Hadron	Source operator	Sink operator	Fit range
P	Smeared	Local	16–22
V	Smeared	Local	17–22
Λ_Q	Smeared	Local	16–22

Table 3.1: Best fit parameters for hadrons.

For local operators at the sink, χ^2/d.o.f. decreases sharply from time–slice 10 to approximately time–slice 15, and remains approximately equal to 1. For smeared operators at the sink χ^2/d.o.f. remains approximately constant for all t_{min}. If $t_{max} = 23$ however, χ^2/d.o.f. increases noticeably as $t_{min} \to 21$, for all three hadron correlators, indicating that the SNR decreased significantly at this time–slice. An example of this behaviour is shown in Fig.(3.7). Using these criteria, the masses were determined from the parameters in Table 3.1.

As the “light” quarks simulated have masses approximately equal to the strange mass, the masses obtained were extrapolated to the chiral limit. This extrapolation, and the behaviour of the resulting mass differences is explored in the following sections.

3.3.2 Chiral extrapolation

Using the time–slice ranges in Table 3.1, the correlators were again fitted to the appropriate asymptotic function. For a given hadron and fixed heavy–quark mass (heavy κ value), the three correlators of the light quark masses, i.e. $\kappa_l = 0.14144$, 0.14226 and 0.14262, were simultaneously fitted; correlations between different time–slices and different light κ values were included in the fit. The bootstrap algorithm was used, using 1000 subsamples of the configurations. The resulting masses are shown in Table 3.2. For each heavy quark mass, the hadron masses were extrapolated to the zero light quark mass limit by linear extrapolation. The

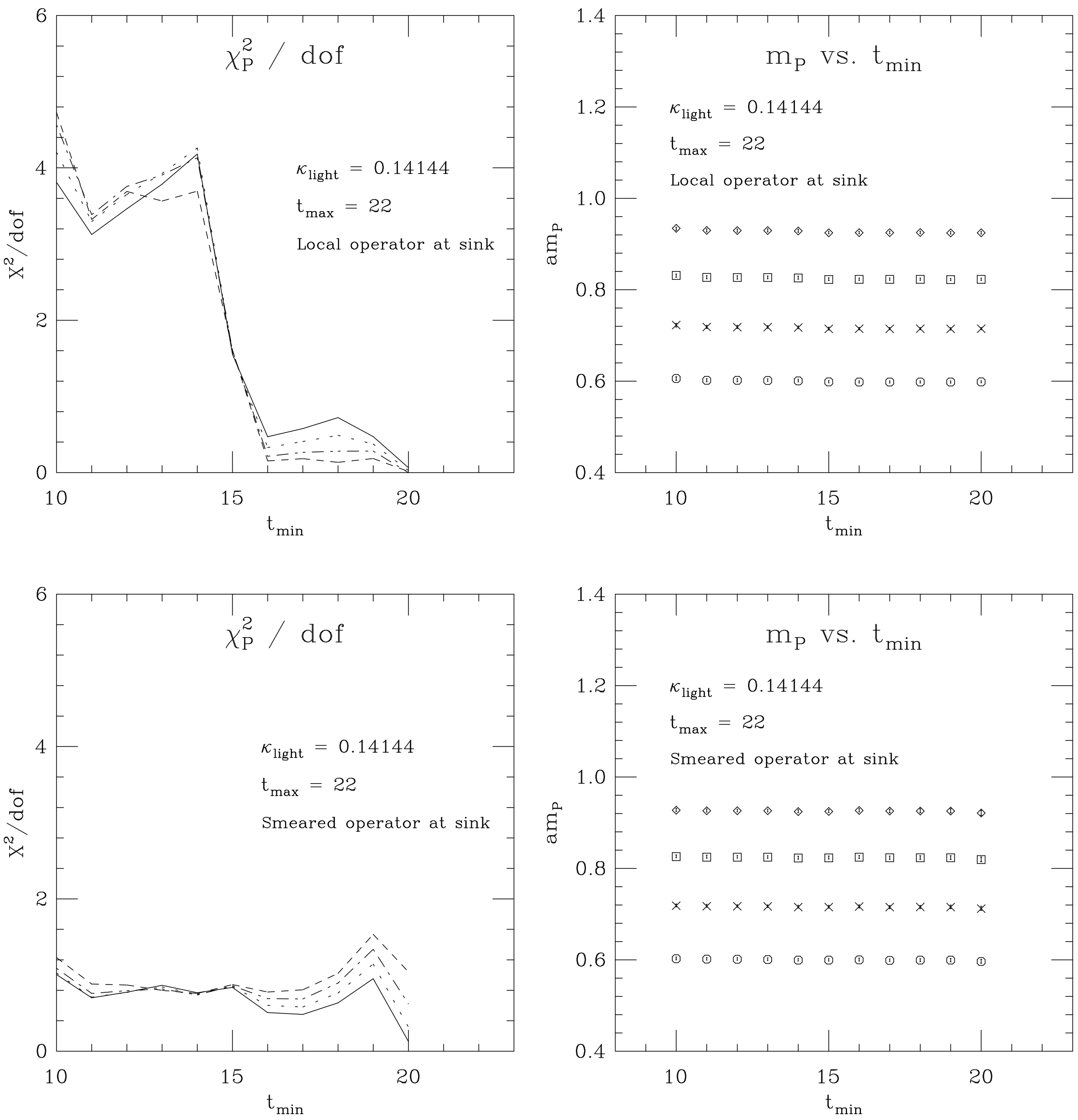

Figure 3.4: An example of χ^2/d.o.f. and the best mass for a pseudoscalar correlator, using local and smeared operators at the sink, as a function of the minimum time–slice for a fixed maximum time–slice. The different line styles and plotting symbols indicate different heavy quark masses.

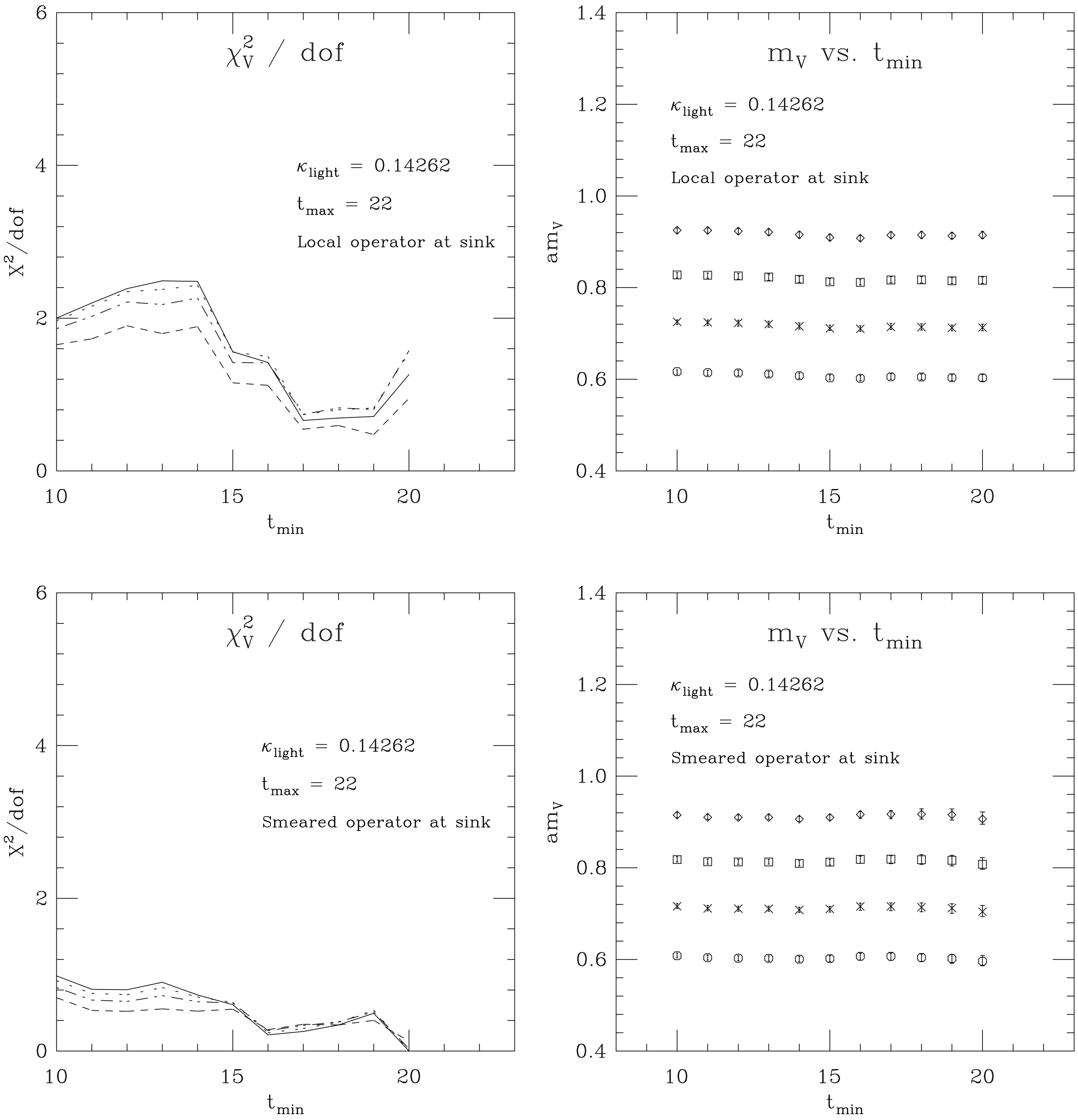

Figure 3.5: An example of χ^2/d.o.f. and the best mass for a vector correlator, using local and smeared operators at the sink, as a function of the minimum time–slice for a fixed maximum time–slice. The different line styles and plotting symbols indicate different heavy quark masses.

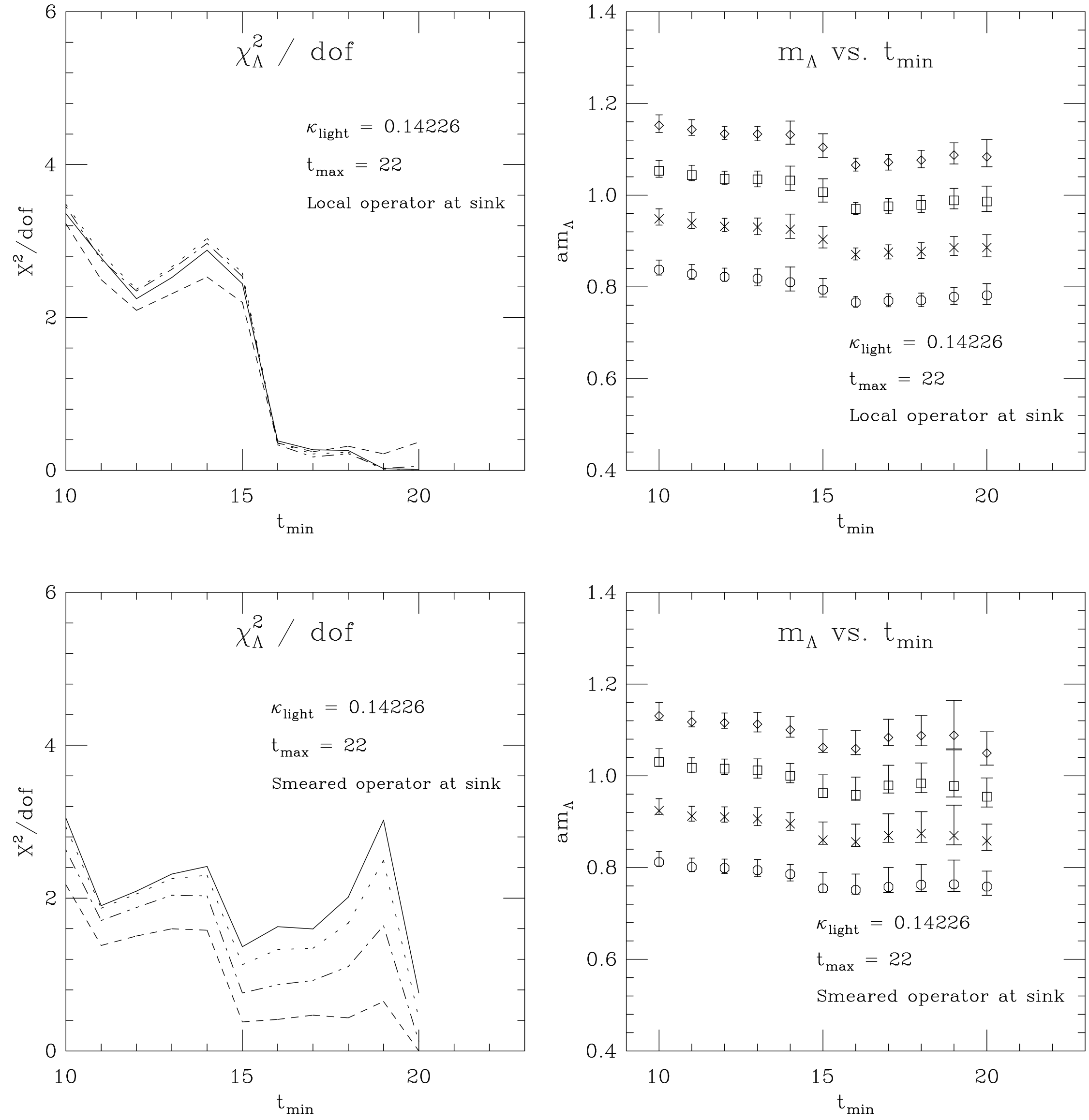

Figure 3.6: An example of χ^2/d.o.f. and the best mass for the correlator $C_\Lambda(t)$, using local and smeared operators at the sink, as a function of the minimum time–slice for a fixed maximum time–slice. The different line styles and plotting symbols indicate different heavy quark masses.

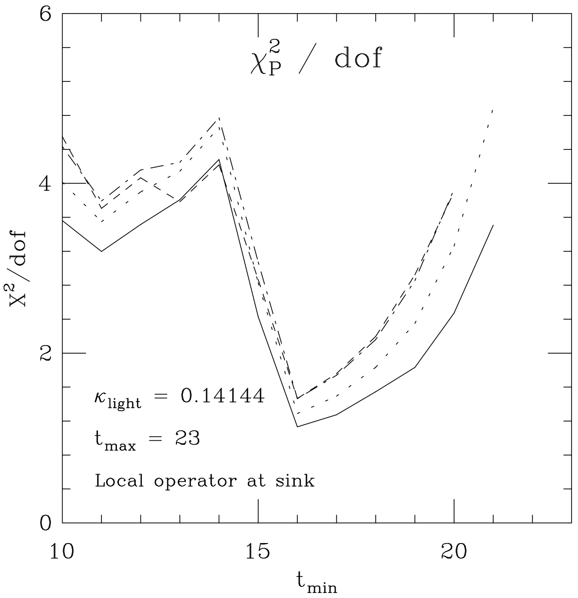

Figure 3.7: An example of the behaviour of χ^2/d.o.f. as a function of the minimum time–slice range, if the maximum time–slice is 23. The different line styles indicate different heavy quark masses.

masses were fitted to the function

$$m_P(\kappa_h; m_l) = m_P(\kappa_h) + b_P(\kappa_h)m_l \quad , \tag{3.16}$$

$$m_V(\kappa_h; m_l) = m_V(\kappa_h) + b_V(\kappa_h)m_l \quad , \tag{3.17}$$

$$m_\Lambda(\kappa_h; m_l) = m_\Lambda(\kappa_h) + b_\Lambda(\kappa_h)m_l \quad , \tag{3.18}$$

where $\kappa_h = 0.121,\ 0.125,\ 0.129$ and 0.133 and m_l is the pole mass of the light quark, defined as

$$m_l = \frac{1}{2}\left(\frac{1}{\kappa_l} - \frac{1}{\kappa_{crit}}\right), \tag{3.19}$$

The parameter κ_{crit} is determined by extrapolating the pion mass to zero. For this lattice $\kappa_{crit} = 0.14315(2)$ [100]. The bootstrap subsamples for each mass were used to obtain the covariance matrix allowing for correlations between the different light κ values. Examples of these fits are shown in Fig.(3.8), and Fig.(3.9). The resulting masses are shown in Table 3.3.

κ_h	κ_l	$m_P a$	χ^2_P/d.o.f.	$m_V a$	χ^2_V/d.o.f.	$m_\Lambda a$	χ^2_Λ/d.o.f.
0.121	0.14144	0.927^{+5}_{-3}	24.6/15	0.947^{+5}_{-3}	11.2/12	1.141^{+14}_{-9}	24.4/15
0.121	0.14226	0.901^{+7}_{-4}		0.923^{+8}_{-5}		1.070^{+22}_{-17}	
0.121	0.14262	0.888^{+9}_{-6}		0.912^{+11}_{-7}		1.011^{+30}_{-21}	
0.125	0.14144	0.826^{+5}_{-3}	25.1/15	0.849^{+5}_{-3}	11.1/12	1.042^{+13}_{-9}	23.3/15
0.125	0.14226	0.800^{+7}_{-4}		0.826^{+7}_{-5}		0.972^{+20}_{-15}	
0.125	0.14262	0.788^{+8}_{-6}		0.816^{+11}_{-7}		0.913^{+34}_{-19}	
0.129	0.14144	0.718^{+5}_{-3}	26.4/15	0.747^{+5}_{-4}	11.5/12	0.941^{+11}_{-8}	22.4/15
0.129	0.14226	0.692^{+6}_{-4}		0.725^{+7}_{-5}		0.873^{+20}_{-16}	
0.129	0.14262	0.680^{+7}_{-6}		0.716^{+10}_{-7}		0.816^{+34}_{-20}	
0.133	0.14144	0.601^{+4}_{-3}	29.5/15	0.639^{+4}_{-4}	12.4/12	0.836^{+10}_{-9}	22.6/15
0.133	0.14226	0.574^{+5}_{-4}		0.616^{+6}_{-6}		0.771^{+18}_{-17}	
0.133	0.14262	0.562^{+7}_{-5}		0.607^{+8}_{-8}		0.719^{+30}_{-25}	

Table 3.2: Masses obtained from simultaneous fit.

κ_h	Hadron	$m_H(\kappa_h)\,a$	$b_H(\kappa_h)$	χ^2/d.o.f.
0.12100	P	0.878^{+7}_{-5}	1.18^{+6}_{-7}	0.88
	V	0.902^{+7}_{-6}	1.09^{+9}_{-10}	0.27
	Λ_Q	0.996^{+30}_{-27}	3.35^{+51}_{-41}	7.08
0.12500	P	0.774^{+7}_{-5}	1.28^{+11}_{-12}	0.56
	V	0.803^{+7}_{-6}	1.10^{+10}_{-10}	0.02
	Λ_Q	0.917^{+26}_{-27}	3.06^{+51}_{-36}	6.69
0.12900	P	0.667^{+10}_{-9}	1.26^{+9}_{-9}	2.76
	V	0.700^{+7}_{-7}	1.11^{+10}_{-9}	0.03
	Λ_Q	0.819^{+25}_{-28}	2.88^{+54}_{-41}	5.84
0.13300	P	0.544^{+6}_{-5}	1.35^{+6}_{-7}	0.003
	V	0.591^{+6}_{-7}	1.13^{+11}_{-8}	0.05
	Λ_Q	0.715^{+25}_{-29}	2.83^{+58}_{-44}	3.44

Table 3.3: Masses obtained from extrapolations.

3.3.3 Extrapolation of mass differences to B and D

The mass differences of Eq.(3.1) and Eq.(3.2) were evaluated for each heavy quark mass. The pole mass m_Q is taken to be approximately equal to $1/4(m_P + 3m_V)$. From chapter 2, it is clear that

$$\frac{4}{m_P + 3m_V} = \frac{1}{m_Q} - \frac{1}{m_Q}\frac{\overline{\Lambda}_m}{m_Q} + \mathcal{O}\left(\frac{1}{m_Q^3}\right). \tag{3.20}$$

Hence, in the linear approximation of Eq.(3.1) and Eq.(3.2), the choice of $4/(m_P + 3m_V)$ is an adequate one.

Both mass differences and the ratio in Eq.(3.3) were linearly fitted to $4/(m_P + 3m_V)$, using the bootstrap subsamples from the chiral extrapolations of the masses to determine the covariance matrix. The final fits are shown in Fig.(3.10) and Fig.(3.11).

The fit parameters for the mass differences are shown in Table 3.4. Using these fit parameters allows a comparison with experimental data, where[4]

$$\begin{aligned}\frac{1}{4}(m_D + 3m_{D^*}) &= 1.9731 \pm 0.0005\,\mathrm{GeV},\\ \frac{1}{4}(m_B + 3m_{B^*}) &= 5.3134 \pm 0.0020\,\mathrm{GeV}.\end{aligned} \tag{3.21}$$

As demonstrated in Table 3.4, the calculated value of these differences at the charm quark mass is consistent with experimental data to within one standard deviation. At the bottom quark mass, the calculated value is consistent to within two standard deviations. It is also noted that the intercept for both differences are in agreement with each other to within one standard deviation. However, both intercepts are also consistent with zero, which is not confirmed by experimental data. Despite large errors, the slope of the "weighted" difference is less than the slope of the "simple" difference.

[4] In order to eliminate isospin splitting, masses were averaged over different charge combinations.

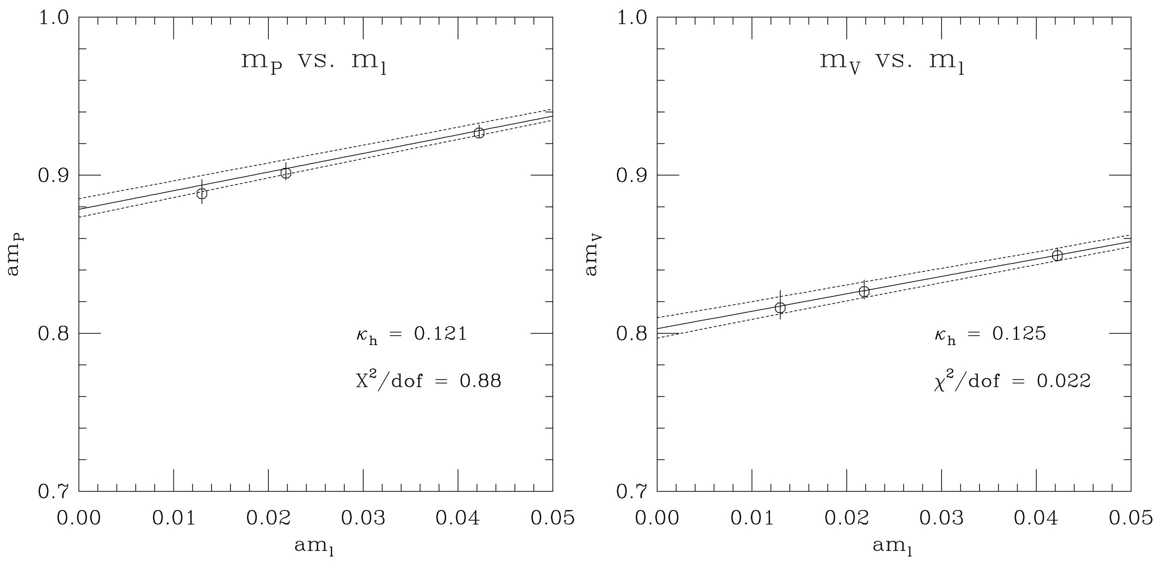

Figure 3.8: An example of chiral extrapolations of the pseudoscalar and vector masses. The dotted lines indicate 68% confidence levels of the fit.

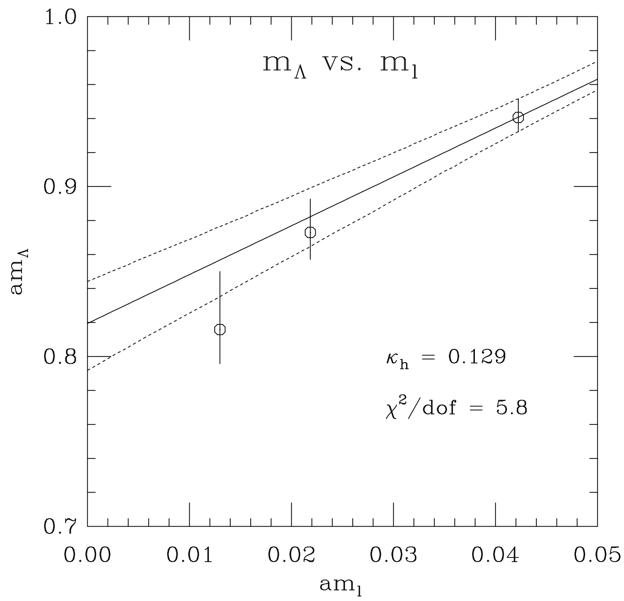

Figure 3.9: An example of chiral extrapolations of m_Λ. The dotted lines indicate 68% confidence levels of the fit.

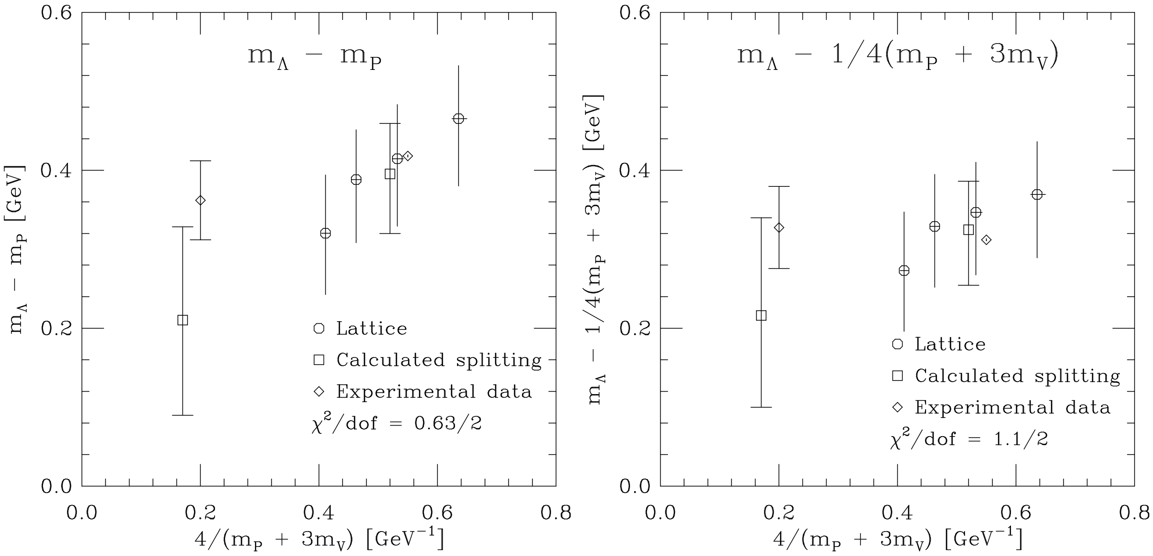

Figure 3.10: Linear extrapolation of mass differences. The statistical errors for the fit include the error due to the lattice spacing. The calculated and experimental point for b and c are slightly displaced for clarity.

The intercept from the linear fit to the ratio is $0.98\,^{+17}_{-16}$. As demonstrated in Eq.(3.3), this is consistent with the predicted behaviour from HQET.

	$m_\Lambda - m_P$	$m_\Lambda - \frac{1}{4}(m_P + 3m_V)$
Intercept [GeV]	$0.10\,^{+18}_{-16}$	$0.15\,^{+17}_{-15}$
Slope [GeV^2]	$0.58\,^{+25}_{-32}$	$0.34\,^{+25}_{-31}$
B (Calculated) [GeV]	$0.21\,^{+\,12}_{-\,12}$	$0.22\,^{+12}_{-12}$
B(Experimental) [GeV]	0.362 ± 0.050	0.328 ± 0.052
D (Calculated) [GeV]	$0.40\,^{+\,6}_{-\,8}$	$0.33\,^{+\,6}_{-\,7}$
D(Experimental) [GeV]	0.418 ± 0.001	0.312 ± 0.001

Table 3.4: Best linear fit parameters to differences, and a comparison with the experimental data.

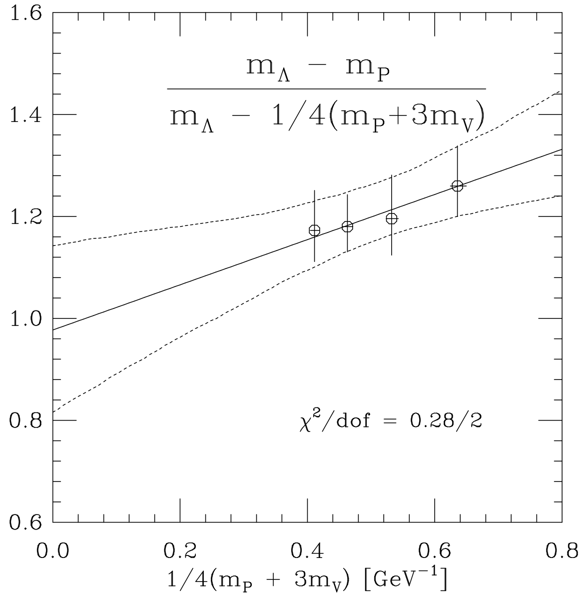

Figure 3.11: Linear extrapolation of ratio of mass splittings to the static limit. The dotted lines indicate 68% confidence levels of the fit.

Chapter 4

The Radiative Decay $b \to s\gamma$

4.1 The Standard Model and New Physics

Theoretical interest in the flavour–changing neutral process $b \to s\gamma$ as a test of the Standard Model (SM) has been renewed by the experimental results from the CLEO collaboration [101] of the decay $B \to K^*\gamma$. For the first time, this mode has been positively identified and a preliminary determination of its branching ratio given.

The radiative decays of the B meson are remarkable for several reasons. Firstly, $b \to s\gamma$ occurs through penguin-type diagrams at one-loop in the SM. As a result, the decay is a purely quantum effect and an extremely subtle test of the SM. Secondly, the process is sensitive to new physics appearing through virtual particles in the internal loops. Existing bounds on the $b \to s\gamma$ branching ratio have been used to place constraints on supersymmetry (SUSY) [102, 103, 104, 105, 106, 107, 108] and other extensions of the SM [109, 110]. A comprehensive review of these results can be found in [111]. Finally, it is also remarkable that $B \to K^*\gamma$ has a sufficiently large branching ratio to be detected experimentally. It is also hoped that other exclusive mode decays, for example $B_s \to \phi\gamma$ will also be detected in the near future. Thus, *accurate* experimental measurements and *accurate* theoretical calculations of these decays could soon probe new physics at comparatively low energies.

In order to compare the experimental branching ratio with a theoretical prediction it is necessary to know the relevant hadronic matrix elements. These

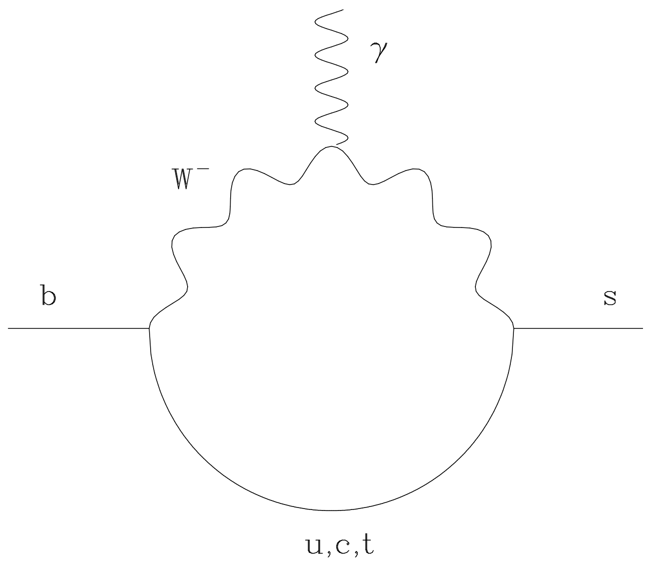

Figure 4.1: An example of a penguin diagram contributing to the decay $b \to s\gamma$

have been estimated using a wide range of methods, including relativistic and nonrelativistic quark models [112, 113, 114], two-point and three-point QCD sum rules [115, 116, 117, 118, 119, 120] and heavy quark symmetry [121], but there remains some disagreement between the different results. It is therefore of interest to perform a direct calculation of the matrix elements using lattice QCD. The viability of the lattice approach was first demonstrated by the work of Bernard, Hsieh and Soni [122] in 1991.

Excluding QCD contributions, the free quark decay $b \to s\gamma$ in the SM proceeds by diagrams similar to that shown in Fig.(4.1). The charm and top quark dominate, because the up quark contribution to the loop is suppressed by the small CKM factor $|V_{ub}V_{us}^*|$.

If the value of the top mass is assumed, the SM can be tested by deriving an independent result for $BR(B \to K^*\gamma)$. Deviations from the expected branching ratio would be an indication of contributions to the decay from physics beyond the SM, to which this decay is potentially sensitive.

Research on such contributions can be classified into supersymmetric and non-supersymmetric extensions of the SM. In the latter case, Cho and Misiak [123] considered $SU(2)_L \times SU(2)_R$ left-right symmetric models and found considerable variations from the SM result for a wide range of the free parameters, while Randall and Sundrum [124] found significant potential deviations from the SM in technicolour models. Anomalous $WW\gamma$ couplings in $b \to s\gamma$ have been analysed and the results found to be consistent with the SM. The bounds obtained from this approach can improve on those from direct searches [125, 126, 127, 128]. The contributions from two Higgs doublet models [129, 130] have been analysed to obtain bounds on the charged Higgs mass and $\tan\beta$, the ratio of the vacuum expectation values of the doublets [131, 132].

SUSY models also involve additional Higgs doublets, but the contribution of other boson-fermion loops, in particular charginos (χ^-) with up type squarks, and gluinos ($\tilde{g}$) or neutralinos (χ^0) with down type squarks must also be included [102, 103, 104, 105, 106, 107, 108, 133]. A comprehensive study of the decay in the Minimal Supersymmetric Standard Model can be found in reference [108]. There are strong contributions from chargino and gluino loops, especially for large $\tan\beta$, which interfere destructively with the Higgs contribution and allow SUSY to mimic the SM in some regions of parameter space. As a result, the current limits on $\tan\beta$ and Higgs masses are weak, but will tighten as more stringent bounds on superpartner masses are obtained.

In the following analysis, the SM will be used as the appropriate model, and possible deviations from the experimental branching ratio searched for. It should be noted that the lattice calculation is needed only to determine the effects of low energy QCD, and these are independent of new physics. The effect of many extensions of the SM will be completely contained within the renormalisation group operator coefficients, and hence it is straightforward to allow for contributions from different models.

4.2 Exclusive vs. Inclusive Decay Modes

Chay *et al.* [134] demonstrated that the inclusive decay $B \to X_u l\nu$ is predominantly a short distance process and can be treated perturbatively in the spectator approximation. Falk *et al.* noted that the same is true for $B \to X_s\gamma$ and used HQET to compute precisely the $1/m_b^2$ leading corrections to it [135]. It has recently been measured experimentally by the CLEO collaboration [136] to be

$$BR(B \to X_s\gamma) = (2.32 \pm 0.51 \pm 0.29 \pm 0.32) \times 10^{-4} \ . \tag{4.1}$$

The procedure for obtaining this result is quite difficult and has a mild model dependence (the final result is a function of m_b). The branching ratios of the exclusive decay modes of $b \to s\gamma$ can be experimentally determined much more accurately, and the present published branching ratio for $B \to K^*\gamma$ from the CLEO collaboration [101] is,

$$BR(B \to K^*\gamma) = (4.5 \pm 1.5 \pm 0.9) \times 10^{-5} \ , \tag{4.2}$$

where the first error is statistical and the second systematic. Hence, a calculation of the branching ratio for this exclusive mode could more accurately utilise experimental data, allowing much more stringent tests of the SM. This requires the determination of long distance QCD contributions which cannot be calculated perturbatively, but can be computed using lattice QCD.

4.3 The Effective Hamiltonian and Hadronic Matrix Elements

In order to determine the low energy QCD contributions to this decay, the high energy degrees of freedom must be integrated out, generating an effective $\Delta B = -1$, $\Delta S = 1$ Hamiltonian. Grinstein, Springer and Wise [137] determined the Hamiltonian $\mathcal{H}_{eff}$, to leading order in weak matrix elements,

$$\mathcal{H}_{eff} = \frac{4G_F}{\sqrt{2}} V_{tb} V_{ts}^* \sum_{i=1}^{8} C_i(\mu) O_i, \tag{4.3}$$

where $C_i(\mu)$ are renormalisation group coefficients multiplying the operators O_i. Six of these operators are four quark operators and two are magnetic moment operators, coupling to the gluon and photon [138]. The operator which mediates the $b \to s\gamma$ transition is,

$$O_7 = \frac{e}{16\pi^2} m_b \bar{s} \sigma_{\mu\nu} \frac{1}{2}(1+\gamma_5) b \; F^{\mu\nu}. \tag{4.4}$$

The coefficients $C_i(\mu)$ are set by matching to the full theory at the scale $\mu = m_W$. The coefficient $C_7(m_b)$ is determined using the renormalisation group to run down to the appropriate physical scale $\mu = m_b$ [139],

$$C_7(m_b) = \eta^{-16/23} \left(C_7(m_W) + \frac{58}{135}(\eta^{10/23} - 1) + \frac{29}{189}(\eta^{28/23} - 1) \right), \tag{4.5}$$

where, in the SM [140],

$$C_7^{SM}(m_W) = \frac{1}{2} \frac{x}{(x-1)^3} \left(\frac{2}{3} x^2 + \frac{5}{12} x - \frac{7}{12} - \frac{x}{2} \frac{(3x-2)}{(x-1)} \log x \right), \tag{4.6}$$

and

$$\eta = \frac{\alpha_s(m_b)}{\alpha_s(m_W)}, \qquad x = \frac{m_t^2}{m_W^2}. \tag{4.7}$$

The effects of scale uncertainty in the leading order approximation have been considered by Buras *et al.* [131].

To leading order, the on-shell matrix element for $B \to K^* \gamma$ is given by,

$$\mathcal{M} = \frac{e G_F m_b}{2\sqrt{2}\pi^2} C_7(m_b) V_{tb} V_{ts}^* \xi^{\mu *} \langle K^* | J_\mu | B \rangle, \tag{4.8}$$

where,

$$J_\mu = \bar{s} \sigma_{\mu\nu} q^\nu b_R, \tag{4.9}$$

and ξ and q are the polarization and momentum of the emitted photon. As outlined by Bernard, Hsieh and Soni [122], the matrix element $\langle K^* | \bar{b} \sigma_{\mu\nu} q^\nu s_R | B \rangle$

can be parametrised by three form factors,

$$\langle K^*|J_\mu|B\rangle = \sum_{i=1}^{3} C_\mu^i T_i(q^2), \tag{4.10}$$

where,

$$\begin{aligned}
C_\mu^1 &= 2\varepsilon_{\mu\nu\lambda\rho}\epsilon^\nu p^\lambda k^\rho \ , && (4.11)\\
C_\mu^2 &= \epsilon_\mu(m_B^2 - m_{K^*}^2) - \epsilon\cdot q(p+k)_\mu \ , && (4.12)\\
C_\mu^3 &= \epsilon\cdot q\left(q_\mu - \frac{q^2}{m_B^2 - m_{K^*}^2}(p+k)_\mu\right) \ , && (4.13)
\end{aligned}$$

where p and k are respectively the momentum of the B and K^* meson. As the photon emitted is on-shell, the form factors need to be evaluated at $q^2{=}0$. In this limit,

$$T_2(q^2{=}0) = -iT_1(q^2{=}0), \tag{4.14}$$

and the coefficient of $T_3(q^2{=}0)$ is zero in the on-shell matrix element. Hence, the branching ratio can be expressed in terms of a single form factor,

$$BR(B\to K^*\gamma) = \frac{\alpha}{8\pi^4} m_b^2 G_F^2 m_B^3 \tau_B \left(1 - \frac{m_{K^*}^2}{m_B^2}\right)^3 |V_{tb}V_{ts}^*|^2 |C_7(m_b)|^2 |T_1(q^2{=}0)|^2. \tag{4.15}$$

From the calculation by Grinstein, Springer and Wise [137] of the inclusive branching ratio, one finds that many of the parameters in Eq.(4.15) cancel in the hadronisation ratio, defined as

$$\begin{aligned}
R &= \frac{BR(B\to K^*\gamma)}{BR(B\to X_s\gamma)}\\
&= 4\left(1 - \frac{m_{K^*}^2}{m_B^2}\right)^3 \left(\frac{m_B}{m_b}\right)^3 |T_1(q^2=0)|^2 \ . && (4.16)
\end{aligned}$$

Hence a comparison can be made to experimental data by evaluating the on–shell form factor $T_1(q^2 = 0)$.

The form factors $T_1(q^2{=}0)$ and $T_2(q^2{=}0)$ will be evaluated using three separate methods in order to determine the systematic error, and compare the calculated value of $BR(B \to K^*\gamma)$ and R with the results from CLEO.

4.4 Computational Details

Sixty $SU(3)$ gauge configurations were generated in the quenched approximation for a $24^3 \times 48$ lattice at $\beta = 6.2$. The calculation of these configurations and the lattice spacing they correspond to is outlined in §3.2. The light quark propagators were again evaluated from the SW action, using the over–relaxed minimal residual algorithm with red–black preconditioning for $\kappa = 0.14144$, 0.14226 and 0.14262, with periodic boundary conditions in the spatial directions and anti–periodic boundary conditions in the temporal direction. Smearing was not used in the calculation of these light propagators. As outlined in chapter 3, these κ values can be used to test the behaviour of the data in the chiral limit. The first two κ values can also be used to interpolate to the strange quark mass which corresponds to $\kappa = 0.1419(1)$ [141].

Heavy propagators, for $\kappa_h = 0.121, 0.125, 0.129$ and 0.133, were evaluated using time–slice 24 of some of the above propagators as the source. For $\kappa_h = 0.121$ and 0.129, the propagators for all of the light κ values were used. For $\kappa_h = 0.125$ and 0.133, the propagators for $\kappa = 0.14144$ and 0.14226 were used. To reduce excited state contamination, these sources were smeared using the gauge–invariant Jacobi algorithm [66], with an r.m.s. smearing radius of 5.2.

Using these propagators, the three–point correlator $C^{3pt}_{\rho\mu\nu}(t, t_f, \vec{p}, \vec{q})$, defined as

$$\begin{aligned} C^{3pt}_{\rho\mu\nu}(t, t_f, \vec{p}, \vec{q}) &= \sum_{\vec{x},\vec{y}} e^{i\vec{p}\cdot\vec{x}} e^{-i\vec{q}\cdot\vec{y}} \langle J_P(t_f, \vec{x}) T_{\mu\nu}(t, \vec{y}) J^\dagger_{V\rho}(0) \rangle \\ &\xrightarrow[t, t_f - t, T \to \infty]{} \sum_{\epsilon} \frac{Z_P}{2E_P} \frac{Z_V}{2E_V} e^{-E_P(t_f - t)} e^{-E_V t} \epsilon_\rho \langle P(p) | \overline{h} \sigma_{\mu\nu} s | V(k, \epsilon) \rangle \end{aligned} \tag{4.17}$$

was calculated, where

$$\begin{aligned} J_P(x) &= \bar{l}(x)\gamma_5 h(x), & (4.18)\\ J_\rho^V(x) &= \bar{l}(x)\gamma_\rho s(x), & (4.19)\\ T_{\mu\nu}(y) &= \bar{h}(y)\sigma_{\mu\nu}s(y). & (4.20) \end{aligned}$$

As outlined in chapter 1, to obtain the matrix element $\langle P|\bar{h}\sigma_{\mu\nu}s|V\rangle$, the ratio

$$C_{\rho\mu\nu}(t,t_f,\vec{p},\vec{q}) = \frac{C^{3pt}_{\rho\mu\nu}(t,t_f,\vec{p},\vec{q})}{C_P^{2pt}(t_f-t,\vec{p})C_V^{2pt}(t,\vec{p}-\vec{q})}, \tag{4.21}$$

where C_P^{2pt} and C_V^{2pt} are the two–point functions constructed from the operators J_P and J_ρ^V, was computed. By time–reversal invariance and assuming that t_f, t and 0 are sufficiently separated, a term proportional to the required matrix element dominates:

$$C_{\rho\mu\nu}(t,t_f,\vec{p},\vec{q}) \underset{t,t_f-t,T\to\infty}{\longrightarrow} \frac{1}{Z_P Z_V}\sum_\epsilon \epsilon_\rho \langle V(k,\epsilon)|\bar{s}\sigma_{\mu\nu}h|P(p)\rangle + \dots\ , \tag{4.22}$$

and $C_{\rho\mu\nu}$ approaches a plateau. The full matrix element $\langle V|\bar{s}\sigma_{\mu\nu}\frac{1}{2}(1+\gamma_5)h|P\rangle$ can be derived from (4.21) using the Minkowski space relation

$$\gamma^5\sigma^{\mu\nu} = \frac{i}{2}\varepsilon^{\mu\nu\rho\lambda}\sigma_{\rho\lambda}. \tag{4.23}$$

Because of memory limitations, these propagators were evaluated only for time–slices 7 to 16 and 32 to 41. The spatial momentum $\vec{p}$ was chosen to be $(0,0,0)$ or $(\pi/12,0,0)$ (the lowest unit of momentum in lattice units that can be injected). All possible choices of $\vec{q}$ were calculated such that the magnitude of the spatial momentum of the vector meson $\vec{k}$ was less than $\sqrt{2}\pi/12$. This is because the signal of light hadrons degrades rapidly as the momentum is increased [142].

In order to obtain $\langle V|\bar{s}\sigma_{\mu\nu}h|P\rangle$, the decay constant and energy were determined for the pseudoscalar of each heavy–light κ combination and the vector of each possible light κ combination, for all possible momenta used. The process of

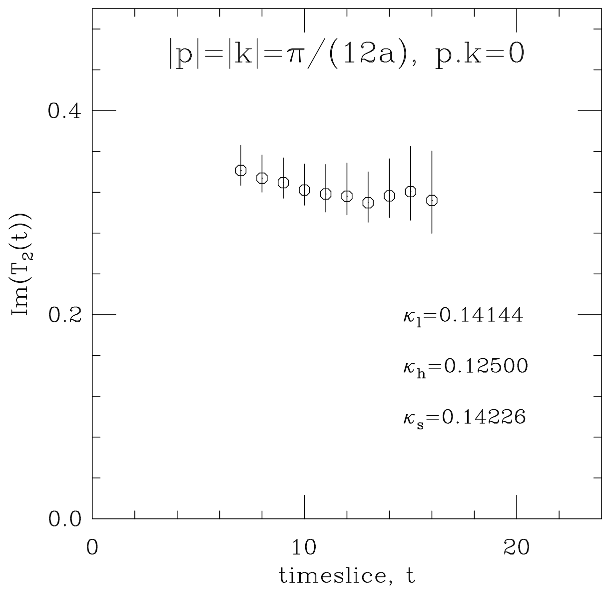

Figure 4.2: $Im(T_2)$, for a typical momentum used. From the application of the time reversal operator, it can be shown that only the imaginary component of T_2 is non–zero. The variables κ_l, κ_h and κ_s are the κ values for the light, heavy and strange quarks.

extracting these is well understood and has been discussed in detail in chapter 3. As the two–point functions are periodic, a correlator at a time $0 \leq t \leq 24$ was averaged with the same correlator at $48 - t$ to improve the signal. This “folded” data was fitted to Eq.(3.4) or Eq.(3.5) for time–slices 15 to 23. For both the two–point and three–point functions the discrete symmetries C, P and T (folding) were used wherever possible, in addition to averaging over equivalent momenta. The statistical errors for all correlators were determined by the bootstrap procedure [99], using 1000 bootstrap subsamples from the original configurations.

As outlined in chapter 1, the weak matrix elements $C_{\rho\mu\nu}$ were extracted from the three–point data and the fits to the two–point data. Having divided out the contributions from the two–point amplitudes and energies, the matrix element $\langle V|\bar{s}\sigma_{\mu\nu}h|P\rangle$ was isolated. These matrix elements were combined to determine the form factors $T_1(q^2)$, $T_2(q^2_{max})$ and $T_2(q^2)$. Each form factor was extracted by a correlated fit to a constant for time–slices 11, 12 and 13. An example of a fit for $T_2(q^2)$ is shown in Fig.(4.2).

The data for unphysical masses, and off-shell photons must be combined to isolate the form factors and extrapolate to the physical regime. It is clear from Eq.(4.14) and Eq.(4.15) that the branching ratio can be evaluated from $T_1(q^2{=}0; m_B; m_{K^*})$ or $T_2(q^2{=}0; m_B; m_{K^*})$. As demonstrated by Bowler *et al.* [143], the evaluation of the form factor $T_1(q^2{=}0; m_P; m_{K^*})$ is relatively straightforward, and $T_2(q^2 = 0; m_P; m_{K^*})$ can be determined in a similar way. In order to test heavy quark scaling, the form factor T_2 is extracted at maximum recoil, where $q^2 = q^2_{max} = (m_P - m_V)^2$, in the same way as Bernard *et al.* [144]. These form factors were extrapolated to the physical mass $m_P{=}m_B$, and an estimate of systematic errors in the extrapolation made by comparing the different methods.

4.5 Extraction of Form Factors

4.5.1 $T_1(q^2)$

The form factor T_1 can be conveniently extracted from the matrix elements by considering different components of the relation,

$$4(k^\alpha p^\beta - p^\alpha k^\beta) T_1(q^2) = \varepsilon^{\alpha\beta\rho\mu} C_{\rho\mu\nu} q^\nu. \tag{4.24}$$

There is a plateau in T_1 about $t = 12$. The use of smeared operators for the heavy quarks provides a very clean signal, with stable plateaux forming before time–slice 11. The data for the heaviest of the light quarks, $\kappa_l = \kappa_s = 0.14144$, with the smallest statistical errors, is shown in Fig.(4.3).

The form factor is evaluated for each of the five possible values of q^2. In order to obtain the on-shell form factor $T_1(q^2{=}0)$, $T_1(q^2)$ is fitted to a pole model,

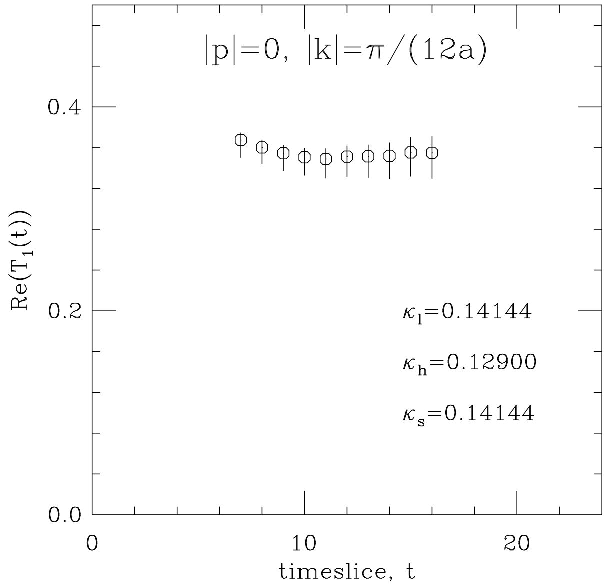

Figure 4.3: A typical plot of $T_1(q^2; m_P; m_V)$ vs. time. From the application of the time reversal operator, it can be shown that only real component of T_1 is non–zero.

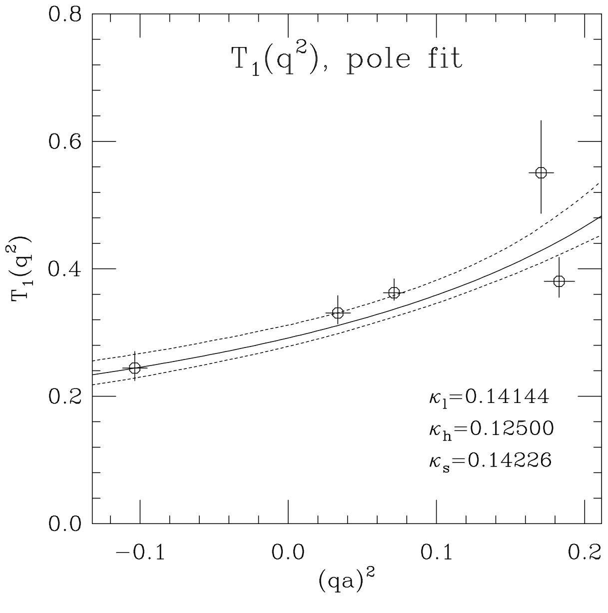

Figure 4.4: $T_1(q^2)$, using a pole fit. The dotted lines represent the 68% confidence levels of the fit at each q^2.

κ_h	κ_s	κ_l	low $(qa)^2$	high $(qa)^2$	$T_1(0)$	χ^2/d.o.f.
0.12100	0.14144	0.14144	-0.032 $^{+7}_{-7}$	0.258 $^{+8}_{-9}$	0.283 $^{+19}_{-12}$	10.2/3
0.12100	0.14144	0.14226	-0.035 $^{+10}_{-9}$	0.265 $^{+12}_{-12}$	0.292 $^{+30}_{-21}$	6.7/3
0.12100	0.14144	0.14262	-0.035 $^{+13}_{-12}$	0.271 $^{+18}_{-16}$	0.298 $^{+43}_{-32}$	3.2/3
0.12100	0.14226	0.14144	-0.014 $^{+10}_{-10}$	0.290 $^{+13}_{-12}$	0.275 $^{+23}_{-17}$	9.7/3
0.12100	0.14226	0.14226	-0.022 $^{+16}_{-15}$	0.298 $^{+19}_{-18}$	0.280 $^{+40}_{-36}$	5.8/3
0.12100	0.14226	0.14262	-0.028 $^{+23}_{-21}$	0.306 $^{+29}_{-26}$	0.277 $^{+55}_{-56}$	5.7/3
0.12500	0.14144	0.14144	-0.118 $^{+6}_{-5}$	0.157 $^{+7}_{-7}$	0.307 $^{+18}_{-10}$	8.9/3
0.12500	0.14226	0.14144	-0.104 $^{+8}_{-8}$	0.183 $^{+10}_{-10}$	0.291 $^{+20}_{-13}$	8.8/3
0.12900	0.14144	0.14144	-0.188 $^{+4}_{-4}$	0.086 $^{+4}_{-4}$	0.334 $^{+18}_{-9}$	10.0/3
0.12900	0.14144	0.14226	-0.190 $^{+6}_{-5}$	0.084 $^{+6}_{-5}$	0.337 $^{+22}_{-12}$	7.6/3
0.12900	0.14144	0.14262	-0.190 $^{+8}_{-7}$	0.084 $^{+8}_{-7}$	0.341 $^{+30}_{-20}$	4.5/3
0.12900	0.14226	0.14144	-0.177 $^{+6}_{-6}$	0.097 $^{+6}_{-6}$	0.316 $^{+19}_{-10}$	9.0/3
0.12900	0.14226	0.14226	-0.182 $^{+10}_{-8}$	0.096 $^{+14}_{-12}$	0.318 $^{+25}_{-17}$	6.5/3
0.12900	0.14226	0.14262	-0.186 $^{+13}_{-12}$	0.103 $^{+20}_{-17}$	0.314 $^{+35}_{-28}$	4.3/3
0.13300	0.14144	0.14144	-0.240 $^{+3}_{-2}$	0.034 $^{+3}_{-2}$	0.368 $^{+19}_{-10}$	6.5/3
0.13300	0.14226	0.14144	-0.233 $^{+4}_{-4}$	0.041 $^{+4}_{-4}$	0.347 $^{+20}_{-11}$	7.3/3

Table 4.1: Results of pole fits to $T_1(q^2; m_P; m_V)$. The range of q^2 is demonstrated by listing the minimum and maximum value of q^2 calculated for each fit.

$$T_1(q^2) = \frac{T_1(q^2{=}0)}{1 - q^2/m^2}, \tag{4.25}$$

allowing for correlations between the energies of the vector and pseudoscalar particles and T_1 at each q^2. In order to obtain the best estimate for $T_1(q^2{=}0)$, the parameter m in Eq.(4.25) is not fixed in this fit. In all of the fits, the χ^2/d.o.f. is not very large (approximately 3), indicating that the pole model is a reasonable ansatz for interpolation. An example of such a fit, for $\kappa_l = \kappa_s = 0.14144$, where κ_l and κ_s are the κ values for light and strange quarks, is shown in Fig.(4.4) and the full set of fit parameters and their χ^2/d.o.f. are shown in Table 4.1.

The behaviour of $T_1(q^2{=}0; m_P; m_V)$ in the chiral limit was explored for $\kappa_h =$ 0.121 and 0.129. The fits of the form factor were compared to the functions,

$$\begin{aligned} T_1(q^2_{max}; m_l) &= a + b\, m_l, & (4.26) \\ T_1(q^2_{max}; m_l) &= c, & (4.27) \end{aligned}$$

where m_l is the lattice pole mass, defined in Eq.(3.19). The linear coefficient b was found to be consistent with zero for each combination of κ_s and κ_h. From Table 4.2, the χ^2/d.o.f. for both fits are similar, indicating that for the data available, the assumption that the form factor is a constant is valid. That is the form factor can be assumed to be independent of the spectator quark mass. Hence, the data for $\kappa_l = 0.14144$ was used for the chiral limit, and a simple linear interpolation was carried out between $\kappa_s = 0.14144$ and 0.14226 for the strange quark, in order to obtain $T_1(q^2{=}0; m_P; m_{K^*})$.

4.5.2 $T_2(q^2)$

The form factor T_2 can be extracted from the matrix elements using the same procedure as T_1, by considering the different components of,

$$(m_P^2 - m_V^2) T_2(q^2; m_P; m_V) = C_{ii\nu} q^\nu, \tag{4.28}$$

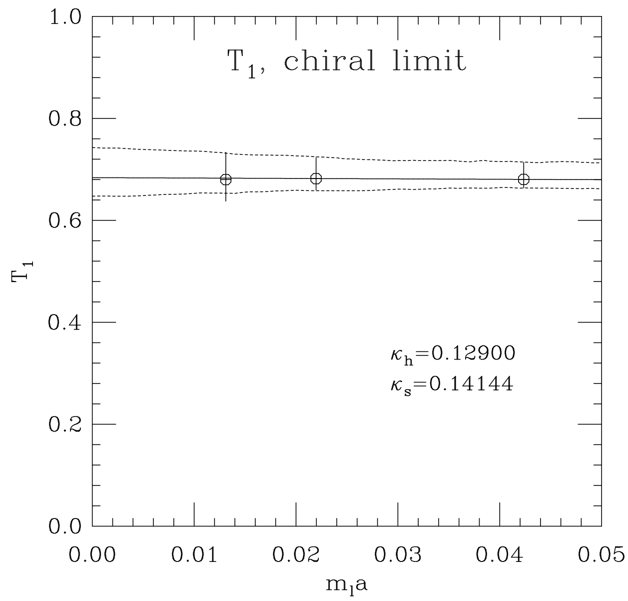

Figure 4.5: Chiral extrapolation of $T_1(q^2{=}0)$. The dotted lines indicate the 68% confidence levels of the fit. m_l is the lattice pole mass.

		$T_1(m_q) = a + bm_q$			$T_1(m_q) = c$	
κ_h	κ_s	a	b	χ^2/d.o.f.	c	χ^2/d.o.f.
0.121	0.14144	$0.291\,^{+45}_{-37}$	$-0.32\,^{+75}_{-74}$	0.09/1	$0.275\,^{+19}_{-13}$	0.3/2
0.121	0.14226	$0.304\,^{+61}_{-60}$	$-0.96\,^{+119}_{-106}$	0.8/1	$0.255\,^{+25}_{-19}$	1.7/2
0.121	0.1419	$0.298\,^{+53}_{-49}$			$0.263\,^{+21}_{-16}$	
0.129	0.14144	$0.336\,^{+27}_{-16}$	$0.03\,^{+\ 34}_{-\ 38}$	0.1/1	$0.337\,^{+18}_{-\ 9}$	0.1/2
0.129	0.14226	$0.333\,^{+29}_{-20}$	$-0.24\,^{+\ 38}_{-\ 38}$	0.2/1	$0.321\,^{+17}_{-\ 9}$	0.5/2
0.129	0.1419	$0.335\,^{+27}_{-17}$			$0.328\,^{+17}_{-\ 9}$	

Table 4.2: Extrapolation of T_1 to the chiral limit, where T_1 is assumed to either have a linear dependence on the pole mass of the light quark, or independent of the pole mass. $\kappa_{strange} = 0.1419$ corresponds to the physical strange quark mass from determining the mass of the K meson on this lattice.

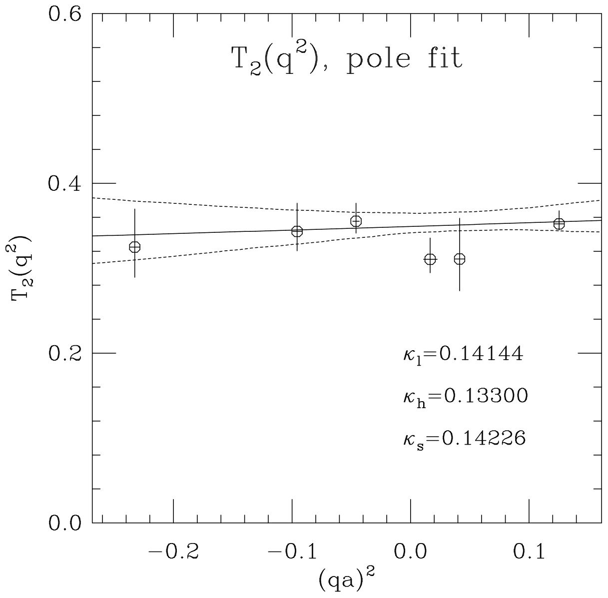

Figure 4.6: $T_2(q^2)$, using a pole fit. The dotted lines represent the 68% confidence levels of the fit at each q^2.

for all i (not summed) such that $q^i = 0$, and interpolating the data to q^2=0 using the pole model. The pole mass was found to be large, and a linear fit to q^2 can be performed. It is noted that this linear behaviour holds well for all possible q^2, including q^2_{max}, as shown in Fig.(4.6). The results of the fits to determine $T_2(q^2{=}0; m_P; m_V)$ using the pole model are shown in Table 4.3.

The chiral behaviour of $T_2(q^2 = 0; m_P; m_V)$ was examined for $\kappa_h = 0.121$ and 0.129, using the same procedure of the previous section. It was determined that the assumption that $T_2(q^2 = 0; m_P; m_V)$ is independent of the spectator quark mass is consistent to within statistical errors of the data available. The results of these fits is shown in Table 4.4 and an example of the chiral extrapolation of $T_2(q^2 = 0; m_P; m_V)$ is shown in Fig.(4.7).

The ratio of $T_1(q^2{=}0; m_P; m_{K^*})/T_2(q^2{=}0; m_P; m_{K^*})$ is shown in Fig.(4.8) and was found, within 2 standard deviations, to be consistent with 1 in accordance with the identity $T_2(0) = -iT_1(0)$, of Eq.(4.14).

κ_h	κ_s	κ_l	low $(qa)^2$	high $(qa)^2$	$T_2(0)$	χ^2/d.o.f.
0.12100	0.14144	0.14144	-0.032^{+7}_{-7}	0.357^{+7}_{-7}	0.306^{+21}_{-14}	5.8/3
0.12100	0.14144	0.14226	-0.035^{+10}_{-9}	0.361^{+11}_{-10}	0.314^{+28}_{-24}	8.5/3
0.12100	0.14144	0.14262	-0.035^{+13}_{-12}	0.365^{+15}_{-15}	0.319^{+24}_{-37}	8.9/3
0.12100	0.14226	0.14144	-0.014^{+10}_{-10}	0.387^{+11}_{-11}	0.292^{+25}_{-16}	2.1/3
0.12100	0.14226	0.14226	-0.022^{+16}_{-15}	0.392^{+17}_{-17}	0.305^{+29}_{-31}	5.3/3
0.12100	0.14226	0.14262	-0.028^{+23}_{-21}	0.398^{+26}_{-24}	0.305^{+20}_{-34}	9.2/3
0.12500	0.14144	0.14144	-0.118^{+6}_{-5}	0.258^{+5}_{-6}	0.328^{+19}_{-11}	5.9/3
0.12500	0.14226	0.14144	-0.104^{+8}_{-8}	0.282^{+9}_{-9}	0.310^{+22}_{-14}	3.9/3
0.12900	0.14144	0.14144	-0.188^{+4}_{-4}	0.176^{+4}_{-4}	0.349^{+16}_{-9}	7.1/3
0.12900	0.14144	0.14226	-0.190^{+6}_{-5}	0.178^{+7}_{-6}	0.355^{+21}_{-13}	9.0/3
0.12900	0.14144	0.14262	-0.190^{+8}_{-7}	0.181^{+9}_{-9}	0.360^{+17}_{-21}	13.2/3
0.12900	0.14226	0.14144	-0.177^{+6}_{-6}	0.194^{+7}_{-7}	0.332^{+18}_{-10}	5.8/3
0.12900	0.14226	0.14226	-0.182^{+10}_{-8}	0.197^{+11}_{-10}	0.337^{+21}_{-20}	8.6/3
0.12900	0.14226	0.14262	-0.186^{+13}_{-12}	0.201^{+17}_{-15}	0.334^{+18}_{-24}	12.3/3
0.13300	0.14144	0.14144	-0.240^{+3}_{-2}	0.113^{+3}_{-3}	0.372^{+14}_{-7}	8.5/3
0.13300	0.14226	0.14144	-0.233^{+4}_{-4}	0.125^{+4}_{-4}	0.349^{+16}_{-8}	6.4/3
0.13300	0.14226	0.14144	-0.233^{+4}_{-4}	0.125^{+4}_{-4}	0.349^{+16}_{-8}	6.4/3

Table 4.3: Results of pole fits to $T_2(q^2; m_P; m_V)$.The range of q^2 is demonstrated by listing the minimum and maximum value of q^2 calculated for each fit.

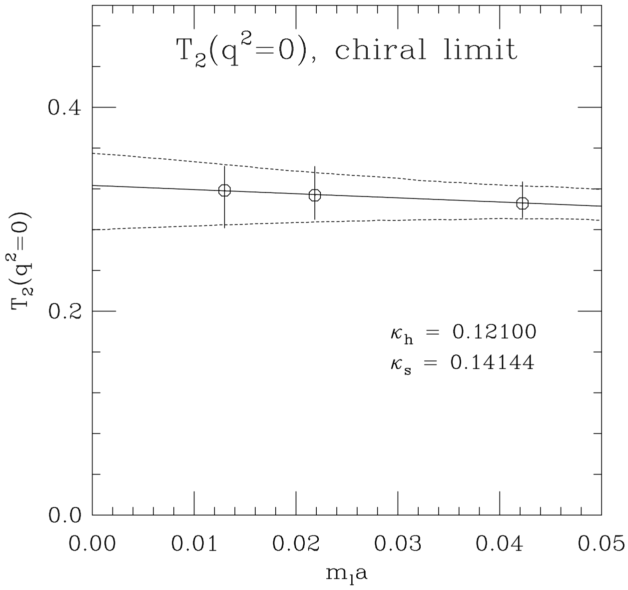

Figure 4.7: Chiral extrapolation of $T_2(q^2{=}0)$. The dotted lines indicate the 68% confidence levels of the fit. m_l is the lattice pole mass.

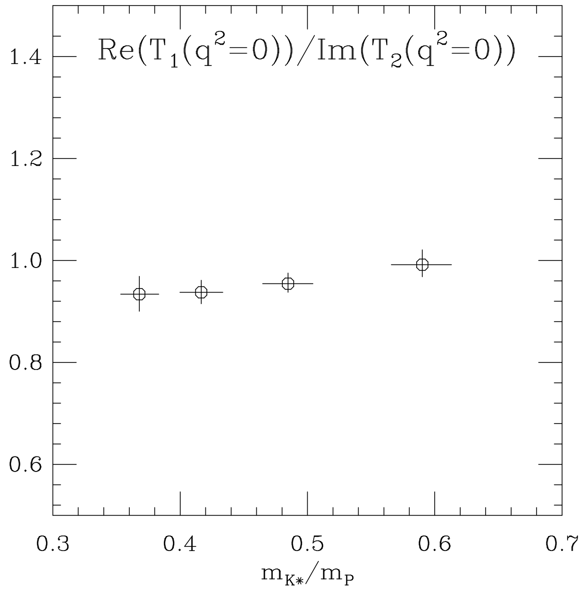

Figure 4.8: The ratio of $T_1(q^2 = 0; m_P; m_{K^*})/T_2(q^2 = 0; m_P; m_{K^*})$.

		$T_2(q^2{=}0; m_q) = a + bm_q$			$T_2(q^2{=}0; m_q) = c$	
κ_h	κ_s	a	b	χ^2/d.o.f.	c	χ^2/d.o.f.
0.12900	0.14144	$0.363\,^{+22}_{-24}$	$-0.31\,^{+46}_{-39}$	0.1/1	$0.348\,^{+13}_{-\ 9}$	0.6/2
0.12900	0.14226	$0.337\,^{+23}_{-31}$	$-0.19\,^{+71}_{-40}$	0.1/1	$0.329\,^{+17}_{-\ 9}$	0.3/2
0.12900	0.14190	$0.349\,^{+22}_{-27}$			$0.337\,^{+15}_{-\ 9}$	
0.12100	0.14144	$0.323\,^{+32}_{-43}$	$-0.41\,^{+83}_{-60}$	0.01/1	$0.304\,^{+17}_{-14}$	0.3/2
0.12100	0.14226	$0.311\,^{+23}_{-47}$	$-0.53\,^{+101}_{-\ 45}$	0.1/1	$0.289\,^{+19}_{-15}$	0.6/2
0.12100	0.14190	$0.317\,^{+25}_{-42}$			$0.337\,^{+15}_{-\ 9}$	

Table 4.4: Extrapolation of $T_2(q^2 = 0)$ to the chiral limit, where T_2 is assumed to either have a linear dependence on the pole mass of the light quark, or independent of the pole mass. $\kappa_{strange} = 0.1419$ corresponds to the physical strange quark mass from determining the mass of the K meson on this lattice.

4.5.3 $T_2(q^2_{max})$

The evaluation of $T_2(q^2_{max}; m_P; m_V)$ is also straightforward, since at zero momentum, $\vec{p}{=}\vec{0}$, $\vec{k}{=}\vec{0}$, the contributions from other form factors vanish,

$$\begin{aligned}(m_P + m_V)\,T_2(q^2_{max}) &= C_{110}(\vec{p} = \vec{0}, \vec{k} = \vec{0}) \\ &= C_{220}(\vec{p} = \vec{0}, \vec{k} = \vec{0}) \\ &= C_{330}(\vec{p} = \vec{0}, \vec{k} = \vec{0}). \end{aligned} \tag{4.29}$$

An example of this data is shown in Fig.(4.9). The behaviour of $T_2(q^2{=}q^2_{max}; m_P; m_V)$ as a function of the spectator quark mass was examined at $\kappa_h = 0.121$ and 0.129 in the same way as for $T_1(q^2{=}0)$. It was again found that the linear coefficient b was consistent with zero for each combination of κ_s and κ_h. From Table 4.5, the χ^2/d.o.f. for both fits are seen to be similar, indicating that for the data available, the assumption that the form factor is independent of the spectator quark mass is valid. Hence, the data for $\kappa_l = 0.14144$ is used for the chiral limit, to obtain $T_2(q^2_{max}; m_P; m_{K^*})$. Bernard *et al.* [144] converted this

		$T_2(q^2_{max}; m_q) = a + bm_q$			$T_2(q^2_{max}; m_q) = c$	
κ_h	κ_s	a	b	χ^2/d.o.f.	c	χ^2/d.o.f.
0.12100	0.14144	$0.331\ ^{+29}_{-14}$	$0.49\ ^{+35}_{-43}$	0.4/1	$0.353\ ^{+15}_{-\ 7}$	1.9/2
0.12100	0.14226	$0.327\ ^{+31}_{-17}$	$-0.03\ ^{+38}_{-47}$	1.9/1	$0.325\ ^{+15}_{-\ 6}$	1.9/2
0.12100	0.14190	$0.328\ ^{+29}_{-16}$			$0.337\ ^{+15}_{-\ 6}$	
0.12900	0.14144	$0.370\ ^{+27}_{-10}$	$-0.14\ ^{+20}_{-37}$	0.9/1	$0.363\ ^{+13}_{-\ 6}$	1.1/2
0.12900	0.14226	$0.349\ ^{+32}_{-16}$	$-0.14\ ^{+31}_{-45}$	0.7/1	$0.341\ ^{+13}_{-\ 6}$	0.8/2
0.12900	0.14190	$0.358\ ^{+29}_{-13}$		0.7/1	$0.351\ ^{+13}_{-\ 6}$	0.8/2

Table 4.5: Extrapolation of $T_2(q^2_{max})$ to the chiral limit, where T_2 is assumed to either have a linear dependence on the pole mass of the light quark, or independent of the pole mass. $\kappa_{strange} = 0.1419$ corresponds to the physical strange quark mass from determining the mass of the K meson on this lattice.

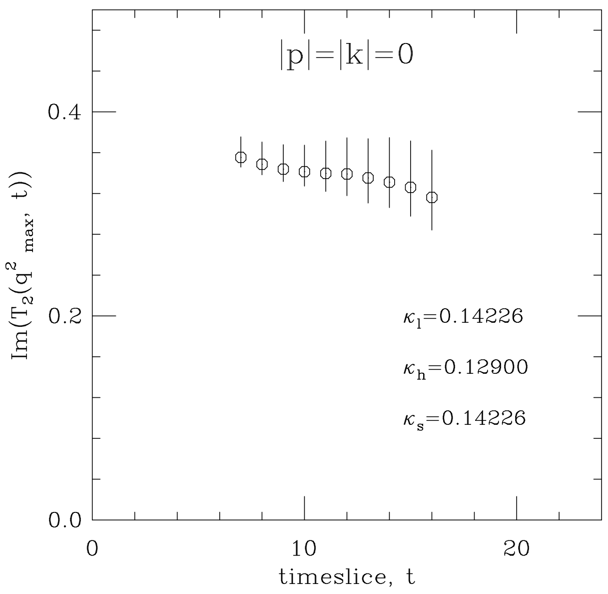

Figure 4.9: A typical plot of $T_2(q^2 = q^2_{max}; m_P; m_V)$ vs. time.

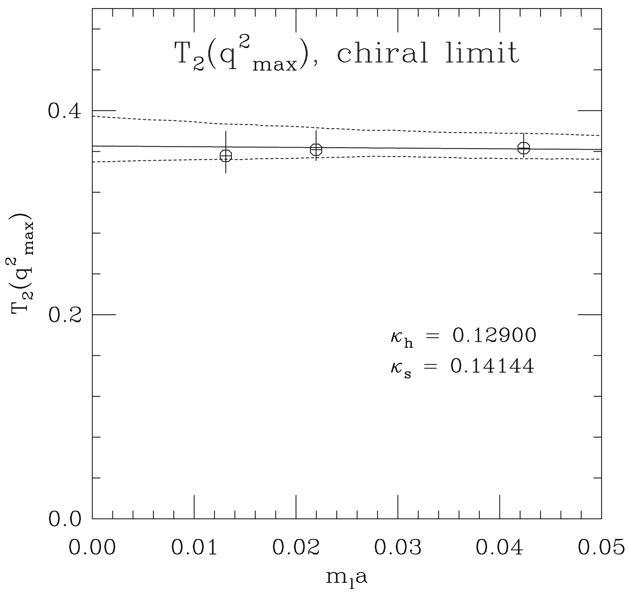

Figure 4.10: Chiral extrapolation of $T_2(q^2{=}q^2_{max})$.

result to $q^2{=}0$ by assuming single pole dominance, i.e.,

$$T_2^{pole}(q^2{=}0) = T_2(q^2_{max})\left(1 - q^2_{max}/m^2_{P^*_{s1}}\right) \ . \tag{4.30}$$

The current J_μ of the matrix element Eq.(4.8) can be expressed in a $V + A$ form, with T_1 corresponding to the vector component and T_2 and T_3 to the axial current. Therefore, in a single pole model, the exchanged particle, P^*_{s1}, for the T_2 form factor would be expected to be the lowest $J^P = 1^+$ state, which carries the correct quantum numbers of spin, parity and strangeness. As outlined in chapter 1, the mass of this state at each heavy quark mass can be obtained from a two–point function of the form found in (1.44), and evaluating the best fit to the function (1.42). In this case, the matrix $\Gamma^{\alpha\beta}$ of Eq.(1.43) is $\gamma^i\gamma^5$. Hence, the two–point function

$$P^*_{s1}(t) = \sum_{i,\vec{x}} \langle J^\dagger_{i,P^*_{s1}}(t,\vec{x}) J_{i,P^*_{s1}}(0)\rangle, \tag{4.31}$$

where

$$J^i_{P^*_{s1}}(t,\vec{x}) = \bar{l}(x)\gamma^i\gamma^5 h(x), \tag{4.32}$$

was evaluated using the same quenched gauge configurations used in the calculation of the matrix elements $C_{\rho\mu\nu}$, the heavy pseudoscalar and light vector mesons. The quark propagators were again computed using the over–relaxed minimal residual algorithm with red–black preconditioning, with periodic boundary conditions in the spatial directions and anti–periodic boundary conditions in the temporal direction. For the heavy quark propagator the κ values $\kappa_h = 0.121$, 0.125, 0.129 and 0.133 were used and $\kappa_s = 0.14144$ and 0.14226 for the strange quark propagator. As stated previously, the choice of κ_s allows for an interpolation to the physical strange quark mass. In order to improve the overlap with ground state, the heavy propagator was smeared at the source, using a smearing radius of 5.2.

By (1.42),

$$P^*_{s1}(t) \underset{t \gg m_{P^*_{s1}}}{\longrightarrow} \frac{Z_s^2}{2m_{P^*_{s1}}} \left(e^{-m_{P^*_{s1}} t} + e^{-m_{P^*_{s1}} (T-t)} \right) . \tag{4.33}$$

For each κ combination, this function was fitted to the data from time–slices 10 to 16, averaged with time–slice 38 to 32 in order to improve the signal. As demonstrated in chapter 3, the best fit range is determined from the effective mass, defined as

$$m^{s1}_{eff}(t) = \ln \left(\frac{P^*_{s1}(t-1)}{P^*_{s1}(t)} \right) . \tag{4.34}$$

An example of the effective mass is shown in figure Fig.(4.11). The errors were generated using the boostrap algorithm with 1000 boostrap subsamples. The result of fits to this data is shown in Table 4.6. Using these masses and the pole model of (4.30), $T_2^{pole}(q^2{=}0; m_P; m_{K^*})$ was determined from $T_2(q^2_{max}; m_P; m_{K^*})$.

The ratio of $T_1(q^2{=}0; m_P; m_{K^*})/T_2^{pole}(q^2{=}0; m_P; m_{K^*})$ is shown in Fig.(4.12). It is, to within 2 standard deviations, consistent with 1. A comparison of the three methods used to obtain $T_1(q^2{=}0; m_P; m_{K^*})$ is shown in Table 4.7. At each heavy quark mass, the three results agree with each other to within 3 standard deviations.

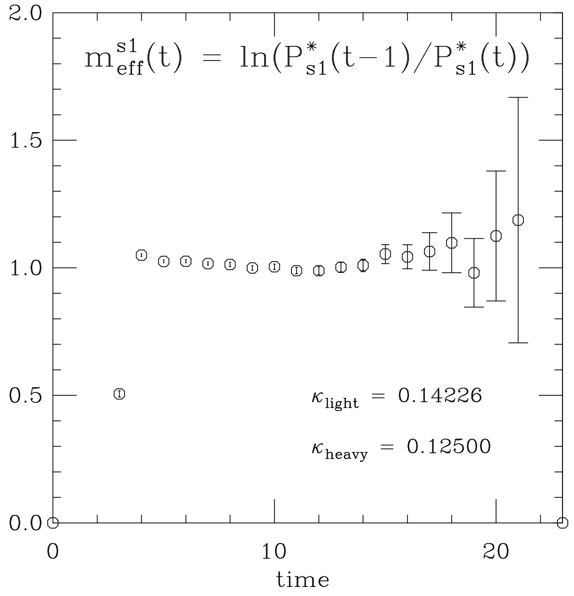

Figure 4.11: An effective mass plot of the meson P_{s1}^*.

κ_h	κ_s	$m_{A1}a$	χ^2/d.o.f.
0.13300	0.14144	$0.802\ ^{+11}_{-10}$	6.59/5
0.13300	0.14226	$0.784\ ^{+12}_{-11}$	5.04/5
0.13300	0.14190	$0.792\ ^{+11}_{-10}$	
0.12900	0.14144	$0.908\ ^{+11}_{-\ 9}$	6.90/5
0.12900	0.14226	$0.891\ ^{+11}_{-11}$	4.63/5
0.12900	0.14190	$0.899\ ^{+11}_{-10}$	
0.12500	0.14144	$1.010\ ^{+10}_{-10}$	6.79/5
0.12500	0.14226	$0.993\ ^{+11}_{-11}$	4.18/5
0.12500	0.14190	$1.000\ ^{+10}_{-10}$	
0.12100	0.14144	$1.107\ ^{+10}_{-10}$	6.52/5
0.12100	0.14226	$1.090\ ^{+10}_{-11}$	3.76/5
0.12100	0.14190	$1.097\ ^{+10}_{-10}$	

Table 4.6: Results of mass fits to P_{s1}^*. The κ value of 0.1419 corresponds to the physical strange quark mass.

κ_h	m_{K^*}/m_P	$T_2(q^2_{max})$	$q^2_{max}/m^2_{P^*_s}$	$T_2^{pole}(0)$	$T_1(0)$	$T_2(0)$
0.133000	$0.59\,^{+\,2}_{-\,2}$	$0.362\,^{+15}_{-\,6}$	$0.08\,^{+\,1}_{-\,1}$	$0.333\,^{+14}_{-\,7}$	$0.356\,^{+19}_{-10}$	$0.359\,^{+15}_{-\,7}$
0.129000	$0.48\,^{+\,2}_{-\,2}$	$0.353\,^{+15}_{-\,6}$	$0.15\,^{+\,1}_{-\,1}$	$0.301\,^{+14}_{-\,7}$	$0.324\,^{+19}_{-\,9}$	$0.339\,^{+17}_{-\,9}$
0.125000	$0.42\,^{+\,2}_{-\,2}$	$0.346\,^{+16}_{-\,6}$	$0.20\,^{+\,1}_{-\,1}$	$0.276\,^{+14}_{-\,7}$	$0.298\,^{+19}_{-11}$	$0.318\,^{+20}_{-12}$
0.121000	$0.37\,^{+\,2}_{-\,1}$	$0.339\,^{+16}_{-\,7}$	$0.26\,^{+\,2}_{-\,1}$	$0.252\,^{+14}_{-\,8}$	$0.278\,^{+22}_{-14}$	$0.298\,^{+23}_{-15}$
	$0.1692\,^{+\,1}_{-\,1}$	$0.269\,^{+17}_{-\,9}$	$0.51\,^{+\,6}_{-\,6}$	$0.112\,^{+\,7}_{-\,7}$	$0.124\,^{+20}_{-18}$	

Table 4.7: Comparison of results from the three methods of extracting $T_{1,2}(q^2{=}0)$. The last row indicates the final extrapolation to the physical regime m_{K^*}/m_B.

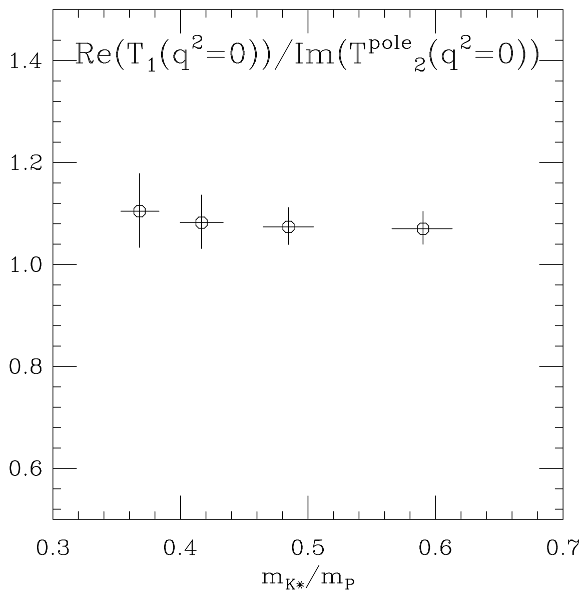

Figure 4.12: The ratio of $T_1(q^2 = 0; m_P; m_{K^*})/T_2^{pole}(q^2 = 0; m_P; m_{K^*})$.

4.6 Extrapolation to M_B

It is not *a priori* clear what the appropriate ansatz is for extrapolating the on-shell form factor in the heavy quark mass to $T_1(q^2{=}0; m_B; m_{K^*})$. Bernard *et al.* [144] demonstrated that there exists a scaling law for the off-shell form factor, $T_2(q^2{=}q^2_{max}; m_P; m_{K^*})$, using HQET. This was used to extrapolate the data to $T_2(q^2_{max}; m_B; m_{K^*})$, but a final step was needed to reach the on-shell point $q^2{=}0$. The pole dominance model was used to obtain $T_2(q^2{=}0; m_B; m_{K^*})$, by estimating the appropriate pole mass. The validity of the pole model over the wide range of momentum transfer from $q^2{=}0$ to q^2_{max} is required, but tests at heavy quark masses around the charm quark mass showed it to be quite accurate.

An alternative method is to combine the pole model and scaling law, by expanding unknown parameters in powers of $1/m_P$, in order to obtain a scaling law for the on-shell form factor $T_1(q^2{=}0)$ directly, using the identity $T_1(0) = iT_2(0)$. In order to get an estimate of the systematic error in the calculation, $T_1(q^2 = 0; m_B, m_{K^*})$ and $T_2(q^2{=}0; m_B; m_{K^*})$ were evaluated by both these methods.

4.6.1 $T_2(q^2_{max})$

At $q^2{=}q^2_{max}$, the initial and final hadronic states have zero spatial momentum and the contributions of form factors other than T_2 vanish,

$$\langle K^*|\bar{b}\sigma_{\mu\nu}q^\nu s_R|B\rangle = \epsilon_\mu(m_B^2 - m_{K^*}^2)T_2(q^2_{max}). \tag{4.35}$$

In the heavy quark limit, the matrix element of Eq.(4.35) scales as $m_B^{3/2}$, due to the normalisation of the heavy quark state ($\sqrt{m_B}$) and the momentum transfer, ($q^0 = m_B - m_{K^*}$). The leading term in heavy quark scaling of $T_2(q^2_{max})$ is expected to be $m_B^{-1/2}$, analogous to the scaling of f_B[72, 40]. Higher order $1/m_B$ and $1/m_B^2$ corrections will also be present, as will radiative corrections [30, 31]. Hence, the form factor $T_2(q^2_{max})$ should scale as,

$$T_2(q^2_{max}; m_P; m_{K^*})\sqrt{m_P} = \text{const.} \times [\alpha_s(m_P)]^{-2/\beta_0}\left(1 + \frac{a_1}{m_P} + \frac{a_2}{m_P^2} + \ldots\right). \tag{4.36}$$

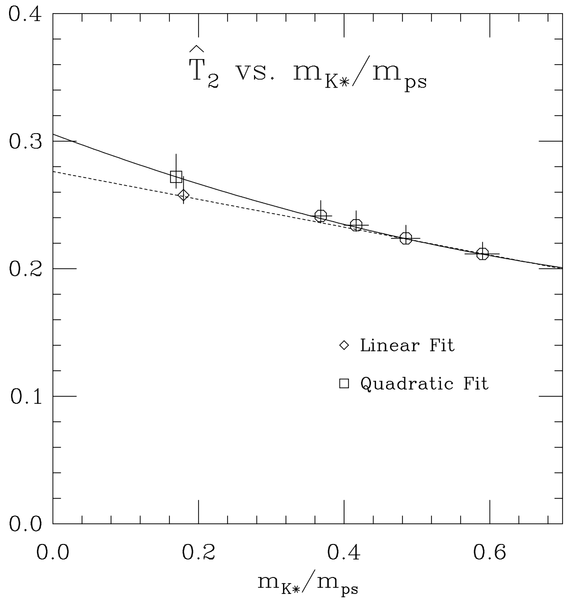

Figure 4.13: Extrapolation of $T_2(q^2{=}q^2_{max})$ to m_B, assuming HQET.

In order to test heavy quark scaling, the following quantity is defined,

$$\hat{T}_2 = T_2(q^2_{max})\sqrt{\frac{m_P}{m_B}}\left(\frac{\alpha_s(m_P)}{\alpha_s(m_B)}\right)^{2/\beta_0}, \tag{4.37}$$

where $\alpha_s(\mu)$ is approximated by,

$$\alpha_s(\mu) = \frac{2\pi}{\beta_0 \ln(\mu/\Lambda_{QCD})}. \tag{4.38}$$

with Λ_{QCD} taken to be 200 MeV and $\beta_0 = 11 - \frac{2}{3}N_f$. In the quenched approximation, N_f is taken to be zero.

The normalisation ensures that $\hat{T}_2 = T_2(q^2_{max})$ at the physical scale m_B. Linear and quadratic correlated fits to Eq.(4.36) were carried out with the functions,

$$\hat{T}_2(m_P) = A\left(1 + \frac{B}{m_P}\right), \tag{4.39}$$

$$\hat{T}_2(m_P) = A\left(1 + \frac{B}{m_P} + \frac{C}{m_P^2}\right), \tag{4.40}$$

and are shown in Fig.(4.13).

Taking the quadratic fit of T_2 at $m_P = m_B$ as the best estimate, and the difference between the central values of the linear and quadratic fits as an estimate of the systematic error, T_2 was found to be

$$T_2(q^2{=}q^2_{max}; m_B; m_{K^*}) = 0.269^{+17}_{-9} \pm 0.011. \tag{4.41}$$

where the first error quoted is statistical and the second is the systematic.

As outlined in §4.5.3, the expected exchange particle in the pole model for T_2 is the 1^+ B^*_{s1} state, but experimental data for its mass is not yet available. However, it is possible to estimate reasonable upper and lower bounds for the mass from HQET. From chapter 2, it is clear that

$$\begin{aligned} m_{Bs1} - m_B &= \Delta\overline{\Lambda} + \frac{A}{m_b} + O(\frac{1}{m_b^2}), & (4.42)\\ m_{Ds1} - m_D &= \Delta\overline{\Lambda} + \frac{A}{m_c} + O(\frac{1}{m_c^2}). & (4.43)\end{aligned}$$

Neglecting terms of order $1/m_c^2$, the upper and lower bounds for Eq.(4.42) are,

$$\frac{m_c}{m_b}(m_{Ds1} - m_D) < m_{Bs1} - m_B < m_{Ds1} - m_D \tag{4.44}$$

Making the approximation,

$$\frac{m_c}{m_b} \sim \frac{m_D + 3m_{D^*}}{m_B + 3m_{B^*}} \tag{4.45}$$

the range of the expected pole mass can be found,

$$m_{B^*_{s1}} = 5.74 \pm 0.21 \text{ GeV}. \tag{4.46}$$

Therefore,

$$T_2^{pole}(q^2 = 0; m_B; m_{K^*}) = 0.112^{+7+16}_{-7-15}, \tag{4.47}$$

where the first error is statistical and the second is the systematic error obtained by combining the variation of the pole mass within its bounds and the systematic error from Eq.(4.41).

4.6.2 $T_1(q^2{=}0)$

If the pole dominance model is assumed for T_2 and the mass of exchanged 1^+ particle expanded as,

$$m_{P^*_{s1}} = m_P \left(1 + \frac{b_1}{m_P} + \frac{b_2}{m_P^2} + \ldots\right), \tag{4.48}$$

then by combining the pole model with the known scaling of $T_2(q^2_{max})$, and the identity $T_1(0) = iT_2(0)$, it can be shown that $T_1(q^2{=}0; m_P; m_{K^*})$ should satisfy a modified scaling law,

$$T_1(0; m_P; m_{K^*})\, m_P^{3/2} = \text{const.} \times [\alpha_s(m_P)]^{-2/\beta_0} \left(1 + \frac{c_1}{m_P} + \frac{c_2}{m_P^2} + \ldots\right), \tag{4.49}$$

where the unknown coefficients in Eq.(4.48) have been absorbed into the unknown scaling coefficients of the matrix element.[1] This was tested in the same way as for T_2, by forming the quantity,

$$\hat{T}_1 = T_1(q^2{=}0) \left(\frac{m_P}{m_B}\right)^{3/2} \left(\frac{\alpha_s(m_P)}{\alpha_s(m_B)}\right)^{2/\beta_0}. \tag{4.50}$$

Linear and quadratic fits were carried out with the same functions as for $\hat{T}_2$, allowing for correlations between masses and form factors, and are shown in Fig.(4.14). The χ^2/d.o.f. was respectively 2.5 and 0.7 for the linear and quadratic fits, indicating that the model is statistically valid in the available mass range.

The correlated quadratic fit with radiative corrections gives,

$$T_1(q^2{=}0; m_B; m_{K^*}) = 0.124^{+20}_{-18}, \tag{4.51}$$

[1] Ali *et al.* found a similar scaling relationship for $T_1(q^2 = 0)$ using the sum rule method [119].

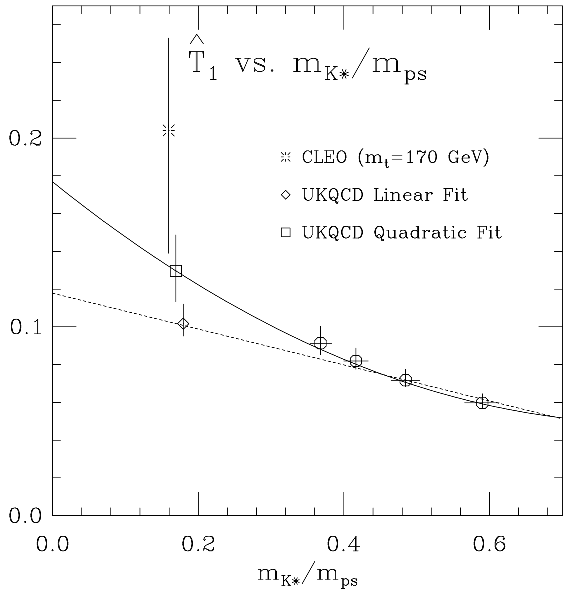

Figure 4.14: Extrapolation of $T_1(q^2{=}0)$ to m_B, assuming pole dominance. As a comparison, the calculated value of T_1 from CLEO is also shown. For clarity, the points at m_K^*/m_B are slightly displaced horizontally.

where the errors quoted are statistical.

All three methods of evaluating $T_1(q^2{=}0; m_P; m_{K^*})$ at intermediate masses are compared in Table 4.7. The differences between the methods are treated as a measure of part of the systematic error. The differences between the methods of determining the form factors at the computed masses are of a similar size ($\sim 10\%$) to the systematic error at the physical B mass, as measured by the two methods of extrapolation.

The final result for $T_1(q^2{=}0; m_B; m_{K^*})$ is taken from the quadratic fit for T_1, with an estimated systematic error in extrapolation given by the difference between linear and quadratic fits,

$$T_1(q^2{=}0; m_B; m_{K^*}) = 0.124^{+20}_{-18}\,(\text{stat.}) \pm 0.022\,(\text{sys.}). \tag{4.52}$$

It is noted that this is consistent with the value obtained from T_2.

To compare this result with experiment, the preliminary branching ratio from CLEO is converted into its corresponding T_1 form factor. The scale is set to $\mu = m_b = 4.39\,\text{GeV}$, in the $\overline{MS}$ scheme, using a pole mass of $m_b^{pole} = 4.95(15)\,\text{GeV}$ [145] to determine m_b [146]. Taking $|V_{ts}V_{tb}| = 0.037(3)$ [147], $\tau_B = 1.5(2)\,\text{ps}$ [148, 149] and all other values from the Particle Data Book combined with Eq.(4.15), T_1^{exp} is respectively 0.23(6), 0.21(5) and 0.19(5) for top quark masses of $m_t = 100$, 150 and 200 GeV. The calculated value for T_1 agrees with these results to within three standard deviations.

In calculating the branching ratio, the perturbative renormalisation of $\sigma_{\mu\nu}$ [150] is used, with a boosted coupling, $g^2 = 1.7 g_0^2$, and the anomalous dimension, $\gamma_{\bar{q}\sigma q} = -(8/3)(g^2/16\pi^2)$, to match the lattice results to the continuum at the scale $\mu = m_b$, giving a matching coefficient of $Z \approx 0.95$. A correction of $Z^2 = 0.90$ is applied in the calculations below. As well as the errors associated from the experimental data, errors due to the scale must also be included. Varying the scale of $C_7(\mu)$ from $\mu = m_b/2$ to $\mu = 2m_b$ changes the final branching ratio by $+27\%$ and -20% respectively. This is due to the perturbative calculation of $C_7(\mu)$ and future work on next–to–leading logarithmic order corrections will reduce this variation significantly [131].

Assuming the recent tentative result for m_t from CDF [151], the lattice results give a branching ratio for the decay $B \to K^*\gamma$ of,

$$BR\,(B \to K^*\gamma) = \Big(1.5^{+5}_{-4}\,(\mathrm{stat.})\ \pm 0.5\,(\mathrm{sys.})\ \pm 0.3\,(\mathrm{exp.})\,{}^{+4}_{-3}\,(\mathrm{scale})\Big) \times 10^{-5}, \tag{4.53}$$

where the statistical and systematic errors have been separated from the lattice, experimental and theoretical (scale) uncertainties. Combining errors to produce an overall result yields,

$$BR\,(B \to K^*\gamma) = \Big(1.5 \pm 0.6\,(\mathrm{stat.})\,{}^{+9}_{-8}\,(\mathrm{sys.})\Big) \times 10^{-5}, \tag{4.54}$$

As stated previously, many of the uncertainties cancel in the hadronisation ratio R, which by Eq.(4.16) gives

$$R = \Big(8.8^{+28}_{-25}\,(\mathrm{stat.})\ \pm 3.0\,(\mathrm{sys.})\ \pm 1.0\,(\mathrm{exp.})\Big)\,\%\ . \tag{4.55}$$

By Eq.(4.1) and Eq.(4.2), the experimental hadronisation ratio is

$$R^{exp} = (19.4 \pm 4.3 \pm 6.5 \pm 3.9)\%\ , \tag{4.56}$$

where the first error is calculated from the combined systematic and statistical error of the inclusive decay [136] and the second and third errors are respectively the statistical and systematic error of the exclusive decay.

4.7 $B_s \to \phi\gamma$

Much of the analysis outlined in this chapter can also be applied to the rare decay $B_s \to \phi\gamma$. ALEPH [152] and DELPHI [153] have looked for this decay and obtained 90% CL upper bounds on its branching ratio of 4.1×10^{-4} and 1.9×10^{-3} respectively. Future research into this decay at LEP is planned. The branching ratio for this decay can be expressed in a form similar to Eq.(4.15),

$$BR(B_s \to \phi\gamma) = \frac{\alpha}{8\pi^4} m_b^2 G_F^2 m_{B_s}^3 \tau_{B_s} \left(1 - \frac{m_\phi^2}{m_{B_s}^2}\right)^3 |V_{tb}V_{ts}^*|^2 |C_7(m_b)|^2 |T_1^s(q^2{=}0)|^2, \tag{4.57}$$

where T_1^s is the relevant form factor from the decomposition of $\langle\phi|J_\mu|B_s\rangle$. Similarly, the hadronisation ratio R_s can also be determined

$$\begin{aligned} R_s &= \frac{BR(B_s \to \phi\gamma)}{BR(B_s \to X_s\gamma)} \\ &= 4\left(1 - \frac{m_\phi^2}{m_{Bs}^2}\right)^3 \left(\frac{m_{Bs}}{m_b}\right)^3 |T_1^s(q^2 = 0)|^2 \,. \end{aligned} \tag{4.58}$$

In determining this matrix element numerically, the interpolating operator $J_\rho^V(x)$ is replaced by the operator $J_\rho^\phi(x)$ defined as,

$$J_\rho^\phi(x) = \overline{s}(x)\gamma_\rho s(x). \tag{4.59}$$

As outlined in chapter 1, the presence of two identical particles in the final state, gives rise to an extra additive term in the trace of the general three–point function Eq.(1.56), which corresponds to $\overline{s}s$ creation from purely gluonic states. It is expected that this process is heavily suppressed by Zweig's rule [54, 55, 56], and hence the extra term is neglected.

As the variation of the form factors for $B \to K^*\gamma$ with respect to the spectator quark mass has been discarded, it can be assumed that,

$$T_1^s(q^2 = 0; m_P; m_\phi) = T_1(q^2 = 0; m_P; m_{K*}), \tag{4.60}$$

$$T_2^s(q^2 = 0; m_P; m_\phi) = T_2(q^2 = 0; m_P; m_{K*}). \tag{4.61}$$

By employing the same *ansätze* for extrapolating T_1 and T_2 as the previous sections, one finds

$$T_1^s(q^2 = 0; m_{B_s}; m_\phi) = 0.125^{+20}_{-18}\,(\text{stat.}) \pm 0.021\,(\text{sys.}) \,, \tag{4.62}$$

$$T_2^s(q^2 = q^2_{max}; m_{B_s}; m_\phi) = 0.270^{+17}_{-9}\,(\text{stat.}) \pm 0.009\,(\text{sys.}) \;, \tag{4.63}$$
$$T_2^{s,pole}(q^2 = 0; m_{B_s}; m_\phi) = 0.114^{+7}_{-4}\,(\text{stat.})\,{}^{+16}_{-15}\,(\text{sys.}) \;. \tag{4.64}$$

It is noted that $T_1^s(q^2{=}0)$ and $T_2^s(q^2{=}0)$ are consistent with each other. As before, by Eq.(4.57) and using $m_{B_s} = 5.3833(5)\,\text{GeV}$ [154, 155] and $\tau_{B_s} = 1.54(15)\,\text{ps}$ [156], the exclusive branching ratio for $B_s \to \phi\gamma$ is

$$\begin{aligned} BR\,(B_s \to \phi\gamma) &= \Big(1.6^{+5}_{-5}\,(\text{stat.}) \pm 0.6\,(\text{sys.}) \pm 0.3\,(\text{exp.})\,{}^{+4}_{-3}\,(\text{scale})\Big) \times 10^{-5}, \\ &= \Big(1.6 \pm 0.6\,(\text{stat.})\,{}^{+10}_{-9}\,(\text{sys.})\Big) \times 10^{-5} \;, \end{aligned} \tag{4.65}$$

and the hadronisation ratio for this decay is

$$R_s = (7.2^{+23}_{-21}\,(\text{stat.}) \pm 2.2\,(\text{sys.}) \pm 1.0\,(\text{exp.}))\% \;. \tag{4.66}$$

Chapter 5

Conclusions

This thesis has presented the non-perturbative calculation of a number of heavy hadron parameters, using lattice QCD. This has been carried out using a single lattice, with a lattice spacing of approximately $0.07\,fm$, a spatial volume of $(1.68\,fm)^3$ and a temporal extension of $3.36\,fm$. In order to simulate the continuum more accurately, a discretised fermionic action has been chosen which eliminates some of the cut–off effects due to the finite lattice spacing. In computational terms, this choice of lattice has a very large volume–to–lattice spacing ratio. As a result, the evaluation of these parameters was carried out in the quenched approximation.

In chapter 3, the calculation of the mass of three heavy–light hadrons, using four heavy quark masses, was detailed. These were the pseudoscalar and vector mesons, where $I(J^P) = \frac{1}{2}(0^-)$ and $\frac{1}{2}(1^-)$, respectively and the baryon Λ_Q ($I(J^P) = 0(\frac{1}{2}^+)$). The signal for the two–point functions of both mesons were quite good, and the behaviour of the masses as a function of the light quark mass is linear, allowing for an extrapolation of the masses to the chiral limit without a sizable increase in the statistical error. On the other hand, the signal for the baryon is noticeably poorer. The derived masses of the baryon are less stable to the choice of time–slice range and its behaviour as a function of the light quark mass is less linear. As the hadron masses were evaluated for only three light quark masses, the chiral extrapolation of the baryon masses was still carried out by means of a linear fit. This, however, increased the statistical error of the final result.

The behaviour of two linear combinations of these masses was examined as a function of the heavy quark mass. This can be compared with experimental data for bottom and charm hadrons and with the predicted behaviour of HQET. In spite of the poor signal for the baryon, both linear combinations agree with the experimental data to within 1 standard deviation at charm and to within 2 standard deviations at bottom, (the linear combinations at bottom must be derived from an extrapolation of the lattice heavy quark masses). The data also agrees with all of the predictions of HQET, albeit with large errors.

For the moderate number of gauge configurations used, the error due to quenching cannot be disentangled from the statistical error and the other systematic errors. Assuming that the statistical errors are Gaussian, a five to ten–fold increase in the number of configurations will reduce the statistical error of both linear combinations at the charm quark mass to less than the probable systematic error (an improvement in the algorithm for evaluating the baryon two–point function will also reduce the statistical error). Repeating this calculation for this high number of configurations (and the evaluation of the masses at different lattice spacings and volumes to allow an extrapolation to the zero–lattice spacing, infinite volume limit) in order to compute the error due to quenching does not appear feasible for the near future.

Nonetheless, exploring the behaviour of these linear combinations in the extrapolation to the bottom quark mass will be a very useful test of new algorithms for increasing the ground–state overlap of interpolating baryonic operators and improving fermionic actions. The heavy quark expansion of $m_\Lambda - m_P$ contains a term proportional to $\bar{\psi}\sigma_{\mu\nu}F^{\mu\nu}\psi$, which, to leading order in the lattice spacing is proportional to the clover term in the SW action. The linear combination $m_\Lambda - 1/4(m_P + 3m_V)$, on the other hand, specifically eliminates this term. The calculated value of $m_{\Lambda b} - 1/4(m_B + m_{B*})$ is in slightly better agreement with experimental data than the calculated value of $m_{\Lambda b} - m_B$. The suggestion by

Lepage and Mackenzie [14] to make the substitution

$$U_\mu \to \frac{U_\mu}{\langle \frac{1}{3} Tr U_{plaq} \rangle^{1/4}} ,$$

where U_{plaq} is the product of a plaquette of gauge links, in order to suppress tadpole diagrams, would in the SW action amount to increasing the size of the clover term. It would be very interesting to see if such an alteration would improve the agreement of the calculated values of $m_{\Lambda b} - m_B$ (and $m_{B*} - m_B$, where the effect also occurs [157]) with experimental data.

In chapter 4 a calculation was presented of some of the exclusive branching ratios of $b \to s\gamma$. An accurate determination of these branching ratios is one of the most important goals in B–physics phenomenology today as experimental data combined with these theoretical predictions will in the near future probe the SM and may detect new physics.

This was carried out by the evaluating the three–point function $\langle 0|J^P O_{\mu\nu} J^{\dagger V}|0\rangle$, where J^P and J^V are respectively the interpolating operators for a heavy pseudoscalar and strange vector meson state and

$$O_{\mu\nu} = \overline{h}\sigma_{\mu\nu} s \ .$$

By combining this data with the masses and amplitudes of the pseudoscalar and vector, the matrix element $\langle P|\overline{h}\sigma_{\mu\nu} s|V\rangle$ was isolated. Unfortunately, the initial and final states of this matrix element are not those of the of the physical matrix element required, nor does the transfer momentum q^μ satisfy the on–shell condition that $q^2 = 0$. As a result a number of extrapolations and interpolations had to be carried out with respect to the spectator, strange and heavy quark mass and q^2.

The chiral extrapolation was neglected as any variation with respect to the spectator quark mass was smaller than the statistical error. If this calculation is repeated with increased statistics, then this variation may well have to be considered. The variation due to the strange quark mass was approximately 10% and could not be neglected. However, the statistical error was not increased in the interpolation to the physical strange quark mass. The interpolation of the data to $q^2 = 0$ using the pole model had χ^2/d.o.f. that were slightly larger than expected. This is probably due to a subset of points in each fit which did not have as high a degree of symmetry as the other points. As a result, there was effectively less data for these points to average over.

The extrapolation of the data in the dimensionless ratio m_V/m_P to m_{K*}/m_B has proved to be quite difficult. By evaluating the two possible form factors, $T_1(q^2)$ and $T_2(q^2)$ for the matrix element and extrapolating both to m_{K*}/m_B, one can derive an estimate of the systematic error. Despite the fact that the determination of $T_1(q^2 = 0; m_B; m_{K*})$ and $T_2(q^2 = 0; m_B; m_{K*})$ depend on the validity of the pole model over a wide range of q^2, the methods of extrapolation in chapter 4 are not equivalent. This is because the coefficients in the fit of $\hat{T}_1$ are not fixed, which essentially allows the pole mass to vary, unlike the derivation of $T_2(q^2 = 0; m_B; m_{K*})$, where the pole mass is fixed to m_{Bs1}. It is only required that the leading order behaviour of T_1 satisfy the $m_P^{3/2}$ dependence. The final on–shell results for these form factors agree to within 1 standard deviation and is consistent with a similar analysis by Bernard, Hsieh and Soni [144].

Nonetheless, as the linear behaviour of $\hat{T}_1$ is quite poor, the recent suggestion by Abada *et al.* [158] that $T_1(q^2 = 0)$ satisfies a $m_P^{1/2}$ dependence merits further research. Such an ansatz would increase the central value of $T_1(q^2 = 0; m_B; m_{K*})$ from 0.124 to approximately 0.2.

As outlined in chapter 1, the effect due to quenching should not have a significant effect on the final result. The mass ratios and form factors are dimensionless and hence one expects that some of the systematic error due to setting the scale will cancel. It has been assumed that the lattice discretisation errors have been sufficiently suppressed by the use of the SW action. This is currently being tested by repeating the the calculation with approximately 30 gauge configurations at $\beta = 6.0$.

The lattice calculation of the branching and hadronisation ratio for $B \to K^*\gamma$ is consistent to within two standard deviations of the available experimental data. The errors for the experimental and lattice data are large. It is expected that the errors for the experimental data will decrease as the present results are based on quite a small number of events (the branching ratio for $B \to K^*\gamma$ was determined from 13 events, while the branching ratio for the inclusive decay $B \to X_s\gamma$ was based on 2 separate analyses, using 100–300 events). It seems reasonable to assume that eventually a lattice calculation of these branching ratios will detect deviations from the SM which are as small as 20% to 30% of the experimental results.

The analysis could also be easily extended to determine the branching ratios for exclusive modes of the decay $b \to d\gamma$. By comparing the ratio of $B.R.^{latt}(B \to \rho\gamma)/B.R.^{latt}(B \to K^*\gamma)$, with future experimental data, one could measure the ratio $|V_{td}|/|V_{ts}|$. If this was carried out, the effects due to the finite volume of the lattice would need to be tested as long distance effects would be enhanced for the light quark field. The use a larger volume would also have the added advantage that the mesons could acquire smaller units of momenta, allowing for a more subtle test of the pole model.

Finally, the exclusive mode decays of other rare b decays, for example $b \to s\bar{s}s$ and $b \to sl^+l^-$, (the inclusive decay of which has a strong dependence on m_t [159]) should also be examined in lattice QCD. These would be more challenging to carry out computationally, but would provide further tests of the SM.

References

[1] S. Glashow, Nucl. Phys. **22**, 579 (1961).

[2] S. Weinberg, Phys. Rev. Lett. **19**, 1264 (1967).

[3] M. Gell-Mann, *The Eightfold Way* (W.A. Benjamin, New York, 1964), (reprint).

[4] D. Gross and F. Wilczek, Phys. Rev. Lett. **30**, 1343 (1973).

[5] P. Renton, *Electroweak Interactions* (Cambridge University Press, Cambridge, 1990).

[6] T.-P. Cheng and L.-F. Li, *Gauge theory of elementary particle physics* (Oxford University Press, New York, 1991).

[7] D. Bailin and A. Love, *Introduction to Gauge Field Theory* (Adam Hilger, Bristol, 1986).

[8] M. Kobayashi and M. Maskawa, Prog. Theor. Phys. **49**, 652 (1973).

[9] A. Ali, Presented at Int. Conf. on High Energy Physics, Glasgow, Scotland, July 20-26, 1994 .

[10] M. Creutz, Phys. Rev. Lett. **43**, 553 (1979), erratum ibid. (1979) 43, 890.

[11] F. Wilczek, Talk given at 16th International Symposium on Lepton and Photon Interactions, Ithaca, NY, 10-15 Aug 1993 , hep-ph 9311302.

[12] S. Bethke, in *QCD: 20 Years Later, Aachen, Germany, 9 -13 Jun*, edited by P. Zerwas and H. Kastrup (World Scientific, Singapore, 1992), Vol. 1.

[13] G. Altarelli, in *Workshop on QCD: 20 Years Later, Aachen, Germany, Jun 9-13*, edited by P. Zerwas and H. A. Kastrup (World Scientific, Singapore, 1992), Vol. 1.

[14] G. Lepage and P. B. Mackenzie, Phys. Rev. D **48**, 2250 (1993), hep-lat 9209022.

[15] A. S. Kronfeld, in *Perspectives in the Standard Model : Proceedings of TASI, Boulder, Colorado, 2–28 June 1991*, edited by R. Ellis, C. Hill, and J. Lykken (World Scientific, Singapore, 1992), pp. 421–474.

[16] C. Sachrajda, in *From Actions to Answers, Proceedings of the 1989 Theoretical Advanced Study Institute in Elementary Particle Physics*, edited by T. DeGrand and D. Toussaint (World Scientific, Singapore, 1990), pp. 293–319.

[17] R. Feynman and A. Hibbs, *Quantum Mechanics and Path Integrals* (McGraw–Hill, New York, 1965).

[18] H. J. Rothe, *Lattice Gauge Theories – An Introduction* (World Scientific, Singapore, 1992).

[19] D. Weingarten, Nucl. Phys. (Proc Suppl.) **B34**, 29 (1994).

[20] C. W. Bernard and M. F. Golterman, Phys. Rev. D **46**, 853 (1992), hep-lat 9204007.

[21] S. R. Sharpe, Nucl. Phys. (Proc. Suppl.) **B30**, 213 (1993), hep-lat 9211005.

[22] V. Lubicz *et al.*, Phys. Lett. B **274**, 415 (1992).

[23] C. Bernard, A. El-Khadra, and A. Soni, Phys. Rev. D **45**, 869 (1992).

[24] UKQCD collaboration, D. Richards *et al.*, Nucl. Phys. (Proc. Suppl.) **34**, 411 (1994).

[25] K. G. Wilson, Phys. Rev. D **10**, 2445 (1974).

[26] A. Simpson, Ph.D. thesis, Physics Department, University of Edinburgh, 1991.

[27] H. Nielsen and M. Ninomiya, Nucl. Phys. **B185**, 20 (1981).

[28] T. Banks, J. Kogut, and L. Susskind, Phys. Rev. D **13**, 1043 (1976).

[29] K. G. Wilson, in *New Phenomena in Subnuclear Physics*, edited by A. Zichichi (Plenum, New York, 1977).

[30] M. Voloshin and M. Shifman, Sov. J. Nucl. Phys. **45**, 292 (1987).

[31] H. Politzer and M. Wise, Phys. Lett. B **206**, 681 (1988).

[32] H. Politzer and M. Wise, Phys. Lett. B **208**, 504 (1988).

[33] G. Lepage, Nucl.Phys. (Proc. Suppl.) **B26**, 45 (1992).

[34] P. B. Mackenzie, Nucl. Phys. (Proc. Suppl.) **B30**, 35 (1993), hep-lat 9212018.

[35] A. S. Kronfeld, Nucl. Phys. (Proc. Suppl.) **B30**, 445 (1993), hep-lat 9211043.

[36] UKQCD Collaboration, J. Simone *et al.*, Nucl. Phys. (Proc. Suppl.) **B30**, 461 (1993).

[37] C. W. Bernard, J. N. Labrenz, and A. Soni, (1993), hep-lat 9306009, UW-PT-93-06, WASH-U-HEP-93-30, BNL-49068.

[38] G. Heatlie *et al.*, Nucl. Phys. **B352**, 266 (1991).

[39] B. Sheikholeslami and R. Wohlert, Nucl. Phys. **B259**, 572 (1985).

[40] UKQCD Collaboration, R. M. Baxter *et al.*, Phys. Rev. D **49**, 1594 (1994).

[41] H. Hoeber, Ph.D. thesis, Physics Department, University of Edinburgh, 1994.

[42] E. Eichten, Nucl. Phys. (Proc. Suppl.) **B4**, 170 .

[43] C. W. Bernard, Nucl. Phys. (Proc. Suppl.) **B34**, 47 (1994), hep-lat 9312086.

[44] G. Lepage and B. Thacker, Nucl. Phys. (Proc. Suppl.) **B4**, 199 (1988).

[45] B. Thacker and G. Lepage, Phys. Rev. D **43**, 196 (1991).

[46] G. Lepage *et al.*, Phys. Rev. D **46**, 4052 (1992), hep-lat 9205007.

[47] C. Davies *et al.*, (1994), hep-lat 9404012, OHSTPY-HEP-T-94-004, SCRI-94-39.

[48] C. Davies, Nucl. Phys. (Proc. Suppl.) **B34**, 135 (1994), hep-lat 9312022.

[49] UKQCD Collaboration, C.T.H. Davies *et al.*, Nucl. Phys. (Proc. Suppl.) **B34**, 437 , hep-lat 9312020.

[50] S. Hashimoto, (1994), hep-lat 9403028, HUPD-9403.

[51] B. Ioffe, Nucl. Phys. **B188**, 317 (1981).

[52] C. Bernard, J. Simone, and A. Soni, Nucl. Phys. (Proc. Suppl.) **B17**, 504 (1990).

[53] J. N. Simone, Ph.D. thesis, University of California, Los Angeles, 1991.

[54] G. Zweig, CERN report no. 8419/TH 412 (1964).

[55] S. Okubo, Phys. Lett. **5**, 163 (1963).

[56] J. Iizuka, Prog. Theor. Phys. Suppl. **37**, 21 (1966).

[57] R. Kenway, Submitted to 22nd Int. Conf. on High Energy Physics, Leipzig, East Germany, Jul 19-25, 1984. Preliminary version appeared as CERN preprint CERN-TH-3952 .

[58] A. Billoire, E. Marinari, and G. Parisi, Phys. Lett. B **162**, 160 (1985).

[59] APE collaboration P. Bacilieri *et al.*, Phys. Lett. B **214**, 115 (1988).

[60] APE collaboration P. Bacilieri *et al.*, Nucl. Phys. **B317**, 509 (1989).

[61] G. Kilcup, Nucl. Phys. (Proc. Suppl.) **B9**, 201 (1989).

[62] T. Degrand and R. Loft, Comp. Phys. Comm. **65**, 84 (1991).

[63] F. Butler, Nucl. Phys. (Proc. Suppl.) **B26**, 369 (1992).

[64] T. Draper and C. McNeile, Nucl. Phys (Proc. Suppl.) **B34**, 453 (1994).

[65] S. Güsken *et al.*, Nucl. Phys. (Proc. Suppl.) **B17**, 361 (1990).

[66] UKQCD collaboration, C.R. Allton *et al.*, Phys. Rev. D **47**, 5128 (1993), hep-lat 9303009.

[67] N. Isgur and M. B. Wise, Phys. Lett. **B232**, 113 (1989).

[68] N. Isgur and M. B. Wise, Phys. Lett. **B237**, 527 (1990).

[69] N. Isgur and M. B. Wise, Nucl. Phys. **B348**, 276 (1991).

[70] H. Georgi, Nucl. Phys. **B348**, 293 (1991).

[71] M. Neubert, Phys. Lett. **B264**, 455 (1991).

[72] M. Neubert, SLAC-PUB-6263, hep-ph 9306320 (1993).

[73] N. Hazel, Nucl. Phys. (Proc. Suppl.) **B34**, 471 (1994), hep–lat 9312001.

[74] N. Isgur and M. B. Wise, Phys. Rev. Lett. **66**, 1130 (1991).

[75] P. Cho, Nucl. Phys. **B396**, 183 (1993), erratum-ibid. **B421**, 683, 1994.

[76] H. Georgi, Phys. Lett. **B240**, 447 (1990).

[77] C. Allton *et al.*, (1994), hep-ph 9406263, ROME-1018-1994.

[78] E. Eichten and B. Hill, Phys. Lett. **B243**, 427 (1990).

[79] A. F. Falk, B. Grinstein, and M. E. Luke, Nucl. Phys. **B357**, 185 (1991).

[80] N. Isgur and M. B. Wise, Invited talk at Hadron 91, College Park, MD, Aug 12-16 , (1991), CEBAF-TH-92-10.

[81] T. Mannel, W. Roberts, and Z. Ryzak, Nucl. Phys. **B368**, 204 (1992).

[82] H. Georgi, Nucl. Phys. **B361**, 339 (1991).

[83] D. Boulware, Phys. Rev. D **23**, 389 (1981).

[84] L. Abbot, Nucl. Phys. **B185**, 189 (1981).

[85] M. Luke and A. V. Manohar, Phys. Lett. **B286**, 348 (1992), hep-ph 9205228.

[86] P. Ball and U. Nierste, (1994), hep–ph 9403407, TUM-T31-56-94.

[87] I. Bigi, M. Shifman, N. Uraltsev, and A. Vainshtein, Phys. Rev. D **50**, 2234 (1994).

[88] A. F. Falk, M. Neubert, and M. Luke, Nucl. Phys. **B388**, 363 (1992), hep-ph 9204229.

[89] A. F. Falk and M. Neubert, Phys. Rev. D **47**, 2965 (1993), hep-ph 9209268.

[90] M. Neubert, Phys. Rev. D **46**, 1076 (1992).

[91] M. Bochicchio *et al.*, Nucl. Phys. **B372**, 403 (1992).

[92] UKQCD collaboration, Nicoletta Stella *et al.*, , to appear in Lattice 94, Proceedings of the 1994 Symposium on Lattice Field Theory, Bielefeld.

[93] C. Alexandrou *et al.*, , hep-lat 9407027, PSI-PR-94-22.

[94] S. Aoki *et al.*, Phys. Rev. D **50**, 486 (1994).

[95] M. Lüscher and P. Weisz, Commun. Math. Phys. **97**, 59 (1985).

[96] UKQCD Collaboration, C. Allton *et al.*, Nucl. Phys. **B407**, 331 (1993).

[97] C. Bernard, in *From Actions to Answers, Proceedings of the 1989 Theoretical Advanced Study Institute in Elementary Particle Physics*, edited by T. DeGrand and D. Toussaint (World Scientific, Singapore, 1990), pp. 233–292.

[98] G. Lepage, in *From Actions to Answers, Proceedings of the 1989 Theoretical Advanced Study Institute in Elementary Particlae Physics*, edited by T. DeGrand and D. Toussaint (World Scientific, Singapore, 1990), pp. 97–120.

[99] B. Efron, SIAM Review **21**, 460 (1979).

[100] UKQCD Collaboration, C. Allton *et al.*, Edinburgh preprint 93/524, Southampton preprint SHEP 92/93-16, hep-lat 9309002 (1993).

[101] CLEO Collaboration, R. Ammar *et al.*, Phys. Rev. Lett. **71**, 674 (1993).

[102] S. Bertolini *et al.*, Nucl. Phys. **B353**, 591 (1991).

[103] N. Oshimo, Nucl. Phys. **B404**, 20 (1993).

[104] R. Barbieri and G. Giudice, Phys. Lett. B **309**, 86 (1993).

[105] J. L. Lopez, D. V. Nanopoulos, and G. T. Park, Phys. Rev. D **48**, 974 (1993).

[106] R. Garisto and J. N. Ng, Phys. Lett. B **315**, 372 (1993).

[107] M. A. Diaz, Phys. Lett. B **304**, 278 (1993).

[108] F. M. Borzumati, DESY 93–090, hep-ph 9310212 (1993).

[109] T. G. Rizzo, Phys. Rev. D **38**, 820 (1988).

[110] W.-S. Hou, A. Soni, and H. Steger, Phys. Lett. B **192**, 441 (1987).

[111] J. L. Hewett, (1994), hep-ph 9406302, SLAC–PUB–6521.

[112] N. G. Deshpande, P. Lo, and J. Trampetic, Z. Phys. **C40**, 369 (1988).

[113] P. J. O'Donnell and H. K. K. Tung, Phys. Rev. D **44**, 741 (1991).

[114] T. Altomari, Phys. Rev. D **37**, 677 (1988).

[115] C. A. Dominguez, N. Paver, and Riazuddin, Phys. Lett. B **214**, 459 (1988).

[116] T. M. Aliev, A. A. Ovchinnikov, and V. A. Slobodenyuk, Phys. Lett. B **237**, 569 (1990).

[117] P. Ball, TUM-T31-43-93, hep-ph 9308244 (1993).

[118] P. Colangelo, C. A. Dominguez, G. Nardulli, and N. Paver, Phys. Lett. B **317**, 183 (1993).

[119] A. Ali, V. M. Braun, and H. Simma, CERN–TH–7118–93, MPI–Ph/93–97, DESY 93–193, hep-ph 9401277 (1993).

[120] S. Narison, Phys. Lett. B **327**, 354 (1994).

[121] A. Ali, T. Mannel, and T. Ohl, Phys. Lett. B **298**, 195 (1993).

[122] C. W. Bernard, P. F. Hsieh, and A. Soni, Nucl. Phys. (Proc Suppl.) **B26**, 347 (1992), note that there is a factor of 2 missing in eq. (4) of this paper.

[123] P. Cho and M. Misiak, CALT–68–1893, TUM–T31–52/93, hep-ph 9310332 (1993).

[124] L. Randall and R. Sundrum, Phys. Lett. B **312**, 148 (1993).

[125] S. Chia, Phys. Lett. B **240**, 465 (1990).

[126] K. Peterson, Phys. Lett. B **282**, 207 (1992).

[127] T. Rizzo, Phys. Lett. B **315**, 471 (1993).

[128] X.-G. He and B. McKellar, Phys. Lett. B **320**, 165 (1994).

[129] S. Glashow and S. Weinberg, Phys. Rev. D **21**, 1393 (1980).

[130] L. F. Abbot, P. Sikivie, and M. B. Wise, Phys. Rev. D **21**, 1393 (1980).

[131] A. Buras, M. Misiak, M. Münz, and S. Pokorski, MPI–Ph/93–77, TUM–T31–50/93, hep-ph 9311345 (1993).

[132] J. L. Hewett, Phys. Rev. Lett. **70**, 1045 (1993).

[133] M. Diaz, Phys. Lett. **B322**, 207 (1994), hep-ph 9311228.

[134] J. Chay, H. Georgi, and B. Grinstein, Phys. Lett. **B247**, 399 (1990).

[135] A. F. Falk, M. Luke, and M. J. Savage, Phys. Rev. D **49**, 3367 (1994), hep-ph 9308288, SLAC-PUB-6317.

[136] B. Barish *et al.*, Presented at Int. Conf. on High Energy Physics, Glasgow, Scotland , July 20-26, 1994 .

[137] B. Grinstein, R. Springer, and M. B. Wise, Nucl. Phys. **B339**, 269 (1990).

[138] H. Simma, (1993), hep-ph 9307274, DESY-93-083.

[139] M. Ciuchini *et al.*, Phys. Lett. B **316**, 127 (1993).

[140] P. Cho and B. Grinstein, Nucl. Phys. **B365**, 279 (1991).

[141] UKQCD Collaboration, C. Allton *et al.*, Phys. Rev. D **49**, 474 (1994).

[142] D. Daniel *et al.*, Phys. Rev. D **46**, 3130 (1992).

[143] UKQCD Collaboration, K. C. Bowler *et al.*, Phys. Rev. Lett. **72**, 1398 (1994), (hep-lat 9311004).

[144] C. Bernard, P. Hsieh, and A. Soni, Phys. Rev. Lett. **72**, 1402 (1994), (hep-lat 9311011).

[145] NRQCD collaboration, C.T.H. Davies *et al.*, hep-lat 9404012, OHSTPY-HEP-T-94-004 (1994).

[146] N. Gray, D. Broadhurst, W. Grafe, and K. Schilcher, Z. Phys. **C48**, 673 (1990).

[147] S. Stone, in *B Decays*, edited by S. Stone (World Scientific, Singapore, 1994), (2nd Ed., to be published).

[148] ALEPH Collaboration, D. Buskulic *et al.*, Phys. Lett. **B307**, 194 (1993).

[149] OPAL collaboration, P.D. Acton *et al.*, Phys. Lett. **B307**, 247 (1993).

[150] A. Borrelli, C. Pittori, R. Frezzotti, and E. Gabrielli, Nucl. Phys. **B409**, 382 (1993).

[151] CDF Collaboration, F. Abe *et al.*, Fermilab Pub 94/097–E .

[152] ALEPH collaboration, A. Bonnssent *et al.*, (1993), talk given at the 28th Rencontres de Moriond (1993).

[153] DELPHI collaboration, M. Battaglia *et al.*, Helsinki University Report No. HU SEFT R 1993–14 , to appear in the proceedings of the 5th International Symposium on Heavy Flavour Physics 1993.

[154] OPAL Collaboration, D. Buskulic *et al.*, Phys. Lett. **B311**, 425 (1993), erratum-ibid. **B316**:631,1993.

[155] CDF Collaboration, F. Abe *et al.*, Phys. Rev. Lett. **71**, 1685 (1993).

[156] R. Forty, to appear in Proc. of XIV Int. Conf. on Physics in Collision, Tallahassee, June 15-17 (1994).

[157] S. Collins, Ph.D. thesis, Physics Department, University of Edinburgh, 1993.

[158] APE collaboration, A. Abada *et al.*, Presented at Int. Conf. on High Energy Physics, Glasgow, Scotland , July 20-26, 1994 , hep-ph 9409338.

[159] N. Deshpande, Presented at Int. Conf. on High Energy Physics, Glasgow, Scotland , July 20-26, 1994 .